

The Development of an Electrochemical Biosensor to Detect and Measure Autophagy Flux

by

Kenneth Jacobs



*Thesis presented in partial fulfilment of the requirements
for the degree of Master of Engineering (Electronic) in the
Department of Electrical and Electronic Engineering at
Stellenbosch University*

Supervisor: Prof. W. J. Perold

Co-supervisor: Prof. B. Loos

December 2022

Declaration

By submitting this thesis electronically, I declare that the entirety of the work contained therein is my own, original work, that I am the owner of the copyright thereof (unless to the extent explicitly otherwise stated) and that I have not previously in its entirety or in part submitted it for obtaining any qualification.

December 2022

Copyright © 2022 Stellenbosch University

All rights reserved

Abstract

The Development of an Electrochemical Biosensor to Detect and Measure Autophagy Flux

K. H. Jacobs

*Department of Electrical and Electronic Engineering
Stellenbosch University*

Thesis: MEng (Electronic Engineering)

December 2022

Autophagy is a cellular process, which a cell undergoes self-degradation to remove unwanted and dysfunctional cellular material. The autophagic process is associated with various diseases such as cancers, neurodegenerative, and infectious diseases, as well as longevity and health. The protein LC3-II is the most common biomarker used to detect the autophagic process. LC3-II is directly related to the formation of autophagosomes, a double-membraned vesicle that contains cellular material for degradation, therefore the change in the concentration of LC3-II is a good estimate of autophagy flux. A label-free electrochemical DNA biosensor is developed to measure the concentration of the DNA that encodes the protein LC3-II. Through covalent immobilization of thiol modified ssDNA probes onto a planar gold electrode, a self-assembled monolayer of ssDNA probes is formed, which acts as the integrated transducer and recognition layer. The ssDNA targets are detected through the hybridization reaction of complementary ssDNA targets and ssDNA probes. A low cost potentiostat is developed to apply square-wave voltammetry to the sensor, which is submerged in an electrolyte solution of potassium ferrocyanide in potassium chloride. The hybridization reaction results in a change in the electrical properties of the sensor which is exploited to measure the concentration of the ssDNA targets. The results indicated that the decreasing peak current measured by the biosensor is directly related to the increasing concentration of the ssDNA targets.

Uittreksel

Die Ontwikkeling van 'n Elektrochemiese Biosensor om Outofagie Vloed waar te neem en te meet

("The Development of an Electrochemical Biosensor to Detect and Measure Autophagy Flux")

K. H. Jacobs

*Departement Elektries en Elektroniese Ingenieurswese
Universiteit van Stellenbosch*

Tesis: MScIng (Elektroniese Ingenieurswese)

Desember 2022

Outofagie is 'n sellulêre proses waar selle selfdegradasie ondergaan om ongewenste en disfunksionele sellulêre materiaal te verwyder. Die outofagiese proses word geassosieer met kanker, neurodegeneratiewe, aansteeklike siektes, sowel as langlewendheid en gesondheid. Die proteïen LC3-II is die mees algemene biomerker wat gebruik word om die outofagiese proses op te spoor. LC3-II is direk verwant aan die vorming van outofagosome, 'n dubbelmembraan vesikel wat sellulêre materiaal vir degradasie bevat en daarom is die verandering in die konsentrasie van LC3-II 'n goeie skatting van outofagie vloed. 'n Etiketvrye elektrochemiese DNS biosensor word ontwikkel wat die konsentrasie van die DNS wat die proteïen LC3-II kodeer, meet. Deur kovalente immobilisasie van thiolgemodifiseerde ssDNS-probes op 'n plat goue elektrode, is 'n self-saamgestelde monolaag van ssDNS-probes gevorm, wat dien as die geïntegreerde omsetter en herkenningslaag. Die ssDNS-teikens word opgespoor deur die hibridisasiereaksie van komplementêre ssDNS-teikens en ssDNS-probes. 'n Laekoste potensiostaat word ontwikkel om vierkantgolfvoltageammetrie op die sensor toe te pas, wat in 'n elektrolietoplossing van kaliumferrosianied in kaliumchloried lê. Die hibridisasiereaksie verander die elektriese eienskappe van die sensor. Die dalende piekstroom gemeet deur die biosensor hou direk verband met die toenemende konsentrasie van die ssDNS-teikens.

Acknowledgements

I would like to express my sincere gratitude to Prof. W. J. Perold, Prof B. Loos, and Dr. A. Du Toit, for their dedication, support, and sharing of their knowledge throughout this study.

Dedications

This thesis is dedicated to my friends and family who have continued to encourage and support me through the challenges of this study.

Contents

Declaration	i
Abstract	ii
Uittreksel	iii
Acknowledgements	iv
Dedications	v
Contents	vi
List of Figures	ix
List of Tables	xii
Nomenclature & Abbreviations	xiii
1 Introduction	1
1.1 Background	1
1.2 Research aims and objectives	3
1.3 Project scope	3
1.4 Thesis Outline	4
2 Literature review	6
2.1 Autophagy	6
2.2 Application of autophagy	7
2.3 Basic autophagy machinery	10
2.4 Autophagy flux	13
2.5 Biosensors	15
2.6 Historical background of biosensors	16
2.7 Biosensor characteristics	18

<i>CONTENTS</i>	vii
2.8 Types of biosensors	18
2.9 DNA immobilization	26
2.10 Summary	30
3 Design and development of sensor	31
3.1 Biosensor overview	31
3.2 Biosensor type	32
3.3 Electrolyte solution	33
3.4 Transducer	33
3.5 Recognition layer - Immobilization	34
3.6 Analyte recognition - Hybridization	37
3.7 Detection method - Square wave voltammetry	39
3.8 Summary	41
4 Design and development of potentiostat	42
4.1 Micro-controller	43
4.2 Digital to analog converter	44
4.3 Control amplifier	45
4.4 Transimpedance amplifier	46
4.5 Three-electrode system	47
4.6 Spice simulation	47
4.7 Arduino software	48
4.8 Summary	52
5 Results	54
5.1 Concentration of background electrolyte	54
5.2 Square wave voltammetry calibration curve	57
5.3 ssDNA probe immobilization	62
5.4 Target DNA hybridization	69
5.5 SWV time dependence	72
5.6 Potentiostat	73
5.7 Summary	81
6 Discussion	84
6.1 Introduction	84
6.2 Overview of the project	84
6.3 Conclusion	86
Appendices	88

<i>CONTENTS</i>	viii
A Datasheets	89
A.1 Screen-printed electrode	90
A.2 Interdigitated electrode	92
A.3 MCP4922	93
A.4 TLC2272	97
B Protocols	103
B.1 DNA preparation	104
B.2 Sybr nucleic acid stain	108
C Code	110
C.1 Arduino code	111
Bibliography	113

List of Figures

2.1	Roles of apoptosis and autophagy in tumor formation. Reprinted from "Eaten alive: A history of macro-autophagy" [14]	8
2.2	The autophagic process. Reprinted from "Frontiers in Cell and Developmental Biology" [17]	11
2.3	Defining autophagy flux through the autophagic pathway. Reprinted from "Defining and measuring autophagosome flux - concept and reality" [18]	14
2.4	Schematic of a biosensor. Reprinted from "Essays in Biochemistry" [21]	15
2.5	Schematic of a three-electrode electrochemical system. Reprinted from "ChemTexts" [35]	22
2.6	Voltammetric excitation signals	24
2.7	DNA immobilization strategies. Reprinted from "Sensors (Switzerland)" [39]	27
3.1	Overview of biosensor prototype	32
3.2	Transducer: Gold WE screen printed electrode	34
3.3	DNA tethered with a C6-thiol	35
3.4	Structure of thiol monolayer	36
3.5	Immobilization of ssDNA probes	37
3.6	Hybridization of ssDNA probes and ssDNA targets	38
3.7	SWV input potential	40
4.1	Potentiostat schematic	42
4.2	Superposition of step and stair wave to form stair-step wave	44
4.3	Control amplifier schematic	45
4.4	Transimpedance amplifier	46
4.5	Spice simulation of potentiostat	48
4.6	Spice output of stair-step wave	48
4.7	Arduino code DAC library	49
4.8	Arduino code DAC setup	49

<i>LIST OF FIGURES</i>	x
4.9 Arduino code setDac function	50
4.10 Arduino code Loop function	51
4.11 Arduino code current sampling	52
4.12 Current sampling of forward and reverse currents	52
5.1 Peak current (mA) vs. background electrolyte concentration (mM)	55
5.2 Peak current (mA) vs. background electrolyte concentration (mM) (a) Logarithmic plot (b) Linear plot	55
5.3 Cyclic voltammogram of electrolyte solution	56
5.4 Calibration curve of DNA sensor (a) Individual peak currents (b) Mean peak current	57
5.5 Calibration curve of various reference electrodes	58
5.6 Calibration curve post MCH treatment	59
5.7 Calibration curve post ultrasonic treatment	59
5.8 Peak currents (mA) of various frequencies	60
5.9 Repeatability of frequency (a) 25 Hz (b) 35 Hz (c) 50 Hz	60
5.10 Calibration curve of various auxiliary electrodes (a) Platinum auxiliary electrode (b) Comparison of platinum and gold	61
5.11 Change in peak current (mA) vs. change in DNA probes concentration (μM) (a) Sensor 1 (b) Sensor 2	62
5.12 The influence of TCEP on immobilization of DNA probes	64
5.13 Voltammograms (a) 1 μM DNA probes (test samples) (b) 1 μM DNA probes (control samples)	65
5.14 Fluorescent microscopy (a) Blank SPE sample (b) Immobilized DNA control sample (c) Immobilized DNA washed in MCH sample (d) Im- mobilized DNA test sample	66
5.15 SEM imaging (a) Blank SPE (b) Blank SPE washed in TE buffer (c) Immobilized DNA control sample (d) Immobilized DNA test sample (e) Hybridized DNA control sample (f) Hybridized DNA test sample	67
5.16 EDX analysis (a) Presence of contaminant (b) Elemental composition	68
5.17 Hybridization of target DNA (a) Sensor 1 (b) Sensor 2 (c) Sensor 3	69
5.18 Peak current of target DNA concentration	70
5.19 Peak currents (mA) vs time (s) (a) Time 0-4500 s (b) Time 0-185 s	72
5.20 Oscilloscope screenshots of the stair-step waveform generated (a) Am- plitude (b) Frequency (c) Step size (d) Start and stop potential	74
5.21 Oscilloscope screenshots of the transimpedance output with various biased input voltages (a) 1 V (b) 1.5 V (c) 2 V (d) 3 V (e) 3.3 V (f) 3.5 V	75
5.22 Spice simulation of 3 V	76

<i>LIST OF FIGURES</i>	xi
5.23 Transimpedance input V_n (a) Spice model (b) prototype	77
5.24 Transimpedance output V_{out} (a) Spice model (b) prototype	77
5.25 Output current of Spice model and prototype design	78
5.26 Output current (a) Spice and prototype model biased at 3.5 V (b) Spice model biased at 1.2 V	79
5.27 Output current when a positive and negative voltage sweep is applied	79
5.28 Output current with Randles circuit dummy cell (a) Uncalibrated pro- totype (b) Calibrated prototype	80
5.29 Output current (a) Uncalibrated prototype, (b) Calibrated prototype .	80
5.30 Output current of Spice simulation and commercial potentiostat	81

List of Tables

2.1	Summary of biosensor development between 1906 and 1999	17
4.1	Micro-controller specifications	43
4.2	DAC MPC4922 pin connections	45
4.3	Bit instructions for DAC register	50
5.1	Peak currents (mA) and potentials (mV) of cyclic voltammogram	56
5.2	Peak current of various ssDNA probes concentration	63
5.3	Decrease in peak current of test samples (TCEP) from control samples (without TCEP)	64
5.4	Change in peak current of target DNA from 1 μ M monolayer	70
5.5	Key parameters of repeated SPE electrochemical activation	73
5.6	Transimpedance voltage biasing	76

Nomenclature & Abbreviations

Variables

J	Steady-state flux	[m ³ /s]
v	Flow rate	[m ³ /s]
t	Time	[s]
A	Voltage amplitude	[Volt]
f	Frequency	[Hz]
v	Scan rate	[mV/s]
V	Voltage	[Volt]
I	Current	[Ampere]
R	Resistance	[Ohm]
n	Bit resolution	[unitless]

Abbreviations

NCD	Noncommunicable disease
DNA	Deoxyribonucleic acid
ssDNA	Single-stranded DNA
dsDNA	Double-stranded DNA
cDNA	Complementary DNA
RNA	Ribonucleic acid
mRNA	Messenger RNA
SWV	Square wave voltammetry

CV	Cyclic voltammetry
DPV	Differential pulse voltammetry
EIS	Electrochemical impedance spectroscopy
Atg	Autophagy related
BCl-2	B-cell lymphoma 2
hVps34	Human phosphatidylinositol 3-kinase
PtdIns3K	Class III phosphatidylinositol 3-kinase
p62	Sequestosome 1
ROS	Reactive oxygen species
TOR	Target of rapamycin
LC3	Microtubule-associated protein
LC3-II	Microtubule-associated protein phosphatidylethanolamine
PRGR-LE	Intracellular pattern-recognition receptor
<i>C. elegans</i>	<i>Caenorhabditis elegans</i>
Vps34	Vesicular protein sorting 34
PI3P	Phosphatidyl inositol trisphosphate
PE	Phosphatidylethanolamine
CMA	Chaperone-mediated autophagy
P	Phagophore
A	Autophagosome
L	Lysosome
AL	Autolysosome
AA	Amino Acids
IUPAC	International Union of Pure and Applied Chemistry
NAHD	Nicotinamide adenine dinucleotide
GOD	Glucose oxidase

GDR	German Democratic Republic
ISFET	Ion-sensitive field-effect transistor
FET	Field-effect transistor
SPR	Surface plasmon resonance
POC	Point of care
LOD	Limit of detection
Ag	Silver
Cl	Chloride
Au	Gold
PCR	Polymerase chain reaction
SELEX	Systematic Evolution of Ligands by Exponential Enrichment
SAM	Self-assembled monolayer
CPG	Contracted pore glass
MCH	Mercaptohexanol
AuNP	Gold nanoparticles
MPA	Mercaptoacetic acid
SPE	Screen-printed electrode
IDE	Interdigitated electrode
CE	Counter electrode
WE	Working electrode
RE	Reference electrode
[Fe(CN) ₆ ^{4-/3-}]	Potassium ferrocyanide
TCEP	Tris (2-carboxyethyl) phosphine hydrochloride
DAC	Digital-to-analog converter
ADC	Analog-to-digital converter
Op-amp	Operational amplifier

NOMENCLATURE & ABBREVIATIONS

xvi

PWL	Piecewise linear
SPI	Serial peripheral interface
CS	Chip select
DI	Deionized
SEM	Scanning electron microscopy
EDX	Energy dispersive x-ray

Chapter 1

Introduction

This chapter provides the relevant background that encouraged this study. It discusses the real-life application of autophagy to the health of human-beings. The aims and objectives are set in order to complete the project. The scope of the project is discussed as well as the limitations to the project, followed by a summary of the subsequent chapters in this thesis.

1.1 Background

Noncommunicable diseases (NCDs) are one of the leading causes of death throughout the globe. In 2016, NCDs killed around 41 million people, which accounted for 71% of all deaths [1]. NCDs are a medical condition, which by definition is non-infectious. They are chronic diseases that result from behavioral, environmental, physiological and genetic factors. They are of slow progression and may result in sudden death. NCDs include cancers, diabetes, neurodegenerative-, chronic respiratory- and cardiovascular diseases [1]. They are one of the biggest challenges facing the 21st century due to their devastating public health, economic, and social impact [2]. Low and middle income countries are disproportionately affected by NCDs, and these countries account for more than 31.4 million of all NCDs deaths.

In 2020, there were almost 10 million deaths due to cancer and an estimated 19.3 million new diagnoses globally. Female breast cancer is the most commonly diagnosed, with 2.3 million new cases. Other common cancers are stomach, prostate, colorectal, and lung. Cancer is the leading hurdle to increase life expectancy around the globe [3]. The most common neurodegenerative diseases are Parkinson's and Alzheimer's. The prevalence of these diseases increase with age, therefore it is expected that the amount of cases will increase as the life expectancy increases in many countries [4]. Alzheimer's goes largely unnoticed as the disease

begins 20 years or more before the onset of symptoms, with the disease causing small changes in the brain that are not easy to detect. Alzheimer's causes complications such as pneumonia, which is found to be the leading cause of death amongst elderly infected with the disease. The long duration of these diseases before death places a large burden on family and public health, as a lot of time is spent on dependence from health care systems [5].

Early detection and diagnosis of cancer increases the chance for successful treatment and survival. Delays in diagnosis introduce more problems during treatment and excessively higher treatment costs. Early diagnoses have contributed to a 2% decrease in premature mortality between 2000 and 2015, but low and middle income countries only had a 5% decrease in deaths due to the lack of affordable and easily accessible cancer detection methods [6]. Early detection of neurodegenerative diseases are important for the development of new drugs and measures to slow down or prevent further deterioration. The current method of diagnosing Alzheimer's is to monitor the mental decline of a patient, which at this time means the disease has already caused severe brain damage. Biomarkers have gained interest in detecting Alzheimer's before the onset of symptoms [7].

In the 1950s, Christian de Duve, Chairman of the Laboratory of Physiology Chemistry at the University of Louvain discovered a new cellular organelle, which de Duve named "lysosomes". This led to the term "autophagy" being defined "as a phenomenon during which cells fuse protein-containing vesicles with lysosomes, leading to the decomposition of cellular protein" [8]. Autophagy was discovered as an essential cellular and metabolic process, which involves the selective or non-selective degradation of cell to rid the cell of unwanted and dysfunctional cellular components. There is evidence that autophagy dysfunction associated with deletion or mutation of autophagy-related genes (Atg) is linked to neurodegenerative diseases and tumorigenesis [8]. Autophagy is linked to Alzheimer's through misfolded protein accumulation that are the cause of neuronal death [9]. Tumors use the autophagy pathway to survive under stressed metabolic conditions such as chemotherapy or radiotherapy [10]. Autophagy activation and inhibition are both contributors in tumor development via different pathways [8].

Autophagy has also been linked to longevity and general health. Caloric restrictions, while having maintained sufficient nutrient levels, induce autophagy, which can increase longevity of various animal species [11]. Therefore autophagy flux has the potential to be a trustworthy indicator of general health.

1.2 Research aims and objectives

The aim of this project is to develop a low cost biosensor to detect and measure autophagy flux. This will be done through the development of a prototype electrochemical DNA biosensor. The biosensor is designed to measure different concentrations of DNA that encodes LC3-II, which is a biomarker for autophagy flux. This study hopes to contribute to the ongoing research into autophagy and its relation to general health and diseases that affect millions of people daily. The aims and objectives are to:

- Identify the biosensor type and sensing method for detection of the analyte.
- Identify the immobilization technique of the recognition element and confirm binding of the recognition element to the transducer.
- Identify the mechanism of interaction between the recognition element and the analyte and confirm successful interaction.
- Design and develop a low cost measurement system for the sensing technique.
- Validate and test the measurement system.

1.3 Project scope

The scope of the project includes:

- Research on the various studies on autophagy, nucleic acids, and biosensors.
- Sourcing of all materials and reagents.
- The design of the entire biosensor including the type of detection method, recognition element, transducer, and potentiostat used.
- Implementation and testing of the immobilization and hybridization strategy.
- Design, manufacturing, and testing of a prototype potentiostat.

The scope of the project is limited to the development and testing of the sensor using only single-stranded DNA (ssDNA) probes and complementary ssDNA targets. Design and testing of the sensor using messenger-RNA (mRNA)

is excluded due to resource and time limitations. ssDNA is used as the proof-of-concept for an mRNA biosensor. Immobilization and hybridization techniques can be adapted for use on mRNA in future studies.

Excluded is the manufacturing of the transducer (electrode) that is used in the biosensor. Screen-printed electrodes (SPEs) are purchased from DropSens to reduce the time taken in the development and testing of the electrodes, as well as to eliminate manufacturing faults in the biosensor that may lead to errors in the results.

The design of DNA primers are not included in the scope of the project, as well as the synthesis and polymerase chain reaction (PCR) amplification of the DNA. The DNA primers are purchased from WhiteSci, synthesis and amplification are performed by the Physiology Department at Stellenbosch University.

The optimization of the immobilization and hybridization strategy will not be addressed in this project. This includes ensuring the optimal orientation of the immobilized DNA probes, the surface density of the DNA probes, as well as the ideal chemical conditions of the DNA samples. Determining the optimal hybridization time, temperature, and chemical conditions of the hybridization procedure are also excluded from the scope of the project.

1.4 Thesis Outline

Chapter One is the introduction to the project. This includes the background that motivated the project, aims and objectives necessary to complete the project successfully, as well as the scope and limitations of the project.

Chapter Two is the literature study of the project. The literature covered serves as important information on all topics in the design and development of the biosensor. The literature includes background on autophagy, biosensors, and immobilization techniques.

Chapter Three is dedicated to the design and development of the DNA sensor. This includes the decisions made behind the electrode chosen, the electrolyte solution, detection method and quantification of the analyte's concentration.

Chapter Four describes the development of a low cost potentiostat. The design of the potentiostat includes the software created to apply square-wave voltammetry (SWV) to the cell.

Chapter Five discusses the results of the various tests that are applied to the sensor and the potentiostat to validate the working of the biosensor.

Chapter Six critically evaluates the design choices and results. The project aims and objectives are analyzed against the final prototype to determine whether or not they were met. It discusses the applicability of the biosensor to the intended application, and makes some suggestions for future research and improvements.

Chapter 2

Literature review

An in-depth literature study is done on the topics that are necessary to complete the project. The topics discussed include the definition of autophagy, its application in biological sciences, and its molecular machinery in the autophagic process. The study also links autophagy to the development of biosensors, the history of biosensors, the different types of biosensors, and the various immobilization techniques that are used to detect biomarkers that indicate the presence of autophagy.

2.1 Autophagy

Autophagy is a powerful cellular process that involves the self-degradation of a cell to remove unwanted cellular material. The term autophagy is ancient greek for "self-eating". The term was first coined in 1963 by Belgian biochemist and cytologist Christian De Duve. The term is used to define the existence of single and or double-membraned intracellular vesicles which hold pieces of the organelles and cytoplasm throughout the different stages of disintegration of the vesicles [12]. Autophagy is a highly regulated process that involves the removal of regions of the cytosol within double-membrane-bound compartments that then mature and age into their cytoplasmic contents [13]. The most commonly studied type of autophagy is macro-autophagy. Macro-autophagy differs from other types of autophagy as the selected matter for degradation is first encapsulated within the autophagosome before being recruited to the lysosomes for digestion [11].

When autophagy was discovered, the question arose: "why would the cell digest its own components?" A simple hypothesis was formed, that autophagy plays the role of a cellular disposal-recycling system. Since the discovery, the purpose of autophagy has expanded, it is understood that autophagy not only clears the cell of intracellular aged and or misfolded proteins, unwanted micro-

organisms, and damaged organelle, but autophagy is also an adaptive response to the metabolic system for provision of energy and nutrients when different types of stresses arise [14]. Defective autophagy is linked to a range of human pathophysiologicals. These include pathogen infections, cancers, neurodegeneration, immune responses, and even development and ageing [14]. There is an hypothesis that the degradation of cytosolic structures by autophagy might play a role in removing intracellular pathogens from cells. This comes from observations of electron-microscopy (EM) studies of intracellular bacteria and viruses within multi-vesicular bodies. An unexplained phenomenon in autophagy has peaked interest among researchers, this is the hepatic purging seen in chimpanzees infected with hepatitis-B. It is shown that 75% of hepatic cells in chimpanzees have viral proteins after 10 weeks since infection. The number of viral proteins decreased to 0 (virus-free) after 20 weeks in the absence of cell death. This suggests there are antimicrobial mechanisms that get rid of viral proteins in hepatic cells that do not result in the degradation by the immune system of infected hepatic cells, therefore concluding that autophagy has also both antibacterial and antiviral functions [13].

The process of autophagy is found to have remained unchanged throughout evolution from yeast to mammals [15]. The genetic screening in yeast has led to the identification of 32 different autophagy-related genes. A number of the identified genes are found in mammals, slime mould, worms, plants, and flies [16].

2.2 Application of autophagy

The machinery of autophagy and autophagy itself are important for many parts of a cell's function and ultimately the development of organisms. Evidence indicates that there are changes that occur in autophagy in the presence of various human diseases [14]. Examples of the new-found research include the discovery that the human gene, a phylogenetic protein, named beclin 1 is important for autophagy. Beclin 1 is a homologue of the yeast gene Atg6, and is shown to be a tumor suppressing gene. The discovery was made by Levine's laboratory. Beclin 1 was at first sequestered as a B-cell lymphoma 2 (Bcl-2) interacting protein. Autophagy is inhibited due to a reduction in beclin 1 associated hVps34 PtdIns3K activity when beclin 1 binds to the anti-apoptotic protein Bcl-2. Excessive apoptosis causes cell atrophy, while insufficient amounts of apoptosis causes uncontrollable rapid cell production. Beclin1 monoallelic deletion on chromosome locus 17q21 is shown to be present in 40-75% of human breast, prostate and ovarian cancers. Mice with

heterozygous loss of beclin 1, and Atg4C show an increase in the speed of tumor development. Reasons why autophagy plays a role in tumor cell survival and suppression are illustrated in Figure 2.1. Stressed autophagy-defective tumor cells acquire an increasing number of p62/sequestosome 1, reactive oxygen species (ROS), damaged mitochondria, and protein masses. The accumulation can be the cause of tumorigenesis, DNA harm and oncogene. In apoptosis-defective cells, autophagy prevents the death of the cells from necrosis, which is a process that promotes the growth of tumors and exacerbates local inflammation. Autophagy has also been linked to an increase in tumor cells, by promoting tumor cell survival under certain conditions (hypoxia and low nutrients) during metabolic stresses in the tumor environment. Pharmacological slowing down of autophagy is shown to promote tumor regression by increasing the cytotoxicity of cancer chemotherapy agents [14].

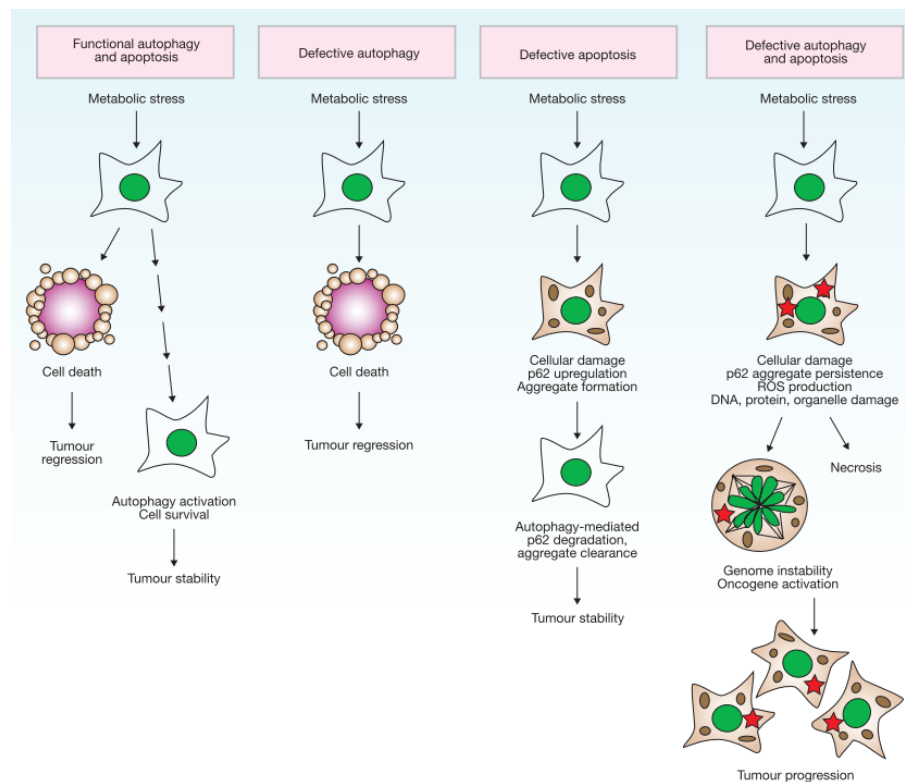


Figure 2.1: Roles of apoptosis and autophagy in tumor formation. Reprinted from "Eaten alive: A history of macro-autophagy" [14]

Other studies have shown that there is a close relationship between neurodegenerative diseases and autophagy. A study performed with mice using neuronal-specific knockouts of Atg7 or Atg5 showed that constant yield of soluble, cytosolic proteins is controlled by basal autophagy for the prevention of abnormal neuropro-

tein growth that may be the cause of neurodegeneration symptoms. Autophagy receptors, p62 and NBR1, are shown through autophagy to be content receptors which deliver misfolded protein masses, as well as possibly detrimental organelles for clearing in *Drosophila*, as well as mammals [14]. Rubinsztein's laboratory showed that specific aggregate-prone proteins undergoing degradation are affected by autophagy. These proteins are involved in Huntington's disease, a genetic disease that is the cause of nerve cells to undergo degeneration in the brain. In fly and mice models it is shown that activation of autophagy by the constraint of target of rapamycin (TOR) reduces the growth of mutant Huntington aggregates, therefore protecting against neurodegeneration.

In 2004 two separate groups, the laboratories of Deretic and Colombo, and Yoshimori's group, released studies indicating that autophagy is an essential defence mechanism against specific bacterial pathogens, including *Streptococcus pyogenes*, which results in diseases such as tonsillitis and pharyngitis, and *Mycobacterium tuberculosis*, which 1.5 million people died from in 2020. Other studies later showed that autophagy does indeed interact with invading microorganisms. Randow's laboratory showed that another human autophagy receptor, NDP52, is able to detect ubiquitin-coated *Salmonella enterica* and redirects the bacteria through binding to microtubule-associated protein (LC3) into autophagosomes. Kurata's group, in collaboration with Yoshimori's laboratory, proved that intracellular pattern-recognition receptor (PRGR-LE) delivers unwanted *Listeria monocytogenes* to the autophagy-mediated defence system in *Drosophila*. Autophagy is not only linked to bacteria, but also to viruses. Studies in mice show that beclin1 protects mice against alphavirus replication and encephalitis. The reduction in autophagy is shown to be important for viruses to evade the immune system and cause disease [14].

Autophagy is also linked to ageing and longevity. Studies from Bergamini's laboratory show that autophagy functionality diminishes with ageing in rodents, as well as the chief functional cells of the liver. Ageing cells are different to normal cells as they progressively accumulate damaged organelles and proteins. Further studies confirm that autophagy plays a role in increasing longevity. One study observed that an increased basal level of autophagy and autophagy activity during cellular growth, increases the lifespan of flies, while flies with *Atg7* deficiency have short lifespans [14]. A phylogenetically maintained NAD-dependent histone deacetylase, named sirtuin 1, was found and identified in a screening for genes that specifically lengthen the replicative lifecycle in yeast. Transgenic expression of sirtuin 1 induces autophagy in mammalian cells and *Caenorhabditis elegans*

(*C. elegans*). The pharmacological restriction of sirtuin 1 prevents activation of autophagy [11]. Attempts to increase longevity and to decrease autophagy function with maturing cells include the use of an anti-lipolytic drug that imitates the positive response of caloric restriction [14]. Rapamycin is one of the best characterized pharmacological autophagy inducers, it restricts target of rapamycin complex 1 (TORC1) and therefore is shown to extend life in all studied organisms. A polyphenol that is found in red wine named resveratrol is shown to extend the lifespan of flies, worms and yeast. Studies on mice have shown that resveratrol also prolongs their life if they are held on a high calorie diet. A polyamine spermidine is shown to also extend life of flies, worms, and yeast in an autophagy manner. A diet rich in physiologically relevant polyamines also prolongs the life of mice [11].

Autophagy has also been found in a response to starvation. Caloric restriction is currently the only treatment known to inhibit ageing by preventing the decline of autophagy related activities, which is beneficial to ageing cells. Dauer formation in *C. elegans*, a non-pathogenic, non-infectious, non-hazardous, and non-parasitic organism, requires functional beclin 1 genes. In order for *Dictyostelium discoideum*, commonly referred to as slime mould, to survive during the starvation of nitrogen, it requires functional homologues of yeast ATG5 and ATG7. It is also found that prevention of organisms, such as *Arabidopsis* (small flowering plants) and *C. elegans*, from premature senescence, wild-type autophagy genes are required [13].

2.3 Basic autophagy machinery

There are different kinds of autophagy: micro-autophagy, macro-autophagy, and chaperone-mediated autophagy. They all allow the increase in proteolytic break down of cytosolic parts at the lysosome. In macro-autophagy the cytoplasmic contents is delivered through the autophagosome, a double membrane-bound vesicle to the lysosome, the vesicle binds with the lysosome to form an autolysosome. In micro-autophagy, the cytosolic parts are delivered directly by the lysosome through the invagination of the lysosomal membrane. Micro- and macro-autophagy are processes that are able to envelop large molecular and cellular material through selective and non-selective mechanisms. In chaperone-mediated autophagy, the targeted proteins are delivered with chaperone proteins across the lysosomal membrane. These complex protein pairs are identified by the lysosomal membrane receptor, which results in the unfolding and degradation of the protein [16].

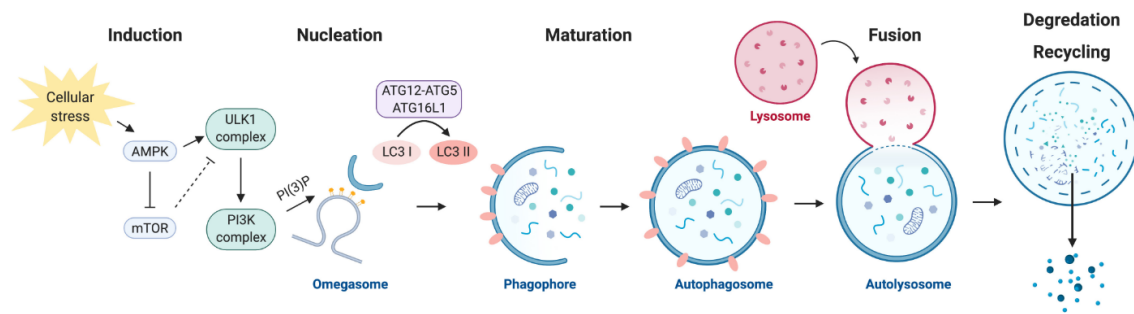


Figure 2.2: The autophagic process. Reprinted from "Frontiers in Cell and Developmental Biology" [17]

The autophagic process, seen in Figure 2.2, can be seen as recycling of damaged and unwanted organelles to create usable by-products that can be re-used for building macro-molecules. In summary, the autophagic process starts with an isolation membrane, the phagophore. The phagophore increases in size to envelop intracellular contents of organelles, ribosomes, and protein masses. The phagophore with all its contents then matures through merging with the lysosome, which allows for the breakdown of the phagophore matter by lysosomal acid proteases. Then lysosomal permeases and delivers by-products and amino acids from the process out of the cytoplasm for recycling [16]. There are five key stages to autophagy [16]:

1. Phagophore nucleation or formation.
2. Atg5-12 conjugation and interaction with Atg16L, and the multimerization at the phagophore.
3. LC3 processing and entering into the expanding membrane of the phagophore.
4. The engulfing of targets for degradation.
5. Merging of the lysosome with the autophagosome for breakdown by lysosomal proteases.

2.3.1 Phagophore formation

The formation of a phagophore is generally found in mammals near the ER-mitochondria contact sites in the presence of specific cytosolic membrane structures [12]. Phagophore possibly even forms from the nuclear envelope under controlled conditions. In yeast, phagophore is formed by the regulating acquirement of transmembrane protein Atg9. The protein may increase lipid accumulation to expand the phagophore. Energy sensing TOR kinase that phosphorylates Atg13 is

used to regulate the step. The regulation prevents the phagophore from interacting with Atg1 and preventing the initial step in autophagy that is sensitive to nutrient availability and the growth factor. Vesicular protein sorting 34 (Vps34), is involved discriminatorily in autophagy when grouped with regulatory proteins and beclin 1. It generates phosphatidyl inositol trisphosphate (PI3P), which is important in the elongation of the phagophore and the acquisition of other Atg proteins for the phagophore [16].

2.3.2 Atg5-12 conjugation

Atg7 performs similar to an E1 ubiquitin activating enzyme. The protein activates Atg12 in an ATP-dependent method through the attachment to its carboxyterminal glycine residue. The activated protein Atg12 is then transferred to Atg10, which increases the covalent strength of the covalent bond of Atg12 to lysine 130 of Atg5. The conjugation of Atg5-12 in pairs with Atg16L dimers to form a multi-metric Atg5-Atg12-Atg16L complex. The complex is associated with the expansion of the phagophore. The complexes are believed to introduce a curvature into the expanding phagophore by acquiring the processed LC3B-II. When the autophagosomes are formed, the complex dissociates from the membrane, therefore the Atg5-Atg12-Atg16L complex is an insignificant biomarker for autophagy [16].

2.3.3 LC3 processing

The protein LC3 is an important marker in the measurement of autophagy. The processing and synthesis of LC3 increases during the autophagic process. A protein that is encoded by the mammalian homologue of Atg8, LC3, is conveyed in most cells as a cytosolic protein. Upon the gene activation of autophagy, the protein is proteolytically cleaved by Atg4. Atg4 is a cysteine protease that generates LC3B-I. Atg4-dependent cleavage exposes carboxyterminal glycine. The exposed glycine is activated by the E1-like Atg7 in a related processes by Atg7 on Atg12. Once the LC3B-I is activated, it is then transferred to Atg3 before phosphatidylethanolamine (PE) is conjugated to the exposed glycine in order to generate LC3B-II. Atg5-12 is essential for the acquirement and integration of LC3B-II into the expanding phagophore. LC3B-II can be found on the external and internal surfaces of the autophagosome. LC3B-II plays its part in the hemifusion of membranes and in the selection of the content for degradation [16].

2.3.4 Target selection for degradation

Throughout the study of autophagy it is understood that during the autophagy process, the autophagosome engulfs matter randomly. Electron micrographs have shown on numerous accounts that the contents of autophagosomes varies. There are studies emerging that indicate that the phagophore membrane has the potential to selectively interact with different matter, such as organelles and protein masses. There are proposals that LC3B-II acts at the phagophore as a receptor. LC3B-II interacts with specific molecules on the target matter before engulfing the target to selectively choose which targets are to be degraded [16].

2.3.5 Merging of the autophagosome and the lysosome

After the targets are engulfed in the autophagosome, the autophagosome is then fused with the dedicated endosomal compartment (lysosome) to form autolysosome. Studies suggest that before autolysosome formation, the autophagosome fuses with early and late endosomes, which delivers parts of the membrane-merging machinery and lowers the autophagosome pH. Lysosomal acid proteases occurs to break down the engulfed material once the autolysosome is formed. The fusion of the lysosome with the autophagosome is sometimes blocked by microtubule poisons such as nocadazole, therefore the cytoskeleton plays an essential role in the formation of autolysosome. Proteases B and D found within the lysosome are required for the turnover of autophagosomes for the maturation of the autolysosome [16].

2.4 Autophagy flux

Macro- and micro-autophagy as well as CMA take place at baseline levels. Therefore they contribute to preserving homeostasis of cells by avoiding the accumulation of cytotoxic elements from normal cellular functionality. The different types of autophagy all follow similar processes, during which autophagy elements are detected and isolated from the cytoplasmic milieu, and then delivered to lysosomes for degradation. The rate at which autophagy elements are degraded by the lysosomes is known as "autophagy flux". The increase or decrease in the degradation activity is proportional to the increase or decrease in the rate of degradation [18]. Autophagy flux is a good indicator of the efficiency of autophagy responses. To summarize, "autophagy flux is the rate at which the molecular machinery for autophagy identifies, segregates, and disposes of its substrates (through lysosomal

degradation)"[12].

Cytosolic is the proteolytically processed form of LC3-I. Upon the formation of the phagophore, the cytosolic is lipidated to form LC3-phosphatidylethanolamine (LC3-II). LC3-II is specifically taken up to the phagophore membrane. Throughout the growth process of the autophagosome, LC3-II situated within the autophagosome remains present until the completion of the autophagosome, while LC3-II situated on the outer surface of the autophagosome is removed through de-conjugation. The level of LC3-II is directly related to the autophagosome number. LC3-II is used to detect autophagy flux. However, it only reveals whether autophagy flux is taking place or not, it does not quantify autophagy flux as a rate. A theoretical approach to define autophagy flux is suggested [18].

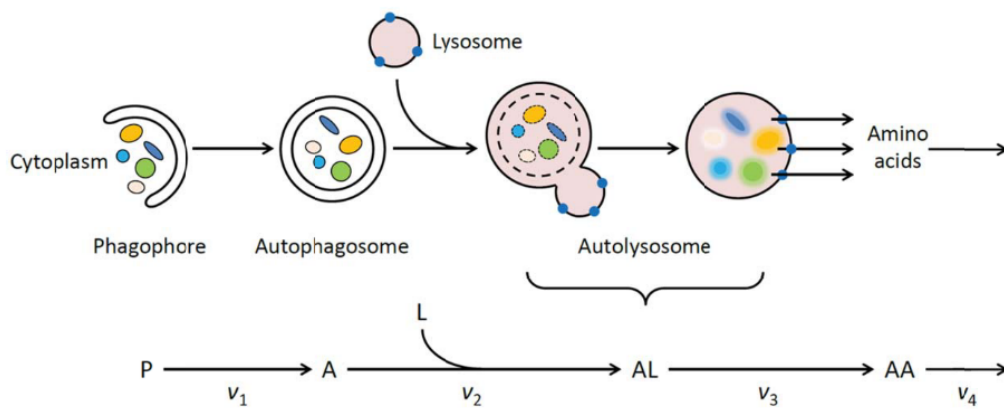


Figure 2.3: Defining autophagy flux through the autophagic pathway. Reprinted from "Defining and measuring autophagosome flux - concept and reality" [18]

The pathway through the autophagic process is distinguished between the flow of material and the flux, which is the rate of flow at steady state as shown in Figure 2.3. Along the pathway, various entities enter and exit the pathway; these entities are the phagophore (P), autophagosome (A), lysosome (L), autolysosome (AL), and Amino Acids (AA). Each process along the pathway has a particular rate, v , which is quantified as the number of entities processed per cell per unit time. The number of entities processed per unit time is defined as n . The rate of change of the different entities is defined by a set of differential equations:

$$\frac{dn_P}{dt} = -v_1, \frac{dn_A}{dt} = -v_1 - v_2, \frac{dn_L}{dt} = -v_2, \frac{dn_{AL}}{dt} = -v_2 - v_3, \frac{dn_{AA}}{dt} = -v_3 - v_4 \quad (2.1)$$

At steady state the rate of change of the entities A, AL, and AA are zero:

$$\frac{dn_A}{dt} = \frac{dn_{AL}}{dt} = \frac{dn_{AA}}{dt} = 0 \quad (2.2)$$

Therefore the rate of change of each process in the pathway is equal to a steady-state flux, J :

$$v_1 = v_2 = v_3 = v_4 = J \quad (2.3)$$

2.5 Biosensors

Quantification of biological elements and processes are essential in the medical and biotechnology fields. Transferring the information provided from these elements and processes into a readable signal to be processed requires the use of biosensors [19]. Biosensors detect and quantify the presence and concentration of a biological analyte [20]. Biosensors are used in the monitoring of diseases, the discovery of drug substances, the detection of pollutants, dangerous micro-organisms that are the cause of various diseases, as well as biomarkers that are indicators of disease in a body [21].

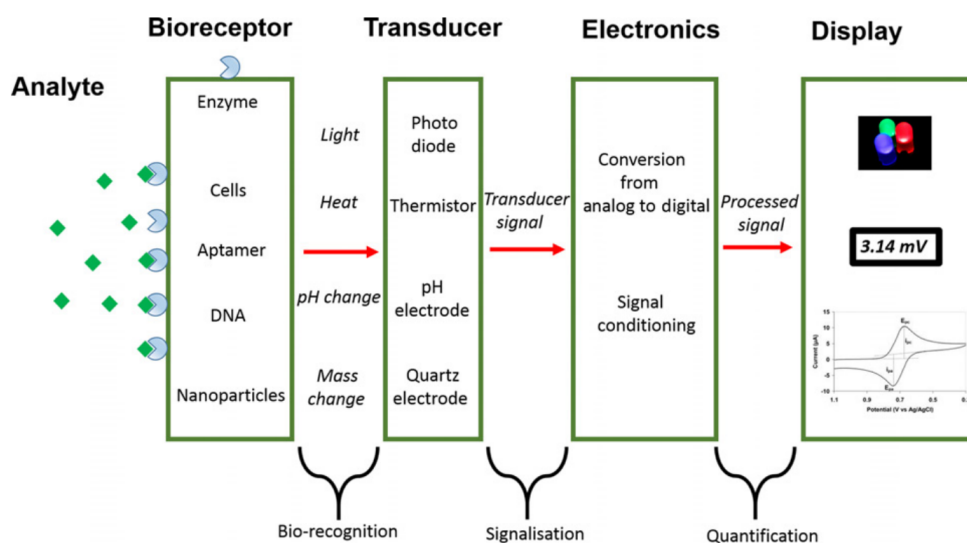


Figure 2.4: Schematic of a biosensor. Reprinted from "Essays in Biochemistry" [21]

Biosensors are constituted of a biological receptor that functions as a recognition layer/entity for the analyte, in conjunction with a transducer, which converts the signal generated from the interaction of the recognition entity and analyte into a signal that is easily detected and measured as shown in Figure 2.4. Typical biological receptors are tissue, living cells, enzymes, antibodies or antigens [20]. The recognition entity detects chemical compounds through several different detection methods that employ thermal, optical or electrical signals [22]. The International Union of Pure and Applied Chemistry (IUPAC) defines a biosensor as "a device

that uses specific biochemical reactions mediated by isolated enzymes, immuno-systems, tissues, organelles or whole cells to detect chemical compounds usually by electrical, thermal or optical signals" [22]. Biosensors are usually sorted based on either their biological receptors to detect the analyte of interest (e.g enzyme sensors or aptamer-based sensors), their transducer type to convert the signal of interest (e.g electrochemical sensors or optical sensors) or according to their final applications (e.g clinical sensors) [20].

2.6 Historical background of biosensors

The first documented concept of a biosensor is in 1906 when M. Cremer showed that the concentration of an acid in a liquid corresponds to a proportional electric voltage within the fluid that is separated by a glass membrane. The first electrode developed for pH measurements was introduced in 1922 by W. S. Hughes, only a few years after Søren Sørensen developed the concept of pH for expressing hydrogen ion concentrations in the year 1909. Between the years of 1909 and 1922, more developments on biosensors were taking place, for example, Griffon and Nelson demonstrated the process of immobilizing the enzyme, invertase, on charcoal and aluminium hydroxide substrates [21]. Otto Warburg is thought as "the father of enzymatic analysis". In the 1930s he developed an optical test to detect Nicotinamide adenine dinucleotide (NADH) at 340 nm. The development of this test facilitated the method to detect dehydrogenases and their substrates [23]. The earliest known application of a biosensor was when Dr. C. Clark designed an "enzyme electrode" for the measurement of the concentration of glucose. The enzyme glucose oxidase (GOD) was used in the measurement [22]. Enzyme biosensors use the method of immobilization through adsorption of enzymes through the strong binding of covalent and ionic bonding, as well as van der Waals forces [24]. In 1974, Bengt Daniellson and Klaus Mosbach introduced the idea of thermal transducers, and coined the term "enzyme thermistors" or "enzyme probes". The technology evolved in 1975 when C. Divies proposed that bacteria can be used as a biological element to form microbial sensors to measure alcohol [23]. In 1975, Yellow Spring Instruments developed the first commercial biosensor, a blood glucose analyzer named YSI 23006 by employing Dr. C. Clark's invention [21]. In 1977, the term "biosensor" was coined by Karl Camman [23].

Research groups and laboratories around the globe entered the biosensor research field. In 1975 in the German Democratic Republic (GDR), otherwise known as East Germany, Frieder Scheller developed an amperometric glucose sensor and

other biosensors that relied on the reactions between sensors and enzymes. In Lithuania, Juozas Kulys conducted research on mediated enzyme sensors engaging organic metals and dehydrogenases almost simultaneously. Studies showing that enzymes are able to communicate directly with electrodes were introduced by Scheller's group in Berlin and Ilya Berezin's group at Moscow State University. The studies showed that the current generated by the electrochemical change of the active site can be increased by the regeneration of the enzyme, while it is in conjunction with the substrate target. In 1983, Masuo Aizawa and Isao Karube in Japan began integrating different transducers with various recognition elements [23].

The historical development of biosensors in different timelines between 1906 and 1999 is summarized in Table 2.1.

Table 2.1: Summary of biosensor development between 1906 and 1999

Year	Biosensor development
1906	Observation of electric voltage between fluid separation by glass [21]
1909	Søren Sørensen developed the concept of pH [21]
1956	Dr. C. Clark designed an "enzyme electrode" [21]
1970	Ion-sensitive field-effect transistor (ISFET) by Bergveld [25]
1975	Fibre-optic biosensor for carbon dioxide and oxygen detection by Lubbers and Opitz [26]
1975	Commercial glucose detection biosensor by Yellow Spring Instruments [21]
1975	Microbe-based immunosensor by Suzuki et al. [27]
1982	Glucose detection by Fibre-optic biosensor by Schultz [28]
1983	Surface plasmon resonance (SPR) immunosensor by Liedberg et al. [29]
1984	Mediated amperometric biosensor: ferrocene used with glucose oxidase for glucose detection [30]
1999	Development of first nano-biosensor by Poncharal et al. [31]

Advancements in the field of optics and communications were due to the first optical biosensor. Previous fiber optic sensors were chemical sensors. Introduction of biological recognition molecules increased sensitivity and specificity of biosensors [23]. The advancement of electronic technology enabled the miniaturization of sensors, therefore introducing point of care (POC) biosensors for glucose monitoring. POC biosensors have been a fundamental element in early recognition of potential life-threatening diseases [22]. The field of biosensors have since evolved to include new technologies such as nano-materials as transducers and bio-recognition elements for biosensing, field-effect transistors (FET), genetic code based sensors, fiber-optic based biosensors, and phone-based optical detectors

with increased efficiency and scalability [22].

2.7 Biosensor characteristics

Every biosensor has certain dynamic and static characteristics. The performance of a biosensor is dependent on the optimization of these characteristics. Some of these are selectivity, reproducibility, stability, sensitivity, and resolution [21].

Selectivity is the ability of the biological receptor/recognition element to only detect the analyte in the presence of other biological elements and contaminants within the sample. To increase the selectivity of a biosensor, it is important to consider the type of biological receptor used. Reproducibility is the ability to produce the same results for duplicated sets of experiments, and is dependent on the accuracy as well as the precision of the electronics and transducer in the biosensor. Accuracy reflects how close the mean value of the results, from duplicated experiments, is to a known value, while precision reflects the ability to provide similar results from duplicated experiments.

In biosensors that require an extended period of incubation steps, the role of stability is essential. Stability relates to the "degree of susceptibility to ambient disturbances in the biosensor's system". Biosensors with a low stability are at risk of drifts in the output signal, which cause errors in the concentration of the analyte measured, which affects the accuracy and precision. Other factors that influence the stability of a biosensor is the temperature sensitivity of electronics, the response from the transducers, the affinity of a the biological receptor to interact with the analyte of interest, and the ability of the biological receptor to degrade over time. Sensitivity, also referred to as the limit of detection (LOD), is the minimum concentration of the analyte that the biosensor can measure. Biosensors require good resolution. Resolution of a biosensor is defined as the smallest change in the analyte's concentration that can induce a change in the output signal measured [21].

2.8 Types of biosensors

Biosensors are generally classified into two main groups: direct label-free detection biosensors, and indirect label-based/labelled detection biosensors. Direct label-free detection biosensors depend on a biological receptor that allows for a biological interaction to be directly measured. Indirect label-based biosensors depend on secondary elements as a catalyst for measurements. The secondary

element can be enzymes, fluorescent tags, etc. Each of the two groups have several detection methods for the biological interactions taking place such as optical, electrochemical or mechanical transducers [22].

2.8.1 Direct label-free detection biosensors

Since direct label-free detection biosensors rely on the specific interaction of the biological interaction, no catalytic label is required. Recognition elements such as enzymes, DNA probes or antibodies are usually used in these biosensors. The detection of the signal induced by the biological interaction typically relies on physical changes that occur. These include changes in the properties of either its electrical, mechanical or optical state. The most common types of detection method for direct label-free biosensors are optical biosensors [22].

2.8.2 Indirect labeled/label-based detection biosensors

Indirect label-based detection biosensors utilize a second recognition element bound to the analyte to generate signals for detection. Labeling or catalytic elements like enzymes are used. Fluorescently tagged DNA, RNA, antibodies, and enzyme alkaline phosphatase are commonly used to enhance the detection of a sandwich complex. Electrochemical transducers translate the detected chemical signal into a readable electrical signal. One kind of indirect label-based detection biosensor uses electrochemical transducers (electrochemical biosensors) to measure the reduction or oxidation of an electro-active chemical compound on the secondary recognition element. Other types of indirect label-based detection biosensors include amperometric devices (detection of ions in a solution, based on the changes in electric current generated, when the analyte goes through a redox reaction by either reduction or oxidation). Optical fluorescence is also commonly used as indirect biosensors. The detection of the fluorescence of the secondary recognition element happens via charged-coupled devices, photomultiplier tubes, photodiodes, fluorescent microscopy, and spectrofluometric analysis [22].

2.8.3 Enzyme biosensor

Enzyme biosensors are devised on biological recognition. The operation of enzyme biosensors are through the ability of enzymes to mobilize a biochemical reaction, whilst remaining stable under the biosensor's operating conditions [32]. They are built on immobilization methods. Immobilization is defined as the technique of fixing cells, organelles, DNA or other enzymes and proteins onto a solid support

system in order to maintain stability [33]. Enzymes are immobilized through adsorption by strong binding forces of covalent and ionic bonding, and van der Waals forces. Minoxidases, oxidoreductases, peroxidases, and polyphenol oxidases are the commonly utilized enzymes [24].

Amperometric enzyme biosensors, based on the production of current from an applied potential to a two-electrode system, are robust, and easy to miniaturize for POC devices. However, amperometric biosensors are vulnerable to the interference of chemicals in the analyte sample. These interferences are due to electrochemical interactions as well as the presence of cells, macromolecules, and proteins. The performance of the biosensor is subject to the influence of pathological conditions on the enzyme activity. The interference can be avoided by pre-treatment. The repeated use of amperometric biosensors results in fouling of the transducers [32].

Amperometric biosensors are commonly classified into three groups according to the generation of the biosensor. These are first, second, and third generation biosensors. They are divided according to the type of electron transfer method used for measuring the biochemical reaction [32].

First generation biosensors, also named mediator-less amperometric biosensors, rely on the electrical current response when analytes or products from the reaction of enzymes diffuse onto the transducer surface through an immobilization process. Enzymes typically used in first generation biosensors belong to two classes, oxidases and dehydrogenases enzymes. These enzymes require co-enzymes during the catalyst reaction. The enzymes need to be able to be regenerated for further catalytic reactions. First generation biosensors are known to be highly sensitive with low response times of usually 1 s. However, they often require pre-treatment of electrodes to produce a reproducible sensor surface [32].

Second generation biosensors, also named mediator amperometric biosensors, use mediators, which act as oxidizing agents for electron carriers. The use of mediators allow the biosensors to operate at low potentials, while avoiding the interference of molecules. Commonly used mediators are ferrocene and ferricyanide. Other mediators also used are inorganic redox ions, methylene blue, and phenazines. Mediators have to remain stable during the reaction, while not taking part in the electron transfer themselves. The mediators used must have a redox potential that is lower than the other electroactive substances in the sample. Improvements on second generation biosensors are through the replacement of oxygen with an electron receptor which can carry electrons to the transducer from the center of the redox enzyme. An advantage of second generation biosensors is the additional option of adding the mediators either to the sample or through

immobilization on the electrode. It is essential that the mediator is entrapped close to the enzyme when immobilized. If the mediator is lost, the exact time during the reaction should be recorded in order to characterize the biosensor's performance through the course of the reaction. Second generation biosensors using immobilized mediators are not used as often due to low stability [32].

Third generation biosensors work on bio-electrocatalysis, which employs a electron transfer between a transducer and the enzyme. There are three parts in a third generation biosensor. These are the enzyme, which acts as the recognition element. The second element is a nano-scale wiring element or a redox polymer to ensure signal generation. The third element is the transducer/electrode. Using a redox polymer as a means to bind the electrode to the center of the sensing enzyme increases the performance of the biosensor. Third generation biosensors are the least used of the three types of enzyme biosensors. However, third generation biosensors are more likely to have short response times, and they are less likely to be dependent on the concentration of oxygen [32].

2.8.4 Electrochemical biosensors

Electrochemical biosensors are capable of providing semi-quantitative and quantitative results by measuring the electrical properties of the interaction of the biological recognition element and the analyte. The biosensor is classified according to the electrochemical transduction method. The transducer is usually a chemically modified electrode [34]. The biological recognition elements in electrochemical biosensors are typically enzymes, nucleic acids, antibodies, cells, and micro-organisms. The bioelectrochemistry and electrophysiological reactions at the electrode are typically amperometric, potentiometric, impedimetric or voltammetric [19]. Electrochemical biosensors are advantageous over other biosensor types due to the the low cost, construction ease, ability for miniaturization, and portability. It can also be interfaced with other types of detection methods to increase performance [20].

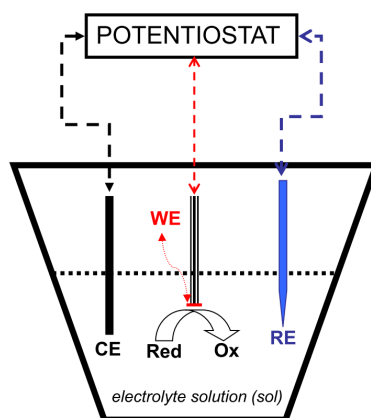


Figure 2.5: Schematic of a three-electrode electrochemical system. Reprinted from "ChemTexts" [35]

In electrochemical biosensors, the reactions take place at the electrode's surface, therefore the role of the electrodes are important in the biosensor's performance. The material of the chosen electrode, the modification of its surface, and the dimensions of the electrode influence the sensitivity of the biosensor. Typically a three-electrode system is used in electrochemical biosensors, namely a reference (RE), counter/auxiliary (CE), and working electrode (WE) as shown in Figure 2.5. The RE is kept as far as possible away from the reaction site to maintain a stable, low potential. It is typically made from silver/silver-chloride (Ag/AgCl). The WE is where the electrochemical reaction takes place, therefore it is also known as the redox or sensing electrode. The CE creates a connection the electrolyte solution in order to apply a current to the WE. The electrodes in the three-electrode system should be chemically stable, while also being conductive, therefore gold, carbon, or platinum are typically used [19].

2.8.4.1 Amperometric

In amperometric biosensors a constant potential is applied between the CE and WE, and the generated current is measured. The current is produced from the reduction and oxidation of the electroactive components (recognition element, analyte, or electrolyte) at the WE [20]. The peak current measured in amperometry is directly proportional to the analyte's concentration. In amperometry, mediated electrochemistry is typically used for electrochemical reactions at the working electrode [19].

2.8.4.2 Potentiometric

In potentiometry the ion activity in the electrochemical reaction is measured. The resulted measurement is used to determine the accumulated charge potential at the WE with respect to the potential of the RE in an electrochemical cell with no current. In potentiometry, the concentration isn't measured by its proportionality to the current. The concentration is determined by its relation to the potential dictated by the Nernst equation,

$$E_{cell} = E^0 - \left(\frac{RT}{nF}\right)\ln Q \quad (2.4)$$

where E_{cell} represents the zero current cell potential, E^0 represents the cell potential under standard conditions, R represents the universal gas constant, T represents the temperature, n being the number of electrons transferred in a single reaction, F represents the Faraday constant, and Q is the reaction quotient. Typically used electrodes are pH, ion, or gas selective electrodes [20].

2.8.4.3 Impedimetric

Impedimetric biosensors use electrochemical impedance spectroscopy (EIS). In EIS, a sinusoidal wave, with a small amplitude, as a function of frequency is applied to the system. The electrochemical capacitance and resistance of materials in response to changes to the surface properties are measured. There are two types of EIS techniques. The first is the measurement of the change in impedance due to the binding of the analyte to the recognition element, which is attached to the surface of the electrode. The second is the measurement of the change in impedance due to the detection of metabolites produced by the growth of bacterial cells. EIS is mostly used in applications where the interaction of the recognition element with the analyte plays a vital role. After the recognition element is immobilized onto the transducer the surface layer is then characterized by using an equivalent circuit that is used to curve-fit experimental data. The characterization of the surface layer is used to determine the electrical parameters that induce the impedance change [20].

2.8.4.4 Voltammetric

In voltammetric biosensors the potential is scanned over a set potential range, and the generated current and potential are then measured. The resulted current can be plotted against the potential, where the position of the peak current against the potential corresponds to a specific measured analyte, while the peak height

of the current is proportional to the measured analyte's concentration. Voltammetry is advantageous as it is able to detect the presence of multiple analytes, which have different characteristics that result in different peak current positions. Voltammetry is a sensitive technique due to the low background signal presence [20]. Voltammetric techniques include cyclic, fast cyclic, AC, normal pulse, linear sweep, square wave, and differential pulse voltammetry. The excitation signals for a few of the voltammetric techniques are shown in Figure 2.6.

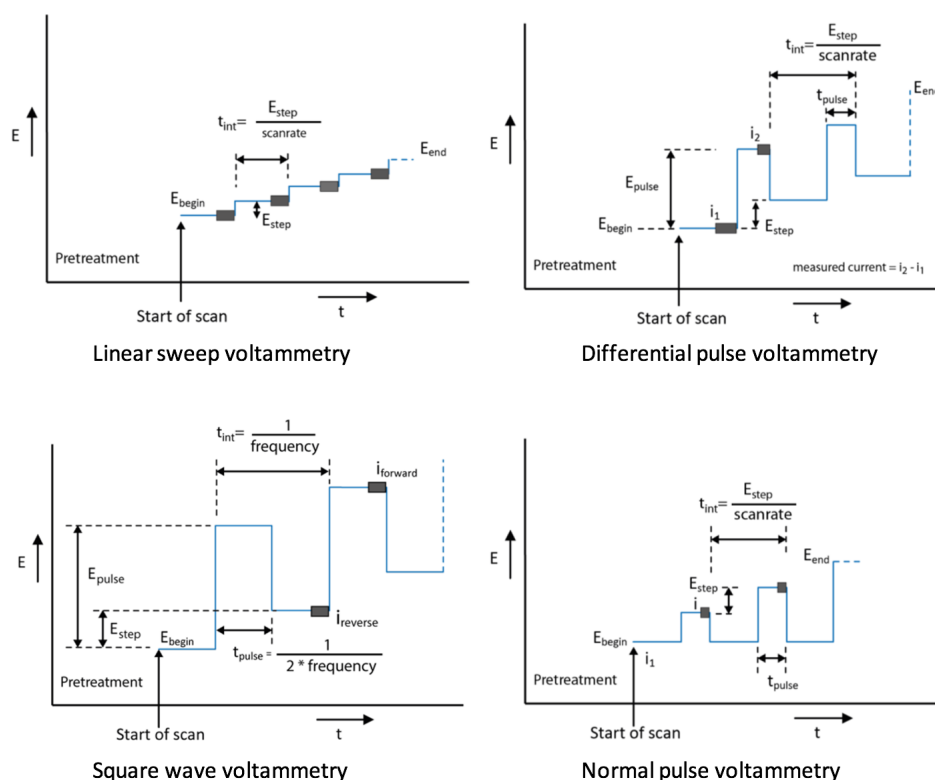


Figure 2.6: Voltammetric excitation signals

2.8.5 DNA biosensor

Nucleic acids have an extensive range of biological, chemical, and physical properties that are highly advantageous in biosensors [36]. DNA biosensors are essential in forensics, biomedical research, food control, and environmental monitoring [37]. In DNA biosensors, oligonucleotides are used as the sensing elements. The oligonucleotides have a fragment or known base sequence of DNA or RNA. They are based on the highly specific binding between the biological elements and its complementary strands of RNA or DNA, known as hybridization. DNA biosensors are of interest due to its capability to gather sequence-specific information in a more simple, cost-effective and quicker way than other biosensing techniques. DNA is advantageous over antibodies and enzymes, because nucleic acid recogni-

tion layers are able to be synthesized and regenerated for repeated use. To increase the specificity and sensitivity of DNA biosensors it can be combined with PCR methods [36].

2.8.5.1 DNA hybridization biosensors

DNA hybridization biosensors are based on the complementary pairing of ssDNA and RNA. The recognition layer is made up of short ssDNA that are able to form double-stranded DNA (dsDNA) through duplex formation with its complementary target ssDNA. The recognition layer is associated with the transducer to translate the hybridization activity into a physical and measurable signal. Short ssDNA, typically between 20 - 40 base pairs, are immobilized onto an electrode. The immobilization step has to be done in such a way that the ssDNA probes are able to retain their properties, being stable, reactive, and accessible to the analyte, while being orientated in an optimal position [37].

When the ssDNA probes are immobilized onto the electrode an electrical signal is produced. This signal changes when the analyte binds to the probe to form dsDNA. When designing the ssDNA probes used in DNA hybridization biosensors there are multiple points to consider. The probe has to hybridize selectively and specifically with the target sequence, the probe should not be self-complementary, and should not hybridize with non-target nucleic acid sequences. Experimental conditions such as the hybridization incubation time, ionic strength, and temperature have to be controlled. Hybridization-based biosensors are highly selective, sensitive, and low cost [37] [36].

2.8.5.2 Aptamer-DNA biosensors

Aptamers are a type of nucleic acid molecule. Aptamers are short synthetic single stranded oligonucleotides that are designed to bind specifically to various types of targets like cells, tissues, nucleic acids and proteins [38]. They are cost-effective and small, which offer convenience and flexibility in their structural design. This has led aptamer-DNA biosensors to be highly sensitive and selective, which can be further improved by combining aptamers with nanomaterials [37]. Aptamers used in aptamer-DNA biosensors are screened through Systematic Evolution of Ligands by Exponential Enrichment (SELEX) [36]. It is the most popular aptamer biosensor system. First introduced in 1990, SELEX was used as an in-vitro selection tool to find new types of aptamers/nucleic acid ligands. There are multiple steps in SELEX: target molecules are incubated with random

sequence pools, the oligonucleotides are separated and bound oligonucleotides are eluted, then the amplification of bound aptamers through PCR [37].

2.8.5.3 Electrochemical DNA biosensors

The detection method plays an important role in the design of DNA biosensors, and electrochemical DNA biosensors are the most commonly used detection method due to their high sensitivity and quick response times [36]. Electrochemical DNA biosensors work on the principle that the biological reaction between the DNA recognition element and the analyte consumes or produces electrons and ions. The movement of these electrons and ions results in a current or potential that can be measured. The signal generated between the transducer, recognition element, and analyte can be converted into a measurable electric signal that is indicative to the analyte's concentration [37].

2.9 DNA immobilization

Immobilization is a technique used in biosensors to bind enzymes, antibodies, and nucleic acids to the surface of the transducer to form an integrated recognition layer. Immobilization of these elements results in the reduction of mobility and loss of these elements. The manner in which DNAs are immobilized determines the property of a microarray. The type of immobilization strategy used is based on the physiochemical properties of the DNA, as well as the surface to which the DNA will be immobilized on. DNA for immobilization can be made base by base on the support or they can be pre-synthesized and then bounded to the surface. In immobilization it is important to minimize non-specific binding of the DNA and to maintain its stability in order to ensure high sensitivity and reactivity [39]. The most commonly used immobilization strategies are covalent bonding, physical adsorption, and avidin/streptavidin-biotin interaction as shown in Figure 2.7.

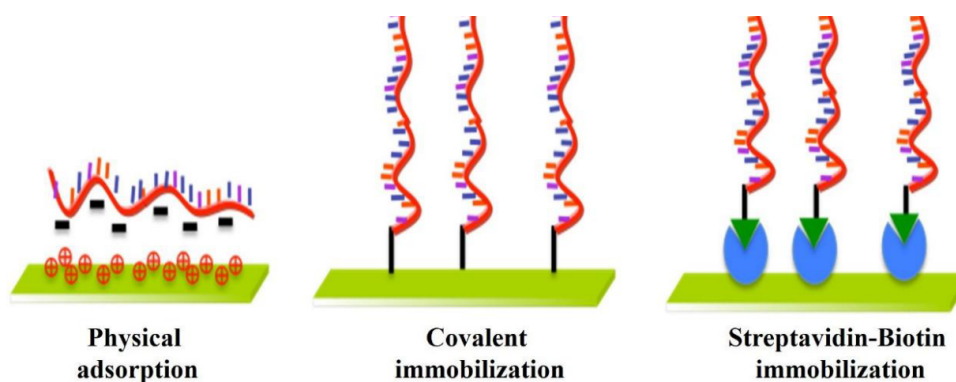


Figure 2.7: DNA immobilization strategies. Reprinted from "Sensors (Switzerland)" [39]

2.9.1 Adsorption

Adsorption is considered to be the simplest immobilization technique. In adsorption, enzymes are physically attached to the support material. Adsorption occurs through the non-specific binding of van der Waals forces, hydrophobic interactions, and hydrogen bonding. These forces are weak and therefore do not change the native structure of DNA or enzymes. Adsorption also occurs through ionic bonding through salt-linkages [40]. Sulfides (R-S-R), disulfides (R-S-S-R), and thiols (R-SH) have a strong affinity to adsorb onto noble metal surfaces like copper, platinum, silver, and gold. These sulfur groups form a well orientated and ordered molecular layer, which is called a self-assembled monolayer (SAM) [41]. Physical adsorption is done by soaking the support, which is commonly an electrode, in a solution containing the enzymes or DNA, and allowing the adsorption during the incubation time. Another method to adsorb a recognition element to a transducer is to allow the solution containing the recognition element to dry on the transducer surface, then rinsing the transducer to remove unbound elements [40].

In the physical adsorption of nucleic acids, modification of the nucleic acid is not required. Immobilization can simply occur through ionic bonding of the negatively charged groups on the DNA and the positively charged surface. Therefore immobilized DNA are randomly orientated, because each molecule on the DNA can form many binding contacts. High background signals due to non-specific binding can result in false positive detection [39]. Physical adsorption is done through very weak bonds, therefore this technique is prone to leaching of enzymes or DNAs. Leaching is made more prone when the system is exposed to high reactant, concentrations, and ionic strengths. The weak bonds also allow enzymes and DNA to be removed from the support using gentle techniques. This does make it more attractive as decayed DNA can be removed and reloaded. This technique

has a higher commercial potential due to its low cost, simple implementation, and relatively chemical-free binding [40].

2.9.2 Covalent bonding

Covalent bonding is one of the most common irreversible immobilization techniques. Covalent bonding results in strong binding, good stability, and flexibility, which prevents desorption of DNA from the surface it is immobilized onto. DNA immobilization through covalent bonding is typically performed through DNA modifications. DNA is synthesized with a group of thiols (S-H) at the 5' or 3' end of the DNA, known as modified or thiolated DNA. The modification binds to the metal surface or a functional group introduced on the electrode surface [42]. This technique allows control over the orientation of the immobilized DNA, therefore making it more accessible for hybridization. It also allows for fine-tuning of the DNA's conformational and electrical properties. At negative electrode potentials, DNA attached to gold via an alkanethiol linker at its 5' end results in an upright orientation, while if it is tethered at its 3' end, it is tilted at 33 degrees [43]. Covalent bonding is beneficial over adsorption, as it leads to very high specific binding of DNA to a support [42].

Chemisorption is typically used to covalently immobilize thiolated DNA to gold to form a SAM of DNA probes on a gold electrode. Thiol groups have a strong affinity to bind to gold and other metals to form a covalent bond of Au-S. The Au-S bond is typically used in biosensors due its high binding strength, high stability, ease of preparation, and the ability to reproduce the monolayer. Thiol modifications can be synthesized at the 3' end of DNA via thiol-modified contracted pore glass (CPG), at the 5' end using thiol phosphoramidite, and onto the backbone of DNA via phosphoramidite chemistry. Different types of thiols are available for DNA modification including Oxa 6-S-s, Dithiol Serinol, 3' Thiol modifier, and a 5' modifier (C6 S-S). Thiol modifications are typically manufactured with a protective disulfide bond. To ensure binding of the thiolated DNA to a metal surface, chemical reduction of the modification is required [42].

A simple chemisorption technique is to pipette the required amount of thiolated DNA probes onto the gold surface followed by an incubation period of 24 hrs to form a strong Au-S bond, followed by washing of the gold surface in TE buffer to remove unbound DNA probes. Other studies suggest washing the modified DNA electrode with mercaptohexanol (MCH) solution to reduce the amount of non-specific binding of the DNA to gold, as well as to control the density of the SAM formed by placing a spacer between each DNA strand to increase the

efficiency of hybridization. MCH treatment is performed by soaking the DNA modified electrode after immobilization in 1 mM MCH for 30 mins at room temperature. MCH incubation time affects the formation of the SAM [42]. Maximum hybridization efficiency does not occur at maximum DNA probe density, because closely packed DNA cannot undergo hybridization due to electrostatic interactions or steric hindrance. Tightly packed SAMs result in high signal to background noise as well as non-specific interactions between the complementary pairs of DNA [39].

To increase the amount of immobilized DNA probes, gold nanoparticles (AuNPs) are used. Any type of working electrode can be functionalized with AuNPs films that will act as the immobilization site for DNA probes. Studies have functionalized AuNPs through chemical linkers. Combinations of AuNPs with other nano-composites offer increased amplification of the electrochemical signal, therefore ultra-sensitive electrochemical DNA biosensors are likely to be introduced in the future [42].

2.9.3 Avidin/streptavidin-biotin interaction

Another non-covalent immobilization technique is based on the formation of avidin/streptavidin-biotin interaction. Biotin molecules, with a molecular weight of 2.44 g/mol, have a high affinity to interact with avidin/streptavidin. This affinity is almost as high as the affinity of covalent bonding. The interaction has strong resistance to high and low temperatures, changes in pH, denatured detergents, as well as organic solvents. Therefore avidin/streptavidin-biotin is highly stable [42].

A benefit of avidin/streptavidin over other molecules is that a large tetrameric protein has the ability to offer four binding sites of the biotin molecule. These interactions are used to immobilize DNA onto solid surfaces. DNA probes are modified at either their 5' or 3' end with a biotin molecule, called biotinylated DNA, and then subsequently exposed to the avidin/streptavidin functionalized surface [42].

Various methods are used for avidin/streptavidin functionalization onto a surface for immobilization of biotinylated DNA. The most widely used functionalization method is EDC/NHS coupling reaction between avidin/streptavidin and the activated carboxyl group. Studies described the activation of the SAM of mercaptoacetic acid (MPA) modified gold surface. Activation is done by submerging the modified electrode in a solution of 30 mM EDC/NHS for 2 hrs, then soaking

of the electrode in 200 $\mu\text{g}/\text{mL}$ avidin solution. This conjugates the avidin onto the surface before the immobilization step. Other methods include the functionalization of avidin and carbon nanotubes using EDC/NHC coupling reaction. Other strategies use a biotin/avidin/biotin sandwich, where the biotin molecule is first immobilized onto the surface of a transducer. This step prepares the avidin layer for biotinylated DNA immobilization. The avidin layer acts as a connection site between the biotinylated DNA and the biotin modified electrode. This is possible because avidin can prepare four binding sites for biotin [42].

2.10 Summary

This chapter introduces autophagy, and defines it as a molecular process that causes the self-degradation of a cell to remove dysfunctional or unwanted cellular material. Autophagy is shown to be linked to various human diseases, including cancer and neurodegenerative diseases. It is linked to ageing, longevity, and is also an adaptive response to metabolic stress. Therefore autophagy is a good indicator of overall wellness. The basic autophagy machinery is explained and the process is summarized into five key stages. From the autophagic process, LC3 is shown to be an important biomarker to detect autophagy. From literature it is found that there is no current measurement of autophagy as rate, hence a theoretical approach to define autophagy flux as a rate is investigated.

Biosensors are introduced as a method to detect and measure autophagy. The general mechanism of a biosensor is explained, followed by a brief history of the development of biosensors over the years. Selectivity, stability, sensitivity, and resolution are shown to be important characteristics of any biosensor. In this chapter a biosensor is classified into two types: Direct label-free and indirect label-based biosensors. Different types of biosensors are explored including enzyme, electrochemical and DNA biosensors. The chapter concludes with a review of the three most common DNA immobilization techniques: adsorption, covalent bonding, and avidin/streptavidin-biotin interaction.

Chapter 3

Design and development of sensor

This chapter discusses the design and development process of the DNA sensor, which includes the type of biosensor to develop, the detection method to use, and the biomarker to detect. The biomarker used to detect autophagy flux is the LC3-II protein. A biosensor that can detect the genetic code of LC3-II is proposed. Therefore the analyte chosen is mRNA that encodes the protein LC3-II. To simplify the design of the biosensor, the complementary DNA (cDNA) of mRNA that encodes LC3-II is used as the analyte.

3.1 Biosensor overview

A label-free electrochemical DNA biosensor is proposed to detect LC3-II. To detect the analyte electrochemically, the ssDNA targets are hybridized with a recognition layer. The recognition layer is made from ssDNA probes complementary to the analyte, that are immobilized onto a transducer to form a SAM. The transducer chosen is SPEs that have planar gold as its WE and CE, and silver as its RE. The analyte is detected by performing SWV on the system and measuring the resulting faradaic current generated from the redox interaction between the analyte, recognition layer, transducer, and a supporting electrolyte solution. SWV is performed using a designed potentiostat that is tested against a commercially available potentiostat, the PalmSens 4. The three main processes of the biosensor is shown in Figure 3.1. Namely the hybridization of the ssDNA targets with the ssDNA probes, the immobilization of the ssDNA probes to gold, and the electrochemical detection of the DNAs.

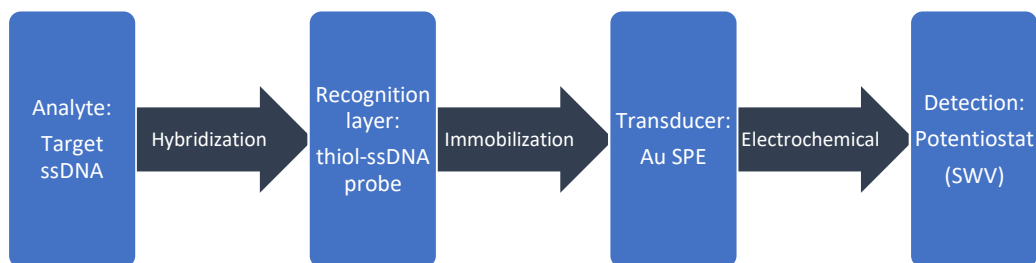


Figure 3.1: Overview of biosensor prototype

3.2 Biosensor type

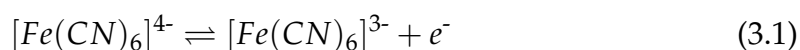
There are various types of biosensors that can be developed to detect LC3-II. These include impedimetric, potentiometric, and optical detection methods. To detect autophagy using mRNA that encodes LC3-II as the biomarker, it is decided that the prototype will utilize ssDNA as a replacement for mRNA. RNA contains ribose sugar molecules instead of the sugar molecules without hydroxyl modifications of deoxyribose as in DNA. This structural difference in the sugar molecule makes RNA more reactive than DNA and therefore less stable than DNA. RNA is not stable in alkaline conditions [44]. It has a short life span due to it being prone to ribonuclease (RNase). RNase is a class of hydrolytic enzymes that catalyzes the degradation of RNA molecules into small components [45]. To obtain ssDNA for the biosensor, RNA is reverse transcribed into cDNA and amplified to the desirable amount [46]. cDNA is the direct complement of mRNA, they contain the entire nucleotide sequence of the corresponding mRNA [47].

Once it is decided that the biosensor will be detecting DNA, the next step is to decide if the biosensor will be a direct label-free biosensor or an indirect labeled biosensor. Indirect labeled biosensors require an additional recognition element that binds to the analyte to generate a signal, however direct label-free biosensors rely on the direct interaction between the recognition layer and the analyte. Label-free biosensors utilize the intrinsic properties of the analyte. Labeled biosensors are more cost- and labor- intensive. It is decided that the biosensor will be label-free due the cost advantages and the simplicity of the principle behind label-free biosensors. The direct interaction between the recognition layer and the analyte is the hybridization reaction between ssDNA probes, that are immobilized onto the transducer to form a SAM, and the ssDNA targets. The hybridization reaction results in a redox reaction that is easily detected through electrochemical

studies. Electrochemical detection methods in biosensors have advantages over other biosensors due to the ease at which it can interface with normal electronic read-out and processing devices, the robustness of the detection method, easy miniaturization for POC development, and the good detection limits especially for small analytes [19]. To understand the complex interactions of the biosensor, such as the type of interactions that result in measurable currents, it is decided to keep the biosensor as simple as possible. The biosensor to detect autophagy flux is therefore decided to be a direct label-free electrochemical biosensor.

3.3 Electrolyte solution

Signal detection of the analyte is increased by the surface interaction between an electrode/recognition layer/analyte, as well as the incorporation of an electrolyte solution. Potassium ferrocyanide ($[Fe(CN)_6]^{4-/3-}$) is chosen as the electrolyte solution due to the potential of the anions. Potassium ferrocyanide has negatively charged ions, which electrostatically repel DNA since DNA has negatively charged phosphate backbones. The electrostatic repulsion aids the detection of DNA in the electrolyte solution. The interaction of potassium ferrocyanide with the transducer is a redox reaction. Oxidation of the electrolyte is as follows:



A supporting electrolyte is required in electrochemical cells to maintain ionic strength of the electrolyte solution. Potassium Chloride (KCl) is chosen as the background electrolyte solution due its high concentration of salt that increases the solution's conductivity.

3.4 Transducer

In the proposed DNA sensor, a transducer is required to convert the interaction of the recognition element and the analyte into a measurable signal for data analysis. The recognition layer is formed through the immobilization process described in Section 3.5. Immobilization is achieved through the interaction of a thiol molecule that covalently bonds to gold. The thiol is linked to the ssDNA to form a modified ssDNA called ssDNA probes. The interaction of the recognition layer and the analyte is through hybridization, which is discussed in detail in Section 3.6. Hybridization causes a redox reaction that results in a faradaic current.

Therefore, the transduction method is electrochemical, converting the signal from the biochemical event into an electrical one.

Transducers in electrochemical biosensors have a two- or three-electrode configuration. Two-electrode transducers are typically interdigitated electrodes (IDEs) and three-electrode transducers are typically SPEs. SPEs are advantageous over IDEs because they are inexpensive, disposable, and do not require polishing before use. The disposable manner of SPEs reduce cross-contamination between measurements, which is a serious problem in sensitive DNA biosensors [20]. The high affinity of the recognition layer to bind to gold, and the disposable nature of the SPEs resulted in the decision to use SPEs with gold as the WE and CE, and silver as the RE. Gold is also inert and the formation of crystal structures that are well-defined greatly influence the formation of the recognition layer [41]. A working electrode with a diameter of 4 mm is chosen to allow a larger surface area for the recognition layer to form. The ceramic substrate has the dimensions $33 \times 10 \times 0.5$ mm as shown in Figure 3.2. SPEs are purchased from Metrohm DropSens [48].

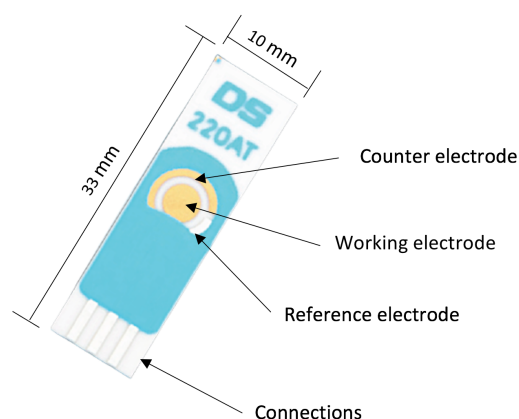


Figure 3.2: Transducer: Gold WE screen printed electrode

3.5 Recognition layer - Immobilization

After the decision to use gold SPEs as the transducer for the biosensor, the recognition layer for the biosensor is characterized. The detection of ssDNA targets requires hybridization of the target ssDNA with a complementary pair of ssDNA. Therefore, the recognition layer is made up of ssDNA probes with which the target ssDNA can hybridize with. For the ssDNA probes to form the recognition layer, they are immobilized onto the SPE to form a SAM. The SAM is only formed onto

the working electrode, which acts as the recognition layer. The sequence of the ssDNA probes is:



DNA's four nucleobases easily adsorb onto gold, with adsorption energy ranked adenine > cytosine > guanine > thymine >> phosphate [49]. Various immobilization techniques are studied. The immobilization technique of covalent bonding is chosen for the design of the biosensor. Covalent bonding of the ssDNA probes to gold provides good vertical orientation of the ssDNA probes, which increases hybridization efficiency. Covalent bonding demonstrates high stability and binding strength between the ssDNA probes and gold, which prevents desorption of the ssDNA probes [42]. In order to covalently bond ssDNA probes to gold, an alkanethiol (thiol) linker between the ssDNA probes and gold is required. Thiol groups have a strong affinity to bind with gold surfaces. The ssDNA probes are therefore synthesized with a C6 Thiol tethered at the 5' end of the ssDNA probes as shown in Figure 3.3. Thiols lead to a high amount of specific binding of ssDNA probes to gold, and therefore reduce the amount of non-specific binding through the four nucleobases.

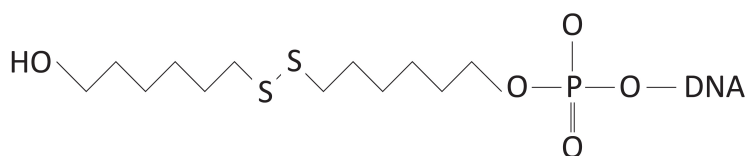


Figure 3.3: DNA tethered with a C6-thiol

The formation of the SAM is done through a three step process: The diffusion-controlled physisorption, then chemisorption of the molecules, and lastly crystallization. Gold's physisorbed state is highly disordered. The only interaction accounting for the adsorption during this stage is van der Waals interactions. During the chemisorption stage, the hydrosulphide head group loses a mercaptan hydrogen atom and then bonds with three gold atoms. This interaction forms a strong covalent bond between the gold and the hydrosulphide head group. The crystallization process follows the alignment of the molecules on the gold's surface in a parallel manner through electrostatic, steric, repellent, and van der Waals forces. The alignment of molecules results in a highly orientated and ordered molecular layer [41]. The structure of a thiol monolayer consists of three parts, a hydrosulphide head group, a molecular backbone, and the end group. The structure of the thiol monolayer is shown in Figure 3.4.

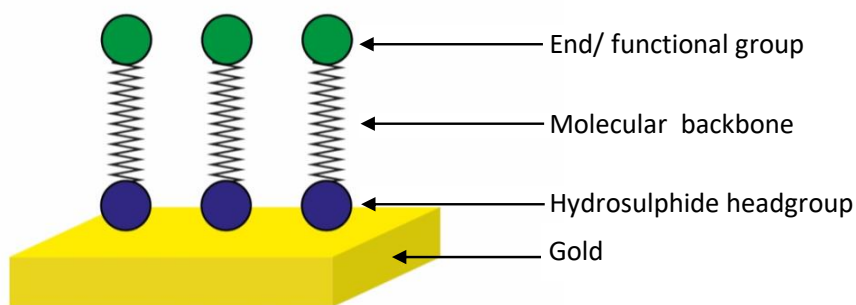


Figure 3.4: Structure of thiol monolayer

After an electrolyte solution of potassium ferrocyanide in potassium chloride is prepared, the ssDNA probes are prepared for immobilization. The synthesis of the ssDNA probes are prepared beforehand in TE pH 8.0 buffer. Two sets of samples of ssDNA probes are prepared: a control sample in which only the ssDNA probes are present in the solution, and a test sample in which the ssDNA probes are mixed with Tris (2-carboxyethyl) phosphine hydrochloride (TCEP) in the solution. TCEP is a potent, thiol-free reducing agent, it is stable and soluble in many aqueous solutions at any pH [50]. The thiol-modified ssDNA probes are not supplied with a free thiol at its 5' end. The thiol is capped with a protective disulfide bond [49]. The test samples of ssDNA probes are treated with TCEP to reduce the disulfide bond on the thiol modified ssDNA probes. The reduction of the disulfide bond exposes the thiol, which allows the ssDNA to covalently bind to gold. TCEP is added to the ssDNA probes solution by the ratio of 1:100, TCEP to DNA. The immobilization of the ssDNA probes are performed according to the following steps:

1. 0.01, 0.1, 1, and 10 μM of ssDNA probes are prepared as test samples in TE buffer.
2. 0.01, 0.1, 1, and 10 μM of ssDNA probes are prepared as control samples in TE buffer.
3. Pipette 15 μL of each concentration of each sample onto the three-electrode system of the SPE.
4. Repeat the pipetting of the ssDNA probe samples for a set of two repeated samples.
5. Incubate the SPEs in a wet chamber at room temperature for 24 hrs.

6. Thoroughly rinse the SPEs with DI water.
7. Dry the SPEs at room temperature before analysis.

Through the process above well organized and orientated SAMs consisting of ssDNA probes are formed, each SAM has a different concentration of ssDNA probes. The formation of the SAM as the recognition layer is used to recognize a signal from the interaction of the analyte and SAM through hybridization in the next step. Figure 3.5 illustrates the immobilized ssDNA probes on gold to form the SAM.

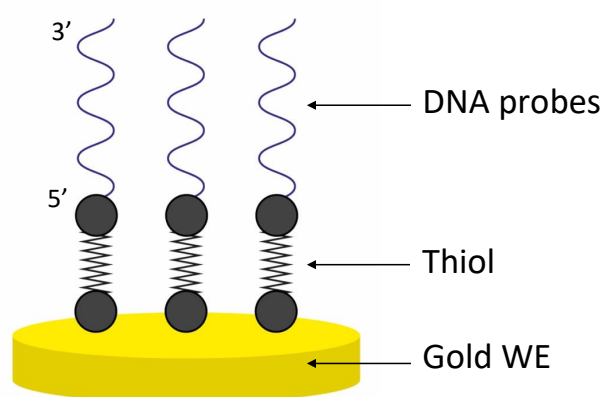


Figure 3.5: Immobilization of ssDNA probes

3.6 Analyte recognition - Hybridization

Once the transducer and the recognition layer are integrated, the analyte can be detected and measured. The analyte is a complementary pair of ssDNA to the ssDNA probes; this ssDNA is referred to as the ssDNA targets. The sequence of the ssDNA target is:

FITC-TGGAGTCTTACACAGCCATTGC

Since the biosensor incorporates the use of a recognition layer, solid-phase hybridization is used as the method of hybridization instead of solution-phase hybridization. This method is performed by adding ssDNA targets to surface-tethered oligonucleotides (SAM) [51]. Even though solid-phase hybridization is more complex, quantification of the SAM before hybridization is essential to detect target ssDNA. Figure 3.6 illustrates the dsDNA formed when the ssDNA targets hybridize with the SAM.

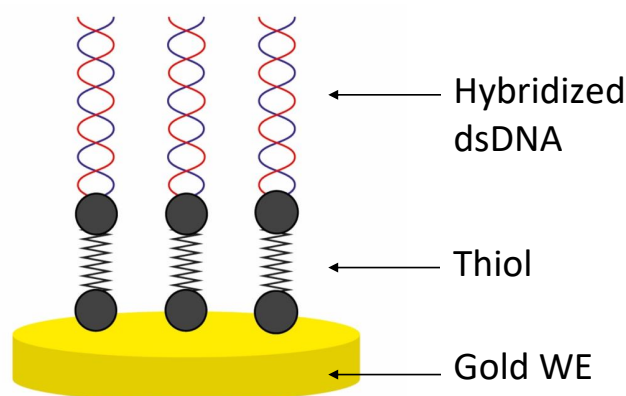


Figure 3.6: Hybridization of ssDNA probes and ssDNA targets

Hybridization changes the overall surface charge of the biosensor from before hybridization. Negatively charged ions of ferrocyanide are electrostatically repelled by increased negatively charged dsDNA compared to ssDNA [52]. The reduction in ferrocyanide ions reaching the gold surface reduces the redox activities taking place between ferrocyanide and gold, and hence reduces the faradaic current generated. This is the most common method to detect hybridization. Another mechanism used to indicate hybridization is through binding of complementary base pairs of both the ssDNA probes and ssDNA targets. By modifying the ssDNA probes with a thiol linker, the ssDNA probes are anchored to the transducer so that less free bases adsorb onto the gold surface, therefore allowing for hybridization through the interaction between the exposed bases of the ssDNA probes and the ssDNA targets. Free adenine and guanine moieties of ssDNA probes bind selectively with their complementary cytosine and thymine bases of the ssDNA targets through hydrogen bonds [42]. By the base-pairing, less of the electroactive bases of guanine and adenine moieties from the ssDNA probes are available to undergo oxidation [53]. In conclusion, the method of detection of the ssDNA targets are mostly through the increased repulsion of the ferrocyanide ions from reaching the electrode surface when dsDNA is formed as well as through the pairing of the base pairs of complementary ssDNA, therefore reducing the amount of free bases on the ssDNA probes available for oxidation with the electrode surface.

To detect the target ssDNA, 1 μM of ssDNA probes immobilized onto SPEs to form SAMs are prepared. Various concentrations of the ssDNA targets are detected. The use of 1 μM of ssDNA probes as the SAM and the substantially smaller amount of ssDNA targets is to ensure saturation of the binding between

the ssDNA targets and the ssDNA probes. The experiment is conducted according to the following instructions:

1. 0.001, 0.01, 0.1, and 0.5 μM of ssDNA targets are prepared in TE buffer pH 8.0.
2. 15 μL of the ssDNA targets are pipetted onto the SAM modified SPEs
3. The SPEs are incubated in a wet chamber for 60 min.
4. After hybridization, the SPEs are rinsed thoroughly with DI water to remove un-hybridized strands of ssDNA targets and dried at room temperature before analysis.

3.7 Detection method - Square wave voltammetry

Since the resulting interactions of the analyte and the recognition layer result in the generation of faradaic current, the sensing method must be able to read small currents. SWV is the voltammetric technique that is used to apply a series of potentials to the transducer and to measure the resulting current.

SWV has several advantages over other techniques, it is highly sensitive, is able to reject background currents, and has a fast scanning speed [54]. In SWV one can avoid the necessity to cycle the overall potential in the reverse direction as required in cyclic voltammetry (CV). Two neighboring pulses imposed at a single potential step complete a full potential cycle in itself by the oppositely orientated forward and reverse pulses as shown in Figure 3.7, which drives the SPE in both the cathodic and anodic direction, while the overall potential remains in a singular direction [35].

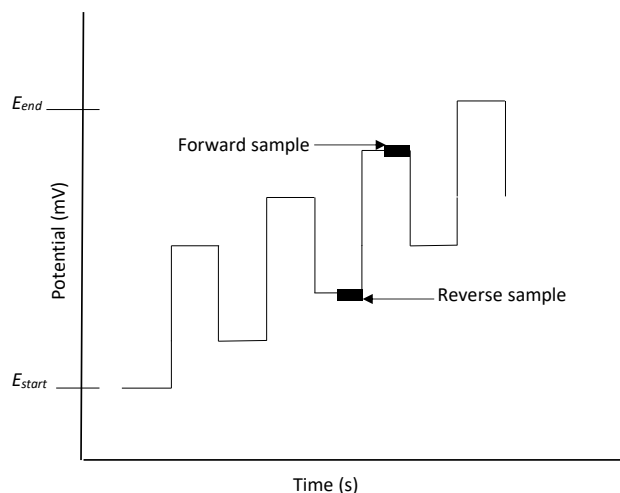


Figure 3.7: SWV input potential

In SWV the net current, the difference between the corresponding forward and reverse currents, is used for analysis. While individual forward and reverse currents do not yield well defined peaks and have a complicated shape, the net current yields a well-defined peak, which is advantageous in an analytical context, as it provides easily measurable parameters of peak current, which is directly related to the concentration of the analyte detected [35]. During voltammetry measurements there is the presence of both capacitive and faradaic currents flowing. Only faradaic currents are the result of the analyte detected. As the concentration of the analyte decreases, the faradaic current decreases however the capacitive current does not change. SWV increases the ratio of faradaic current to capacitive current $\frac{I_f}{I_c}$ [55], therefore increasing the sensitivity of the biosensor.

Electrochemical stability of the SAM is limited to a potential window of -0.6 V to +0.6 V due to structural aspects of thiol-modified ssDNA, the start and end potentials of the SWV analysis is therefore limited within this potential window [56]. SWV is performed with the following setting: Start potential of -0.1 V, end potential of 0.4 V, step size of 0.001 V, amplitude of 0.05 V and frequency of 50 Hz. The analysis of the immobilized and hybridized ssDNA from the previous sections is as follows:

1. Prepare the electrolyte solution with DI water in 5 ml Eppendorf tubes.
2. Connect the immobilized/hybridized modified SPEs to the potentiostat.
3. Place the SPEs in the Eppendorf tube with the electrolyte solution and allow saturation for 1 min.

4. Run SWV on the immersed SPEs for a total of three measurements.
5. Repeat the setup for every SPE sample with an unused electrolyte solution.

3.8 Summary

This chapter presents the methodology behind the development of the sensor. A brief overview of the biosensor is presented. The three main processes of the sensor are established as immobilization, hybridization, and the electrochemical measurement. The biosensor is characterized by its label-free approach to detect ssDNA as well as the electrochemical detection method.

Potassium ferrocyanide in potassium chloride is chosen as the electrolyte solution of the electrochemical cell. A transducer to convert a chemical reaction into an electrical signal is required, therefore a planar gold SPE is chosen as the transducer. A SAM consisting of ssDNA probes, which are immobilized onto the transducer is developed, and the structure of the SAM is investigated. The covalent bonding immobilization procedure is explained and a protocol is developed to implement the procedure.

The mechanisms which induce a current during the hybridization reaction between ssDNA probes and ssDNA targets are investigated. The type of hybridization procedure is established and a protocol is developed. The chapter concludes with the method to detect the concentration of the analyte. SWV is chosen as the electrochemical technique that is applied to the sensor. The applied SWV signal to the sensor is characterized, and a measurement protocol is established to measure the concentration of both the immobilized ssDNA probes as well as the hybridized ssDNA targets.

Chapter 4

Design and development of potentiostat

This section describes the design and development process for a prototype potentiostat that interfaces with the sensor. The principle of the potentiostat is to apply a voltage waveform to the biosensor and record the generated output current signal. The design of the potentiostat is low cost and easy to replicate compared to expensive commercially available potentiostats. The potentiostat consists of a microprocessor (Arduino Uno), a digital to analog converter (DAC), a control amplifier (U1), a transimpedance amplifier (U2), and the cell. A full schematic of the prototype design is shown in Figure 4.1.

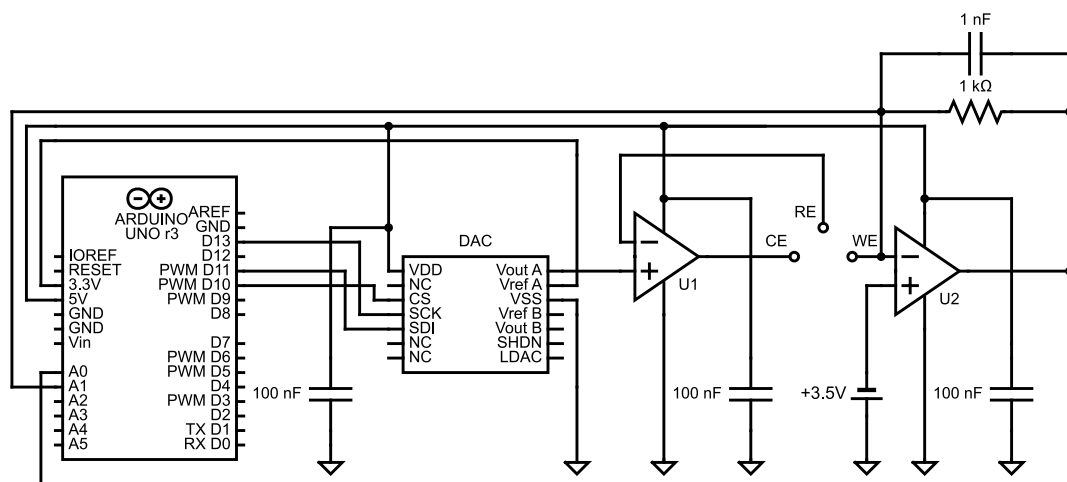


Figure 4.1: Potentiostat schematic

4.1 Micro-controller

A micro-controller is required to supply the desired signal to the potentiostat, as well as to process the output current signal generated by the cell. In conjunction with the external DAC, the micro-controller can generate any desired waveform. Using the micro-controller's analog-to-digital converter (ADC), the output current signal from the cell can be processed. An Arduino Uno R3 is chosen due its low cost and functionality. The relevant specifications of the Arduino Uno are listed in Table 4.1 below.

Table 4.1: Micro-controller specifications

Component	Specification
Name	Arduino Uno Rev 3
Micro-controller	ATmega328P
Operating voltage	5V
Digital I/O pins	6
Analog input pins	6
Clock speed	16 MHz
Analog-digital-converter resolution	10 bit
Digital-analog-converter	none

4.1.1 Stair-step wave

The potentiostat is designed to perform SWV. The waveform that is applied to the cell during SWV is a stair-step waveform. The waveform is formed by the superposition of a step wave and a stair wave as indicated in Figure 4.2. The amplitude (A), step, frequency (f), scan rate (v), and the start and stop potential are chosen according to the discussion in Section 3.7.

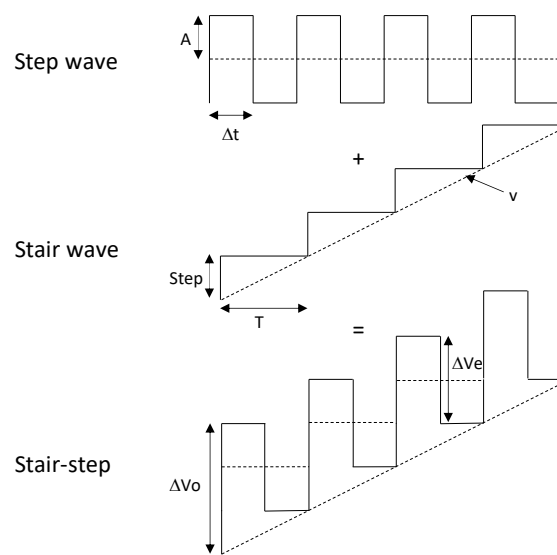


Figure 4.2: Superposition of step and stair wave to form stair-step wave

The characteristics of the stair-step wave are:

$$\Delta V_o = 2A + 2v\Delta t \quad (4.1)$$

$$\Delta V_e = 2A \quad (4.2)$$

$$\Delta t = \frac{1}{2f} \quad (4.3)$$

4.2 Digital to analog converter

An external DAC is interfaced with the Arduino Uno. DAC MCP4922 is a dual 12-bit voltage output DAC that requires an external voltage reference input. The device is supplied by a 2.7 V - 5.5 V voltage supply, and has a SPI interface with a 29 MHz clock support. It is chosen for its low noise performance and accuracy. The pin connections of the DAC are listed in Table 4.2. The DAC values are calculated according to:

$$\begin{aligned} DAC &= \frac{V_{out}}{V_{ref}} \times 2^n \\ &= \frac{V_{out}}{3.3} \times 2^{12} \end{aligned} \quad (4.4)$$

Table 4.2: DAC MPC4922 pin connections

MCP4922 Pin	Connection
Vdd	Arduino 5 V
NC	No connection
CS	Arduino SS Pin 10
SCK	Arduino SCK Pin 13
SDI	Arduino MOSI Pin 11
Vout A	Input to Control Amplifier
Vref A	Arduino 3.3 V
Vss	Ground

4.3 Control amplifier

A control amplifier compares the measured cell voltage with the desired cell voltage. To adjust the measured cell voltage to the desired cell voltage the control amplifier drives current into the cell. The control amplifier is designed using an operational amplifier (op-amp). The desired potential is applied to the positive input terminal of the op-amp, which is then applied to the CE. The measured potential of cell at the RE is fed back through the negative potential of the op-amp as shown in Figure 4.3. TLC2272 dual op-amp is chosen as the op-amp that is used throughout the potentiostat design. It is chosen because of its high input impedance and low noise levels, which are suitable for small signals. The op-amp is powered at the positive power rail with a 5 V potential and grounded at the negative power rail. A 100 nF bypass capacitor is added to the positive power rail. This ensures a low impedance ac path to ground over a large frequency range.

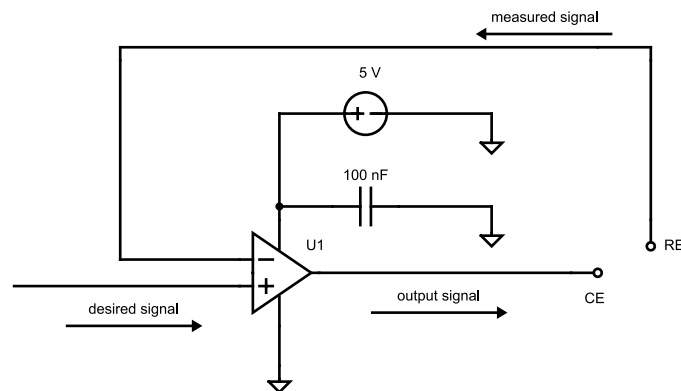


Figure 4.3: Control amplifier schematic

4.4 Transimpedance amplifier

A transimpedance amplifier is a current-to-voltage converter (I/V). Small amounts of current in the electrolyte solution is converted into a measurable voltage for the micro-processor to process digitally. The transimpedance amplifier is designed using a negative feedback op-amp, a resistor, and a capacitor as seen in Figure 4.4.

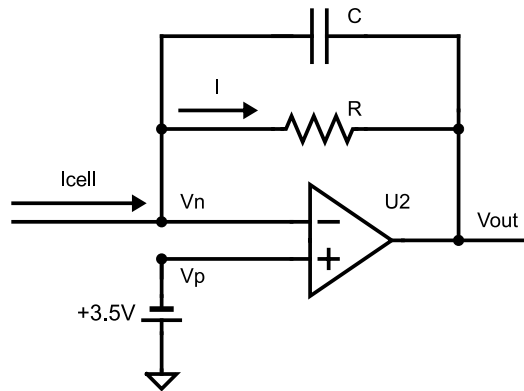


Figure 4.4: Transimpedance amplifier

The $1\text{ k}\Omega$ resistor (R) over the operational amplifier eliminates any DC offset. Adding the 1 nF capacitor (C) in parallel with the resistor eliminates oscillation by acting as a RC filter. The input terminals of the transimpedance amplifier is biased at a potential of 3.5 V by connecting the positive input terminal to a 3.5 V supply. By biasing the operational amplifier at 3.5 V , the transimpedance amplifier is able to measure negative potentials. The potentiostat is limited to detect current according to the potential limit of the ADC. The ADC on the Arduino Uno can only convert voltages between 0 to 5 V . The current in the cell is determined by measuring the current across resistor, R, where $I_{cell} = I$. Therefore the current in the cell is determined as:

$$I_{cell} = \frac{V_n - V_{out}}{R} \quad (4.5)$$

Where according to ideal op-amp characteristics:

$$V_n = V_p = 3.5\text{ V} \quad (4.6)$$

The current limits are determined by the potential limits of the ADC ($V_{out(min)}$ and $V_{out(max)}$). Therefore, the minimum and maximum currents the potentiostat can

measure are:

$$\begin{aligned}
 I_{cell(min)} &= \frac{V_n - V_{out(max)}}{R} \\
 &= \frac{3.5 - 5}{1 \text{ k}\Omega} \\
 &= -1.5 \text{ mA}
 \end{aligned} \tag{4.7}$$

$$\begin{aligned}
 I_{cell(max)} &= \frac{V_n - V_{out(min)}}{R} \\
 &= \frac{3.5 - 0}{1 \text{ k}\Omega} \\
 &= 3.5 \text{ mA}
 \end{aligned} \tag{4.8}$$

4.5 Three-electrode system

The cell is measured with a three-electrode system consisting of a RE, CE, and WE. A potential is applied to the CE, where the electrochemical reactions are unknown [35]. The RE is required to be robust and have a constant chemical composition [35]. It has a constant potential and is used to measure the potential of the cell. The potential of an electrolyte solution is equal to the potential of the metallic phase of the RE [35]. Current in the cell only flows between the CE and the WE. The WE carries information to the potentiostat from the charge transfer across the small electrolyte-electrode interface. Current in the cell is measured at the WE while the relative potential of the WE is controlled by the RE [35].

4.6 Spice simulation

Design of the potentiostat is simulated in LTSpice to compare the prototype potentiostat to a known theoretical result. A Spice schematic of the potentiostat is shown in Figure 4.5. The stair-step wave that is generated by the Arduino and external DAC is simulated using a piecewise linear (PWL) function at voltage source V1. The electrochemical cell is represented by resistor R1.

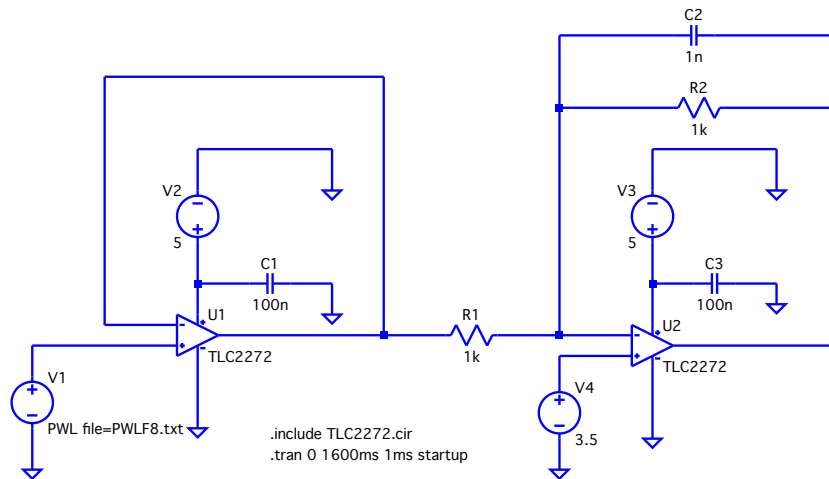


Figure 4.5: Spice simulation of potentiostat

The stair-step wave simulated in Spice using the piecewise linear function is shown in Figure 4.6. The waveform has a potential ranging from 0 mV to 490 mV, a step of 10 mV, an amplitude of 50 mV, and a frequency of 50 Hz. The specifications of the waveform are chosen according to sensor, including the electrode type, analyte, and electrolyte solution.

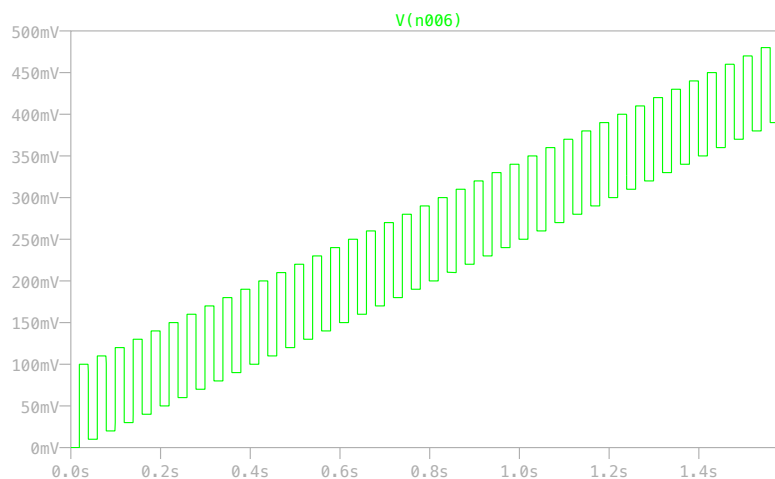


Figure 4.6: Spice output of stair-step wave

4.7 Arduino software

To perform SWV a stair-step wave is applied to the electrochemical cell and the current is measured using the ADC on the Arduino micro-processor. This is achieved by the software implemented. The external DAC is designed to interface

directly with the serial peripheral interface (SPI) port of the Arduino.

The first step in interfacing the DAC with the Arduino is to include the SPI library and to set pin 10 on the Arduino as the chip select (CS) pin of the DAC as indicated in Figure 4.7 [57].

```
// include the library code:
#include <SPI.h>

// Set Constants
const int dacChipSelectPin = 10;    // set pin 10 as the chip select for the DAC:
```

Figure 4.7: Arduino code DAC library

In the setup of the Arduino micro-processor, Figure 4.8, the CS pin is set as an output pin on the Arduino. The CS pin is by default an active low pin, therefore it is set high in the setup. By setting the CS pin high, the peripheral is disconnected from the SPI bus to prevent any unexpected communication from taking place. The CS pin must be held low throughout the duration write command. SPI.begin() initializes the SPI and sets the pin modes for the SPI.

```
// Start setup function:
void setup() {
  Serial.begin(9600);
  pinMode(adcVout, INPUT);
  pinMode(adcVn, INPUT);
  pinMode(dacChipSelectPin, OUTPUT);
  // set the ChipSelectPins high initially:
  digitalWrite(dacChipSelectPin, HIGH);
  // initialise SPI:
  SPI.begin();
  SPI.setBitOrder(MSBFIRST);    // Not strictly needed but just to be sure.
  SPI.setDataMode(SPI_MODE0);  // Not strictly needed but just to be sure.

  TCCR2B = TCCR2B & B11111000 | B00000001; // for PWM frequency of 31372.55 Hz
  pinMode(3, OUTPUT);
  pinMode(7, OUTPUT);
} // End setup function.
```

Figure 4.8: Arduino code DAC setup

Function setDac(), Figure 4.9, is called in the program when a value is sent to the DAC in order to output a potential signal. MCP4922 has two DACs on the module. The two inputs to the function are the DAC value sent to the DAC and the chosen DAC channel. SPI function can only transfer 8 bits at a time, but the value sent to the DAC is 12 bits long. Function setDac() uses masking to separate the 12 bit value into a primary and secondary byte. dacPrimaryByte contains the 4 bit instructions and the the first 4 MSB of value. dacSecondaryByte contains the 8 LSB of value. Case statements switch between the DAC channels according to the user's choice. After the data has been separated into the primary and secondary bytes, the interrupts are disabled, the CS pin is written low to wake up the selected

DAC, and the primary byte and secondary byte are consecutively written to the DAC. The selected DAC is then written high to disable it and the interrupts are enabled.

```
void setDac(int value, int channel) {
  byte dacRegister = 0b00110000;
  int dacSecondaryByteMask = 0b0000000011111111;
  byte dacPrimaryByte = (value >> 8) | dacRegister;
  byte dacSecondaryByte = value & dacSecondaryByteMask;
  switch (channel) {
    case 0:
      dacPrimaryByte &= ~(1 << 7);
      break;
    case 1:
      dacPrimaryByte |= (1 << 7);
  }
  noInterrupts();
  digitalWrite(dacChipSelectPin, LOW);
  SPI.transfer(dacPrimaryByte);
  SPI.transfer(dacSecondaryByte);
  digitalWrite(dacChipSelectPin, HIGH);
  interrupts();
}
```

Figure 4.9: Arduino code setDac function

dacRegister is a binary number that contains the initial information sent to the DAC. The 8 bit binary number of dacRegister consists of data bits and instruction bits, which can be seen in Table 4.3. Zeros in the data bits are place holders for the data that is sent to the DAC.

Table 4.3: Bit instructions for DAC register

Write command for DAC register							
7 (MSB)	6	5	4	3	2	1	1 (LSB)
\bar{A}/B	BUF	$\bar{G}A$	\overline{SHDN}	DATA	DATA	DATA	DATA

- bit 7 \bar{A}/B : DAC selection bit
 0 = Write to DAC_A
 1 = Write to DAC_B
- bit 6 **BUF**: V_{REF} input buffer control bit
 0 = Unbuffered
 1 = Buffered
- bit 5 $\bar{G}A$: Output gain selection bit
 0 = 2 × (V_{OUT} = V_{REF} × D / 4096)
 1 = 1 × (V_{OUT} = V_{REF} × D / 4096)
- bit 4 \overline{SHDN} : output Shutdown control bit
 0 = Shutdown the selected DAC channel
 1 = Active mode operation
- bit 3-0 **DATA**: DAC input data bits

Values in the write command correspond to the stair-step wave sent to the DAC

by using a for loop function, Figure 4.10. The step and amplitude are specified by the user. Values in the write command are converted to values that the DAC can read before being sent to the DAC. Frequency is set by specifying the time (in ms) between the change in the value sent to the DAC. Once the values have been transferred to the DAC, a function to sample current is called (`sampleReverse()` and `sampleForward()`).

```
void loop() {
  float step =0;
  float amp =200;

  for (int i = 0; i <40; i++){
    step = step+25;
    step_DAC[i] = step;
    step_DAC[i] = step / 3300;
    step_DAC[i] =step_DAC[i] *4096;
    step_DAC[i] = (int)step_DAC[i];

    amp = amp +25;
    amp_DAC[i] = amp;
    amp_DAC[i] = amp / 3300;
    amp_DAC[i] =amp_DAC[i] *4096;
    amp_DAC[i] = (int)amp_DAC[i];
    float xyz = amp_DAC[i];

    setDac(step_DAC[i],0);
    delay(15);
    i_rev_arr[i]=sampleReverse();
    Serial.println(i_rev_arr[i]);

    setDac(amp_DAC[i],0);
    delay(15);
    i_for_arr[i]=sampleForward();
    Serial.println(i_for_arr[i]);
  }
  exit(0);
}
```

Figure 4.10: Arduino code Loop function

Current sampling for the forward and reverse sampling are similar to one another and hence, only the reverse current sampling is shown in Figure 4.11.


```

float sampleReverse(){
  float adc_rev =0;
  float v_rev =0;
  float adc_avg_rev =0;
  float adc_tot_rev =0;

  float adc_rev_vn = 0;
  float v_rev_vn =0;
  float adc_avg_rev_vn =0;
  float adc_tot_rev_vn =0;

  float i_rev=0;

  for(int r=0; r<4; r++){
    delay(1);
    adc_rev = analogRead(adcVout);
    adc_tot_rev = adc_tot_rev + adc_rev;

    adc_rev_vn = analogRead(adcVn);
    adc_tot_rev_vn = adc_tot_rev_vn + adc_rev_vn;
  }
  adc_avg_rev = adc_tot_rev/5;
  v_rev =adc_avg_rev*5;
  v_rev = v_rev/1023;

  adc_avg_rev_vn = adc_tot_rev_vn/5;
  v_rev_vn =adc_avg_rev_vn*5;
  v_rev_vn = v_rev_vn/1023;

  i_rev = v_rev - v_rev_vn; // divided by 1k = mA
  return i_rev;
}

```

Figure 4.11: Arduino code current sampling

Sampling takes place for 0.25% of the time of each step as illustrated in Figure 4.12. Five samples are taken using ADC. The average of the five samples are then converted to voltages and the current is calculated.

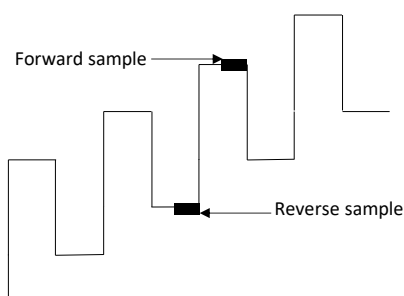


Figure 4.12: Current sampling of forward and reverse currents

4.8 Summary

This chapter explored the development process of the potentiostat, which can be used to apply SWV to the sensor in order to measure the analyte's concentration. A schematic of the entire potentiostat is presented, which consists of a micro-controller, DAC, control amplifier, cell, and a transimpedance amplifier.

An Arduino Uno integrated with an external MCP4922 DAC is designed to

apply a stair-step wave signal through the control amplifier to the cell. The control amplifier is developed to maintain the desired signal applied to the cell by comparing the actual cell potential with the desired applied potential. The resulted current generated in the cell is converted to a voltage using the developed transimpedance amplifier. A Spice simulation of the developed potentiostat is designed in order to compare the theoretical working of the potentiostat to the experimental results. The chapter concludes with a detailed explanation of the Arduino code developed. The code is designed to apply the desired signal to the cell and to sample the measured voltage from the transimpedance amplifier.

Chapter 5

Results

This section discusses the results from the development of an electrochemical DNA sensor. Fluorescent microscopy, Scanning electron microscopy (SEM), and electrochemical studies were conducted to verify the immobilization of the ssDNA probes and the hybridization of the ssDNA targets. Electrochemical studies were conducted using an integrated setup. The setup consisted of a potentiostat, an electrode with a transducer surface, an electrolyte, and the analyte. The potentiostat, Palmsens 4, is used to perform SWV and CV on the sensor. The results of the various tests conducted on the low-cost potentiostat are also discussed.

5.1 Concentration of background electrolyte

10mM of potassium ferrocyanide is used as the electrolyte solution. Potassium chloride is chosen as the background electrolyte. The electrolyte solutions are made up with DI water in 5 ml Eppendorf tubes. To exclude any extraneous variables, such as bacteria contamination, a freshly made batch of electrolyte solution is prepared before every experiment. Before any electrochemical analysis is performed, the electrode is submerged in the electrolyte solution for 1 min and three consecutive measurements are taken. The average of the three measurements are used for comparative studies. This procedure is used for all electrochemical measurements that follow.

Various concentrations of the background electrolyte are tested to determine which combination of the electrolyte solution yields the strongest signal. The square wave voltammograms for concentrations of 0.1, 0.5, 1, 3, 5, 10, 50, and 100 mM potassium chloride in 10 mM of potassium ferrocyanide are plotted in Figure 5.1. From the square wave voltammograms it is observed that as the concentration of the background electrolyte increases, the peak current generated through SWV

increases proportionally. Concentrations above 10 mM of potassium chloride yield higher current peaks, therefore the recommended electrolyte solution of 100 mM potassium chloride in 10 mM potassium ferrocyanide is used for the electrochemical sensor.

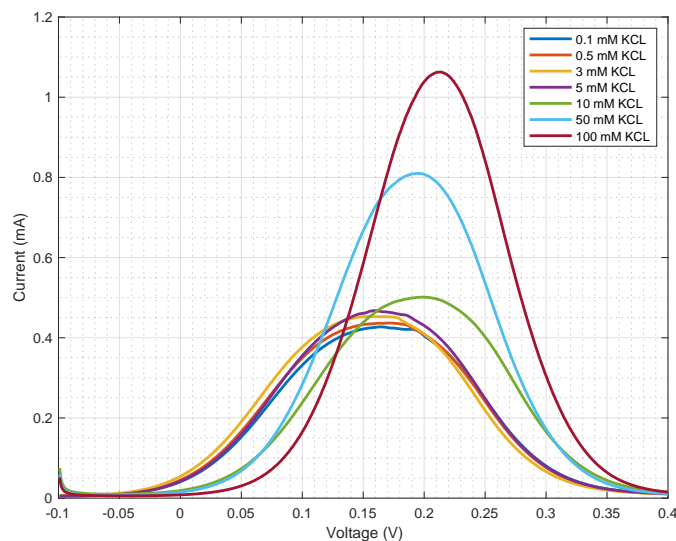


Figure 5.1: Peak current (mA) vs. background electrolyte concentration (mM)

Figure 5.2 show the approximately linear relationship between the peak current measured and the concentration of the background electrolyte when added to the electrolyte solution.

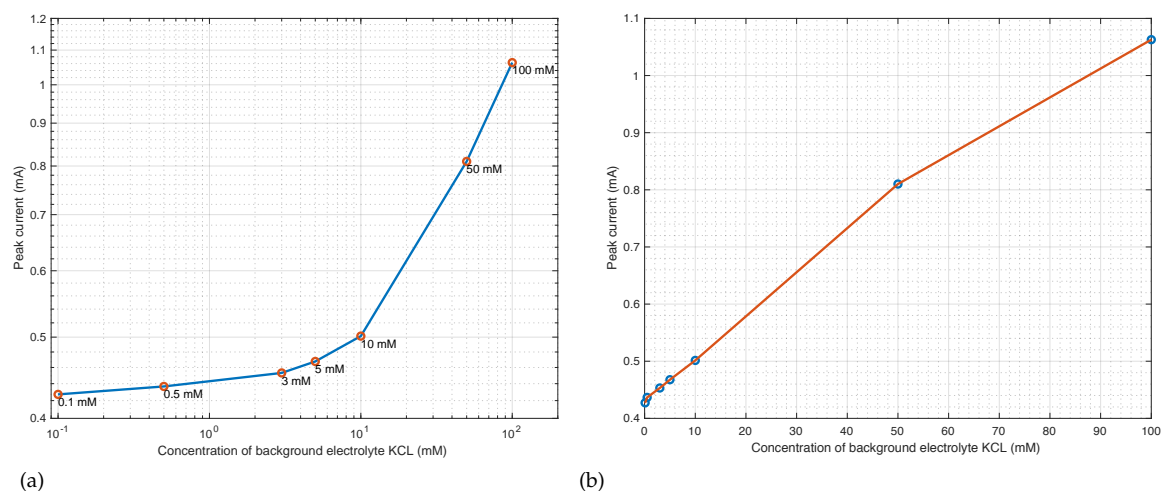


Figure 5.2: Peak current (mA) vs. background electrolyte concentration (mM) (a) Logarithmic plot (b) Linear plot

A CV measurement, Figure 5.3, is performed on the electrolyte solution of 10 mM potassium ferrocyanide and 100 mM potassium chloride. The results indicate that the redox reaction the solution undergoes is reversible as shown by the perfect duck-shape of the voltammogram, with a peak-to-peak separation value (ΔE_p) of

99.92 mV for every scan shown in Table 5.1.

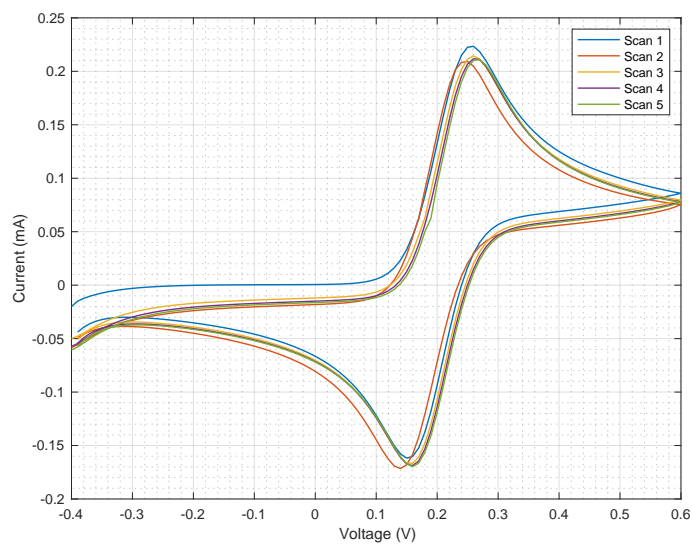


Figure 5.3: Cyclic voltammogram of electrolyte solution

Table 5.1: Peak currents (mA) and potentials (mV) of cyclic voltammogram

Scan	I_{pc} (mA)	E_{pc} (mV)	I_{pa} (mA)	E_{pa} (mV)	ΔE_p (mV)
1	0.22339	249.65	-0.16176	149.73	99.92
2	0.20922	239.65	-0.17152	139.73	99.92
3	0.21447	259.65	-0.16673	159.73	99.92
4	0.21182	259.65	-0.16884	159.73	99.92
5	0.21094	259.65	-0.16973	159.73	99.92

5.2 Square wave voltammetry calibration curve

To determine a change in concentration of the analyte of interest, a calibration curve is required to compare the unknown peak currents of the square wave voltammogram to a known peak current. The calibration curve is determined by submerging a blank electrode into the chosen electrolyte solution and performing SWV on the system. The calibration curve is the subsequent voltammogram that shows the peak current generated when an analyte of concentration 0 mM of DNA per volume is added to the sensor. When the sensor is used to measure the concentration of an analyte, any change in the peak current from the calibration curve is proportional to the concentration of the analyte. The average peak current of the blank electrode is 1.1 mA at 0.18 V as shown in Figure 5.4(b). From the individual measurements, Figure 5.4(a), sensor 1 has a peak current of 1.08 mA, sensor 2 peak current is 1.09 mA and sensor 3 is 1.11 mA. The average peak current of 1.1 mA has a standard deviation of 0.016 mA and a margin of error of 0.009 mA.

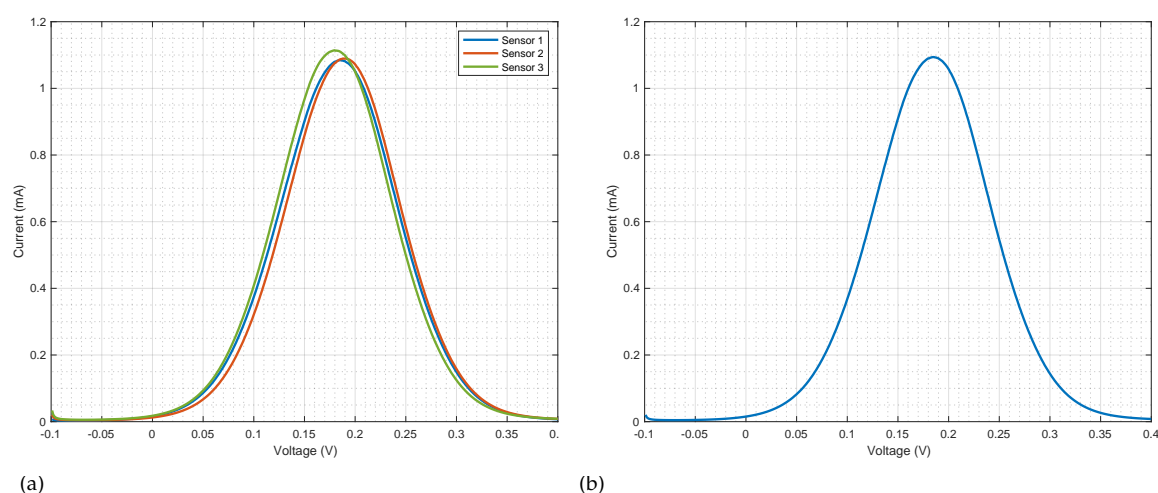


Figure 5.4: Calibration curve of DNA sensor (a) Individual peak currents (b) Mean peak current

5.2.0.1 External reference electrode

Silver and gold are both noble metals and have a high affinity to bind to thiols, hence the use of modified ssDNA probes. It is important in electrochemical studies for the RE to maintain a constant potential. The potential binding of the ssDNA probes to the RE may change the resistance of the electrode. Therefore, the use of an external RE eliminates the unwanted binding of the ssDNA probes to the SPE's RE. Figure 5.5 compares the peak current of the calibration curve between the system when the SPE's own RE is used, and when an external RE is used. A 5 cm long piece of silver wire is used as the external RE. The external RE is placed

as close as possible to the WE to minimize the resistance to the system. By using the external RE, the peak current is reduced by 11.55% to 0.97 mA from 1.1 mA. The change in the peak current is due to the different resistive characteristics of the electrodes, such as surface finishes, and surface areas.

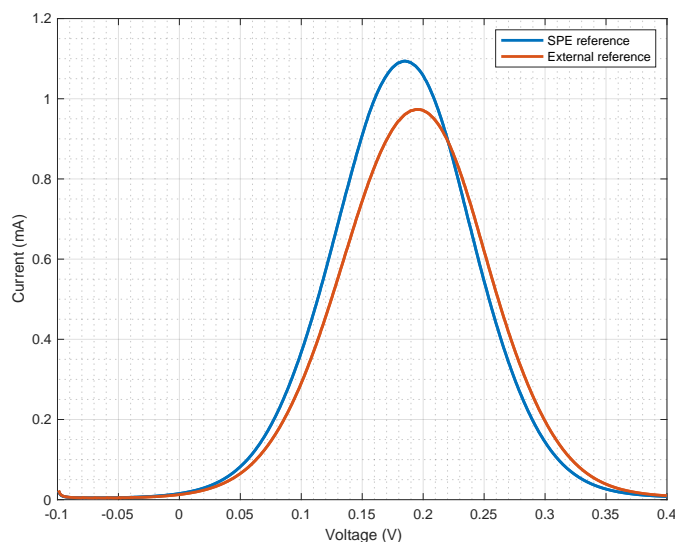


Figure 5.5: Calibration curve of various reference electrodes

5.2.0.2 Mercaptohexanol treatment

Unlike dsDNA, ssDNA's bases are exposed; among the exposed bases guanine and adenine moieties have been shown to be the most electroactive bases. These bases easily oxidize and adsorb onto gold surfaces [42]. MCH is used to prevent non-specific binding of ssDNA probes and target ssDNA, as well controlling the density of immobilized ssDNA probes by placing a spacer between the ssDNA probes and gold. Figure 5.6 shows the effect of treating the blank electrode with MCH before performing SWV. The electrodes are submerged in 1 mM of MCH for 1 hr. The MCH solution is made up with DI water. The SPEs are then thoroughly rinsed with DI water and dried at room temperature before the electrochemical measurements are taken. After the MCH treatment, the peak current decreased by 11.79% from 1.1 mA to 0.96 mA. Due to MCH acting as a blocking agent, the negatively charged MCH molecules repel the negatively charged $[\text{Fe}(\text{CN})_6]^{4-/3-}$ ions and thus reducing the peak current measured.

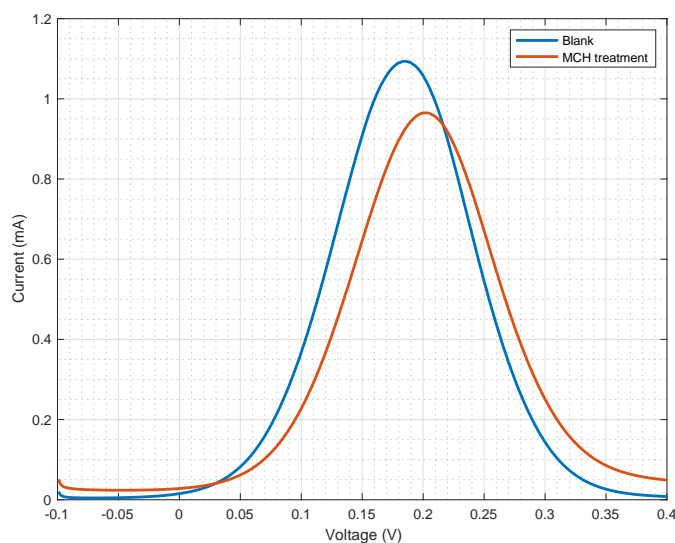


Figure 5.6: Calibration curve post MCH treatment

5.2.0.3 Ultrasonic treatment

To remove any debris from the SPEs they are placed in a beaker with ethanol and placed in the ultrasonic cleaner for 10 mins on a low temperature and high frequency. Figure 5.7 shows what occurs when the electrodes are ultrasonically treated in ethanol. The peak current decreases by 4.68% from 1.1 mA to 1.05 mA. The small change in the peak current can be due to the removal of unwanted contaminants on the electrode surface and thus giving way for more $[\text{Fe}(\text{CN})_6]^{4-/3-}$ ions to bind to the electrode surface.

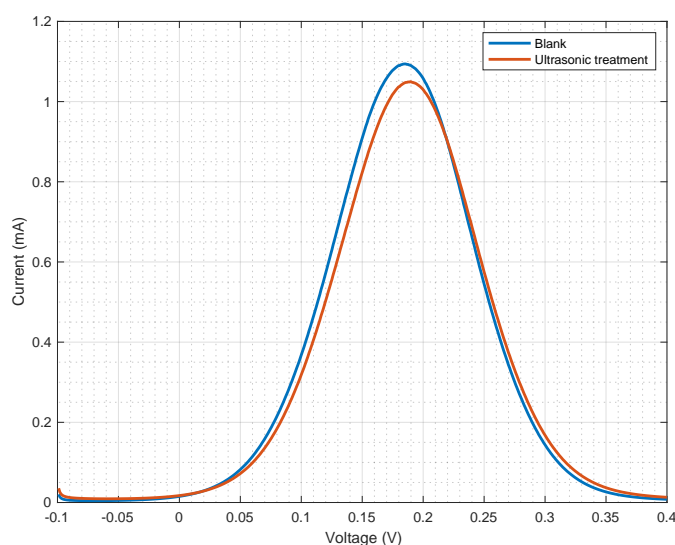


Figure 5.7: Calibration curve post ultrasonic treatment

5.2.1 Frequency

Various frequencies of the signal applied to sensor are tested in SWV. It is observed that the peak current increases as the frequency is increased as shown in Figure 5.8. Increasing the frequency increases the scan rate, which reduces the accuracy of each measurement, therefore only frequencies up until 50 Hz are tested.

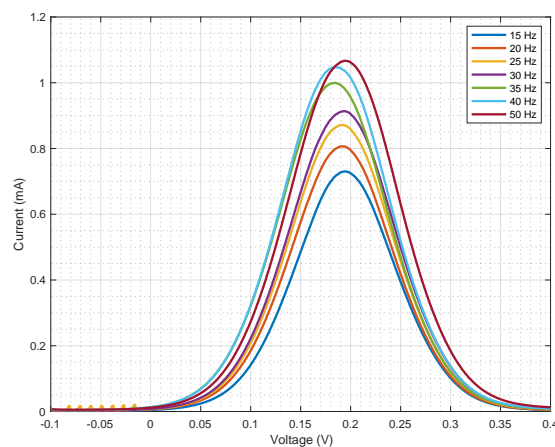


Figure 5.8: Peak currents (mA) of various frequencies

The repeatability of three different frequencies, 25 Hz, 35 Hz, and 50 Hz are tested. It is observed in Figure 5.9 that 50 Hz yields the most repeatable results.

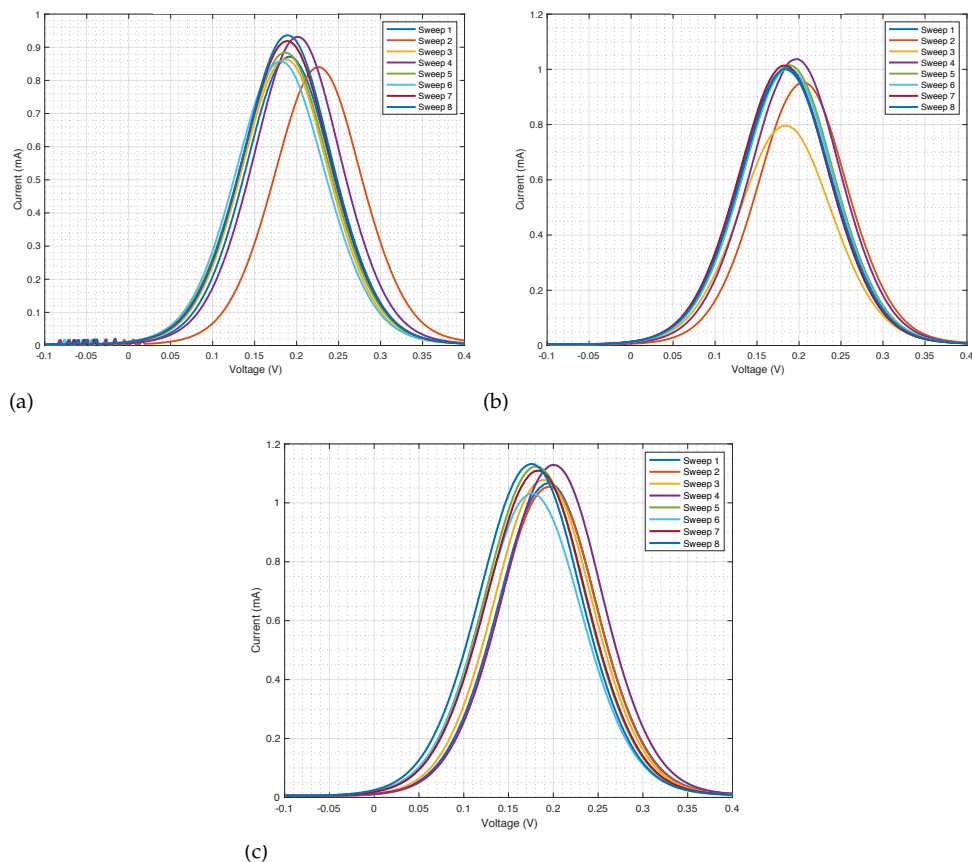


Figure 5.9: Repeatability of frequency (a) 25 Hz (b) 35 Hz (c) 50 Hz

5.2.2 Platinum auxiliary electrode

A comparison test is conducted between a SPE with gold as its CE and a SPE with platinum as its CE. Using a blank electrode submerged in the chosen electrolyte, SWV measurements are conducted on both electrodes. The average voltammetric peak currents are plotted and compared in Figure 5.10(b). Gold yields a higher peak current. It is expected that by loading the blank electrodes with DNA, the measured peak currents will decrease indicating binding is taking place. Therefore, it is beneficial to have a calibration curve with a high peak current in order to see the change more clearly.

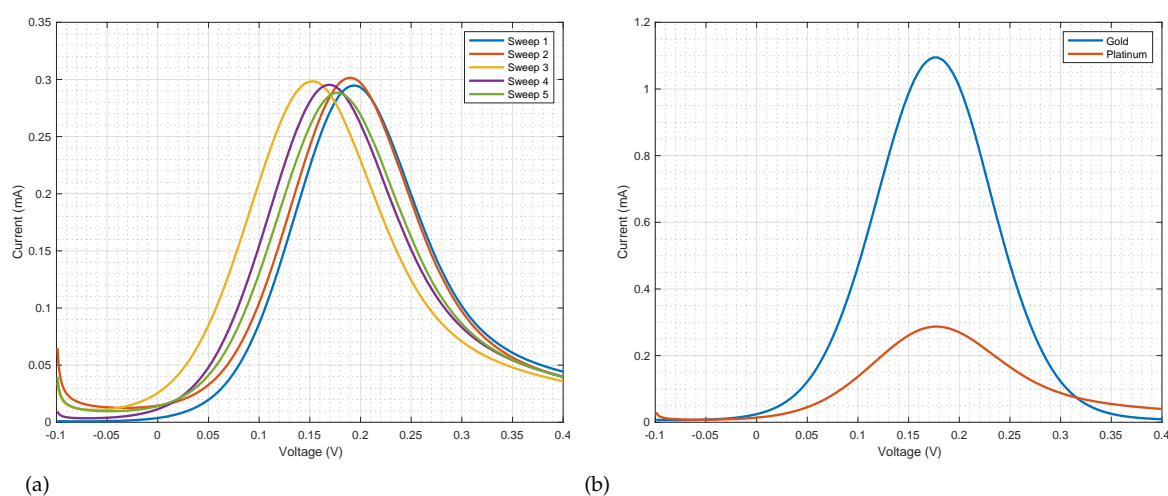


Figure 5.10: Calibration curve of various auxiliary electrodes (a) Platinum auxiliary electrode (b) Comparison of platinum and gold

5.3 ssDNA probe immobilization

An important step in the development of the DNA sensor is generating a recognition layer integrated with a transducer to detect the analyte. This section discusses the results from developing the SAM on the transducer through the immobilization of ssDNA probes on a gold SPE. Electrochemical and imaging techniques are used to confirm the development of the SAM. Concentrations of 0.01, 0.1, 1, and 10 μM of ssDNA probes are tested.

5.3.1 ssDNA probe concentration

Figure 5.11 shows the relationship between the peak current of a square wave voltammogram and the concentration of ssDNA probes immobilized onto a gold SPE. As the concentration of the ssDNA probes increase from 0.01 μM to 10 μM the peak current decreases. Each curve represents the average of three individual measurements taken. Two sensors immobilized with the same concentration of ssDNA probes are used to establish the working of the sensor.

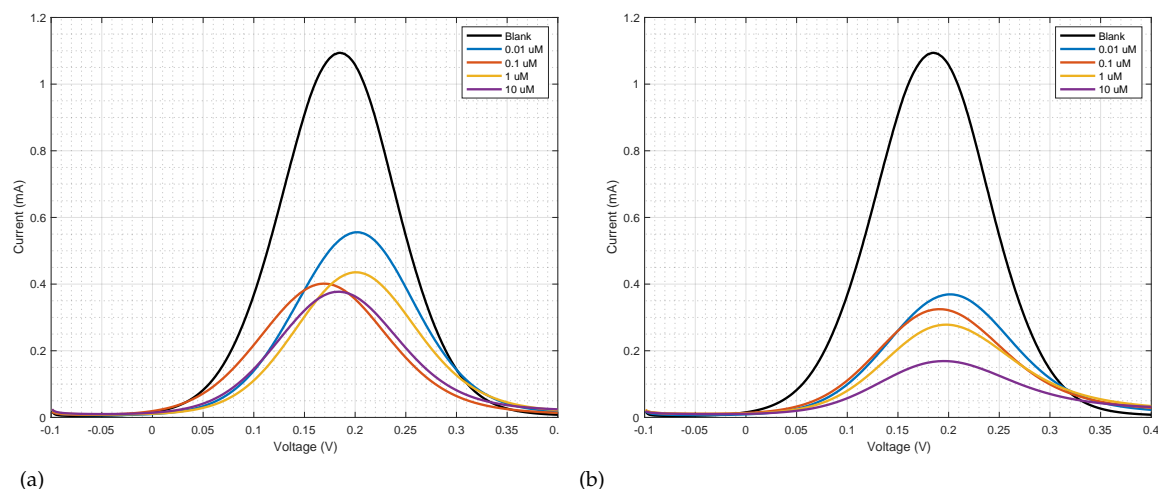


Figure 5.11: Change in peak current (mA) vs. change in DNA probes concentration (μM) (a) Sensor 1 (b) Sensor 2

The peak currents from the immobilization of the ssDNA probes are summarized in Table 5.2. The change in the concentration of the ssDNA probes are detected from the change in the peak current measured from the calibration curve of the blank sample. The results indicate that as the concentration of the ssDNA probes increase, the peak current decreases proportionally. There is a 57.6% decrease in peak current from the calibrated curve of the blank sample when the smallest concentration of 0.01 μM ssDNA probes are immobilized onto the SPE.

The decrease from the calibration curve increases with concentration to a 77.2% reduction in peak current when 10 μM of ssDNA probes are immobilized onto the SPE.

Table 5.2: Peak current of various ssDNA probes concentration

DNA probes (μM)	Sensor 1 (mA)	Sensor 2 (mA)	Average (mA)	Percentage decrease (%)
Blank	1.09	1.09	1.09	
0.01	0.56	0.37	0.46	57.6
0.1	0.40	0.32	0.36	66.7
1	0.43	0.28	0.36	67.3
10	0.38	0.17	0.25	77.2

5.3.2 TCEP

The thiol-modified ssDNA probes are not supplied with a free thiol at its 5' end. TCEP is used to break down the disulfide bond and expose the free thiol. The use of TCEP to increase covalent bonding of the DNA probes to gold is tested. TCEP is used as the test samples in the immobilization of ssDNA probes. Solutions without TCEP are used as the control samples. As shown in Figure 5.12, by incorporating TCEP into the ssDNA probes solution there is a decrease in the peak current, indicating an increase in binding between the ssDNA probes and the gold WE of the SPE. From the experiment it is shown that by adding TCEP to the ssDNA probes solution results in the decrease of the peak current by an average of 19.4% compared to the control samples without TCEP. The peak current is inversely proportional to the binding that takes place, therefore TCEP increases binding by 19.4%.

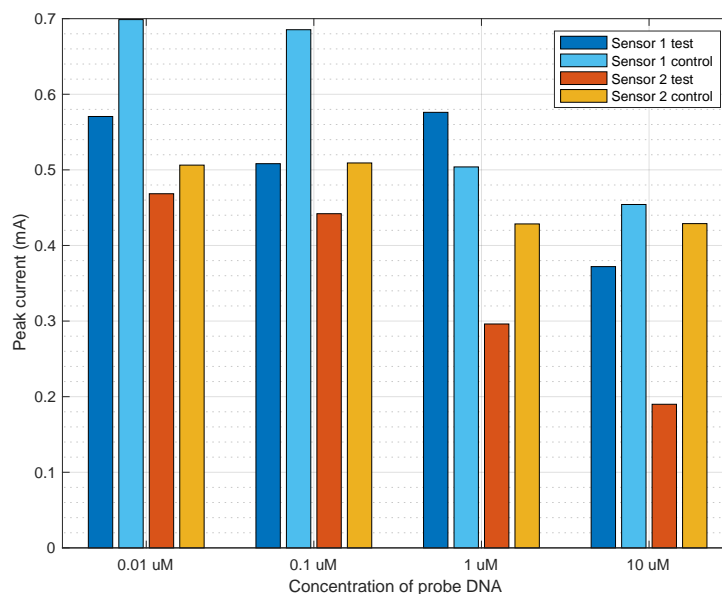


Figure 5.12: The influence of TCEP on immobilization of DNA probes

The change in peak current of each concentration of ssDNA probes are shown in Table 5.3. The results show the percental decrease in peak current between each control and test sample. The average of the percentage decrease between the control and the test samples are calculated from the table. The decrease in the peak current of the control samples, DNA samples without TCEP, is due to the non-specific binding of the exposed bases of the DNA and the disulfide bonds to the gold through adsorption [49].

Table 5.3: Decrease in peak current of test samples (TCEP) from control samples (without TCEP)

DNA probes (μM)	Sensor 1 (%)	Sensor 2 (%)	Mean (%)
0.01	18.35	7.49	12.92
0.1	25.85	13.18	19.52
1	-14.33	30.90	8.29
10	18.10	55.70	36.9

5.3.3 Repeatability of immobilization

To test the reproducibility of the sensor the repeatability of the immobilization step is determined. 1 μM of ssDNA probes are immobilized onto eight separate SPEs. Each of the SPEs are separately tested in a fresh batch of electrolyte solution under the same conditions. Square wave voltammograms of the test and control samples are shown in Figure 5.13. The mean peak current of the test samples is 0.63 mA with a standard deviation of 0.121 mA. The mean peak current of the control samples is 0.59 mA with a standard deviation of 0.131 mA. Comparing the

standard deviation of the test and controls it is shown that the test samples are more repeatable than the control samples.

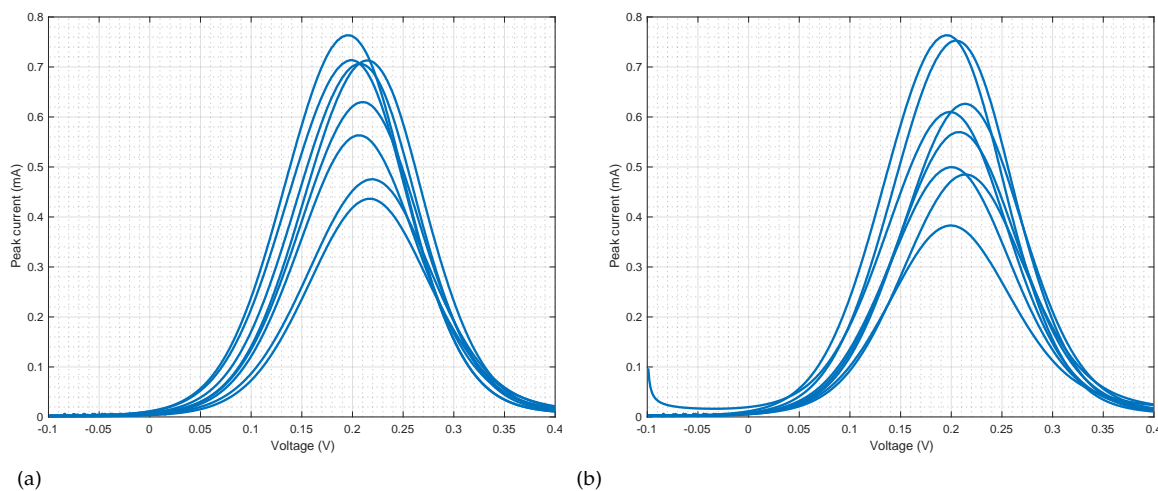


Figure 5.13: Voltammograms (a) 1 μM DNA probes (test samples) (b) 1 μM DNA probes (control samples)

5.3.4 Fluorescent microscopy

To investigate the binding of ssDNA probes to the gold surface through immobilization, fluorescent microscopy tests are done on the SPEs immobilized with ssDNA probes. Different nucleic acid stains are used for the experiment, these stains include GelRed, SybrSafe, GelStar, SmartGlow, and SybrGold. To ensure saturation of the stain onto the ssDNA probes, a dilution of 1:100 is used for all stains except the SMartGlow loading dye, which is diluted 1:5. The stains are prepared in TE buffer. 20 μL of the stain solution are pipetted onto the electrodes immobilized with ssDNA probes and incubated for 15 mins before thoroughly rinsed with DI water. The stains are light sensitive, therefore the experiment is performed in a dimly lit room. The fluorescent imaging is done with the Carl Zeiss Confocal LSM 780 Elyra PS1 with SR-SIM and PALM/dSTORM super-resolution platforms for multiple colour analysis. The experiment requires the use of many electrodes due to the many different stains tested and the multitude of samples that are repeatedly cleaned and re-used in the experiment. Therefore, it is decided to use IDEs for this experiment to investigate binding of the the ssDNA probes to the gold instead of single-use SPEs. The IDEs are reusable by removing the stain and immobilized probes in a UVO cleaner between experiments.

The experiment compares the immobilized test samples with the control samples, blank samples, and the test samples treated with MCH. The results of all samples stained with SmartGlow are shown in Figure 5.14. It is expected that

a high amount of brightly lit spots on the face of the electrode should show on the test sample and test sample treated with MCH, with slightly less spots on the control sample and none on the blank sample. However, the results from the experiment show little difference between the samples with all the stains tested. The brightly lit spots on the control sample in Figure 5.14 (b) and the test sample treated with MCH in Figure 5.14 (c) are contaminants and not related to the immobilized ssDNA probes.

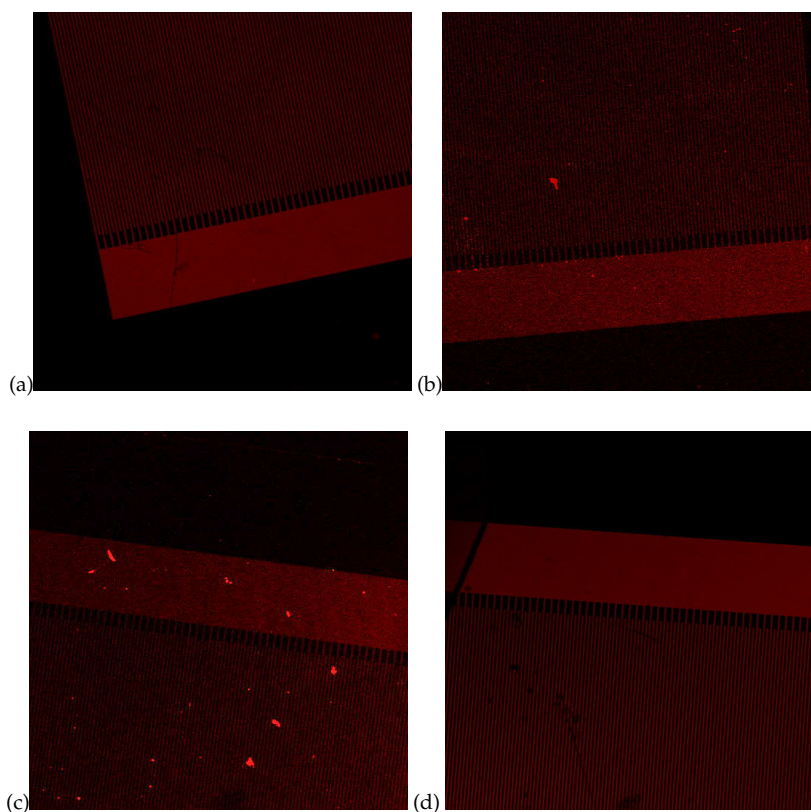


Figure 5.14: Fluorescent microscopy (a) Blank SPE sample (b) Immobilized DNA control sample (c) Immobilized DNA washed in MCH sample (d) Immobilized DNA test sample

5.3.5 Scanning electron microscopy

SEM surface imaging is another technique used to investigate binding of the ssDNA probes to the gold electrode surface. The Zeiss MERLIN SEM unit is used to take images. For this experiment the SPEs are used. IDEs are not suitable for this experiment due to the poor conductivity of the glass substrate, which result in low resolution imaging and electrostatic charging on the surface. SEM images of blank SPE samples, blank SPEs washed in a TE buffer samples, ssDNA probe test and control samples, and target ssDNA test and control samples are taken and

compared. There is no difference in the samples studied as shown in Figure 5.15. Reasons for the lack of evidence on the binding of DNA to gold can be due to the level of conductivity DNA has and the size of the DNA to be detected. ssDNA has an average theoretical width of 0.9 nm [58] and the Zeiss MERLIN SEM has a resolution of 0.8 nm @15kV, while the images were taken at a scale of 20 μm . At the time of the experiment, the limit of zoom was set to 20 μm , which is unsuitable to detect the extremely small DNA particles.

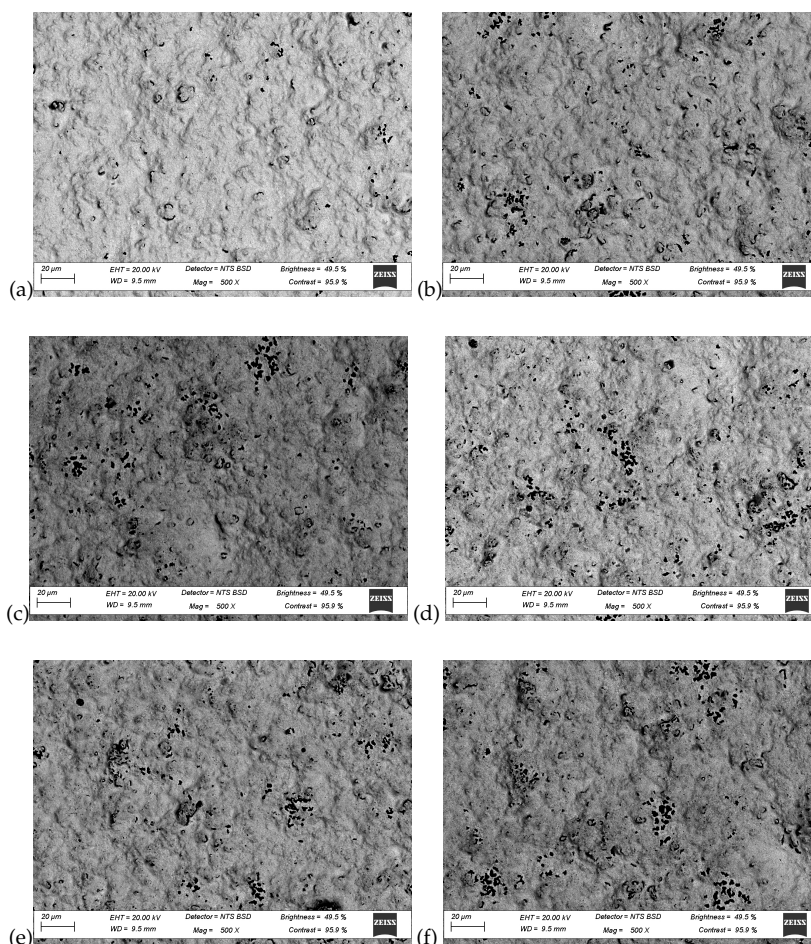


Figure 5.15: SEM imaging (a) Blank SPE (b) Blank SPE washed in TE buffer (c) Immobilized DNA control sample (d) Immobilized DNA test sample (e) Hybridized DNA control sample (f) Hybridized DNA test sample

To further explore DNA binding to gold through immobilization, energy dispersive x-ray analysis (EDX) analysis is performed on the SPEs. High levels of the element Fe (iron) are found on the surface of the gold as shown in Figure 5.16. It is assumed that these contaminants are present after thoroughly rinsing used SPEs in DI water after they are submerged in the electrolyte solution for electrochemical detection. The unsuccessful rinsing of the used SPEs, which results in the presence of Fe contaminants, is undesirable for repeated electrochemical activation of the

SPEs because during SWV, the migration of the Fe ions to the gold surface of the SPE is directly related to the peak current generated.

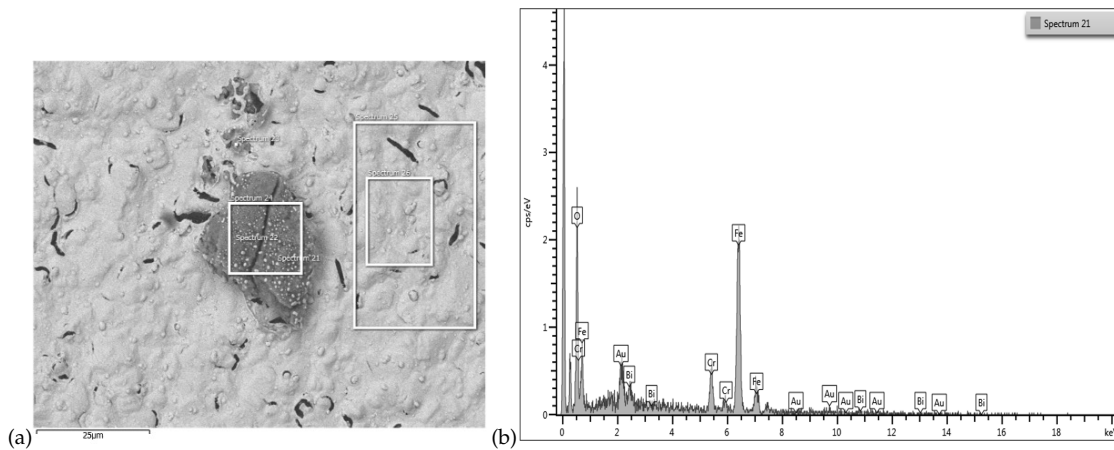


Figure 5.16: EDX analysis (a) Presence of contaminant (b) Elemental composition

5.4 Target DNA hybridization

Hybridization is the main principle of the DNA sensor. ssDNA probes immobilized on the transducer form a SAM. The SAM allows for the recognition of the ssDNA targets by the formation of dsDNA through the hybridization of the ssDNA probes and the ssDNA targets. The voltammograms in Figure 5.17 show the change in the measured peak current when various concentrations of ssDNA targets are hybridized with 1 μM of ssDNA probes immobilized onto a gold SPE. Small concentrations of ssDNA targets starting at 0.001 μM are tested up until 0.5 μM . The experiment is repeated on three separate sensors. Each curve represents the average of three individual measurements for each concentration.

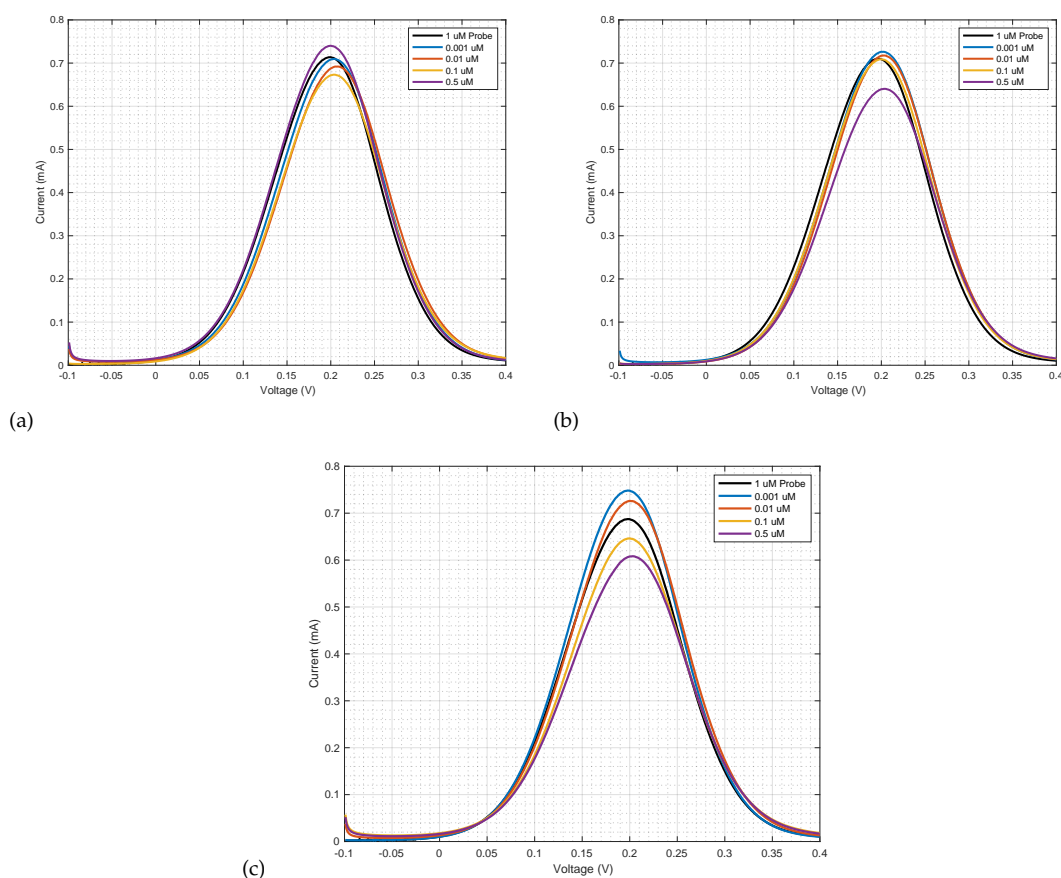


Figure 5.17: Hybridization of target DNA (a) Sensor 1 (b) Sensor 2 (c) Sensor 3

The results from Figure 5.17 indicate a trend that, as the concentration of the ssDNA targets increases, the peak current of the square wave voltammogram decreases. This is used as the method of detection for the DNA sensors. The change in current is also an indication of the successful hybridization of the ssDNA targets to the immobilized ssDNA probes. Free guanine and adenine moieties on the ssDNA probes interact with thymine and cytosine bases of the ssDNA targets

through the hybridization process. The hybridization process results in less free guanine and adenine moieties of the ssDNA probes to undergo redox activities. The increase in the negative charge resulting from the formation of the dsDNA repel more Fe ions away from the electrode. These activities cause a reduction in the peak current [42].

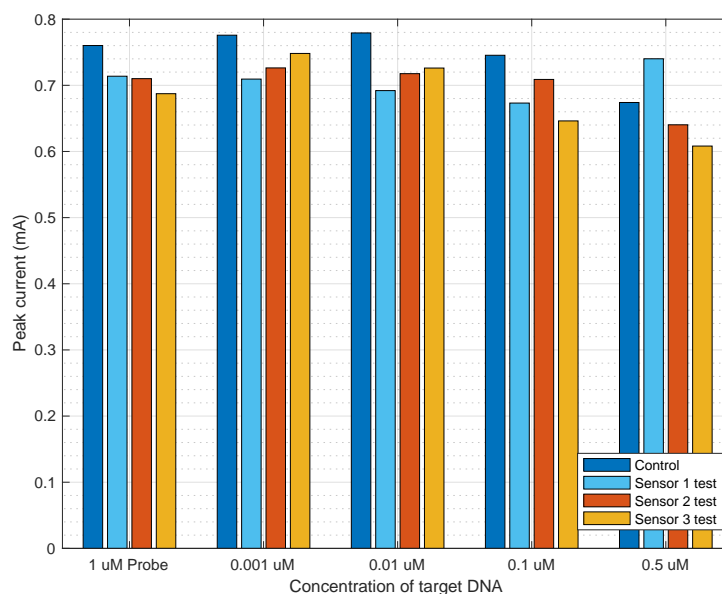


Figure 5.18: Peak current of target DNA concentration

Table 5.4: Change in peak current of target DNA from 1 μ M monolayer

Target DNA (uM)	Control (mA)	Sensor 1 (mA)	Sensor 2 (mA)	Sensor 3 (mA)	Mean decrease (%)
1 Probe	0.7602	0.7138	0.7101	0.6873	
0.001	0.7758	0.7094	0.7263	0.7482	-3.51
0.01	0.7792	0.692	0.7176	0.7261	-1.22
0.1	0.7454	0.6732	0.7089	0.6462	3.83
0.5	0.674	0.7401	0.6403	0.6082	5.88

Figure 5.18 and Table 5.4 compares the peak currents of the square wave voltammograms between the control samples and the test samples when the SPEs are loaded with increasing concentrations of the ssDNA targets. It is concluded that the control sample generally generates a larger peak current, indicating that less hybridization takes place due to the absence of ssDNA probes to hybridize with.

When the sensor is loaded with 0.001 μ M of ssDNA targets, there is an average increase of 3.51% in the peak current among the three test samples instead of a decrease from the base peak current of the 1 μ M of ssDNA probes. The increase

in the peak current after hybridization of 0.001 μM ssDNA targets with the 1 μM of ssDNA probes is an indication of the detection limit. The peak current has a tendency to increase after every SWV sweep as shown in Section 5.5. Therefore, 0.001 μM of ssDNA targets are too small to detect and causes a decrease in the peak current after SWV. When 0.01 μM of ssDNA targets are hybridized with the ssDNA probes, there is 1.22% increase instead of a decrease in the peak current for the same reasons there is an increase in the 0.001 μM of ssDNA targets. When 0.1 μM of ssDNA targets are hybridized with the ssDNA probes there is 3.83% decrease from the peak current of the 1 μM ssDNA probes. The change in the peak current from an increase to a decrease as the concentration of the ssDNA targets increases is an indication that the sensor is able to detect ssDNA targets with a concentration of 0.1 μM or higher. When 0.5 μM of ssDNA targets are hybridized with the ssDNA probes, there is 5.88% decrease from the peak current. The decrease in the peak current from hybridization is proportional to the increase in concentration of the ssDNA targets.

5.5 SWV time dependence

Throughout the design of the DNA sensor, it is observed that the repeatability of SWV measurements are difficult to achieve. Therefore, the following experiment investigates the effect repeated electrochemical activation of the SPEs has on the peak currents generated. Figure 5.19 represents the peak currents of square wave voltammograms taken at 15 s intervals in the same electrolyte solution without washing the SPEs after each measurement. It is to be noted that this experiment is not designed to determine concentration, therefore the difference in concentration between the different samples are not important, but rather the behaviour of the peak current over time.

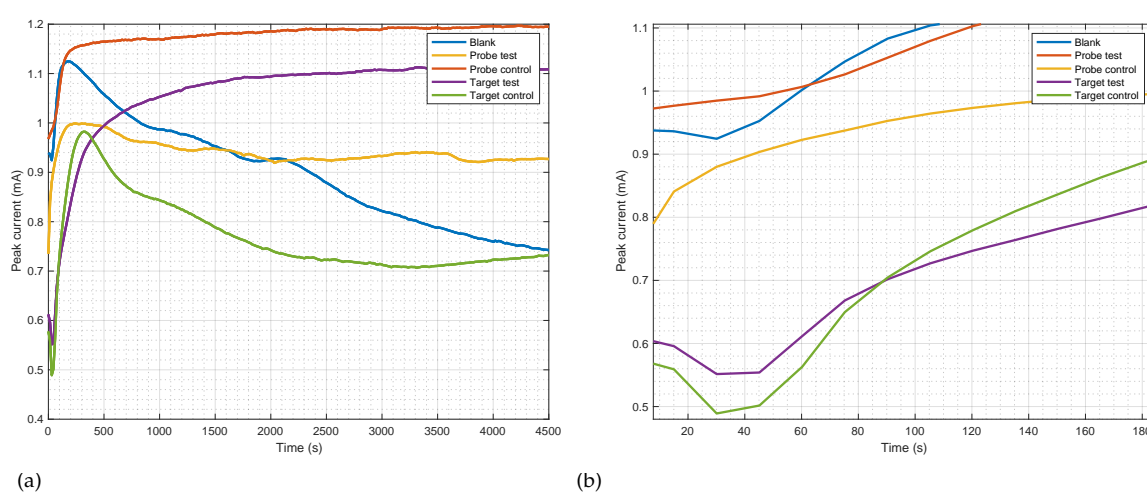


Figure 5.19: Peak currents (mA) vs time (s) (a) Time 0-4500 s (b) Time 0-185 s

Table 5.5 highlights the important current and time stamps of the curves in Figure 5.19. The general trend of the curves in Figure 5.19 show an overall increase in peak current for the first 350 s, the increase is due to the accumulation of Fe molecules on the SPE as a result of the redox reaction. After saturation of Fe molecules on the SPE, most of the samples' peak currents start to reach steady state after 350 s and in some cases starts to decline. For the first three measurements under 40 s, there is a decrease in the peak current for all samples except the ssDNA probes test and control samples. This decrease in peak current can be due to fouling on the electrode surface, an accumulation of product from the electrochemical reaction that forms an impermeable layer on the electrode surface. Electrode fouling can be removed by repeated electrochemical activation. After three cycles of electrochemical activation, at 30 s there is an increase in peak current due to Fe molecules reaching the electrode surface. It is assumed that for both the probe and target ssDNA test samples, the peak current will eventually decrease due to

over-saturation of the electrode surface with Fe molecules, similar to the other samples. The reason that saturation takes longer for these test samples is because DNA has negatively charged phosphate backbones, which repel the negatively charged Fe molecules, and these test samples have more DNA immobilized onto the electrodes.

Table 5.5: Key parameters of repeated SPE electrochemical activation

Sample	Start peak current (mA)	Saturation peak current (mA)	End peak current (mA)	Saturation time (s)
Blank	0.94	1.12	0.74	165.55
Probe test	0.97	1.16	1.19	210.70
Probe control	0.74	1.00	0.93	210.7
Target test	0.61	1.09	1.11	1715.72
Target control	0.58	0.98	0.73	331.10

5.6 Potentiostat

This section highlights the results from the development of the potentiostat through the processes described in Chapter 4 .

5.6.1 Digital to analog converter output waveform

The combination of a stair and step wave to form a stair-step waveform is done using an Arduino which interfaces with the external DAC. The results of the desired waveform that is output from the DAC are shown in Figure 5.20. Figure 5.20(a) shows the amplitude of the stair-step wave, which is shown to have an amplitude of 50 mV as set by the DAC. Figure 5.20(b) shows the desired frequency of 50 Hz for the stair-step wave. Figure 5.20(c) shows that the DAC can output the waveform with a step of 10 mV as set by the DAC. Figure 5.20(d) indicates the start and stop potential of the waveform. The start potential is 0 mV and the stop potential is 400 mV.

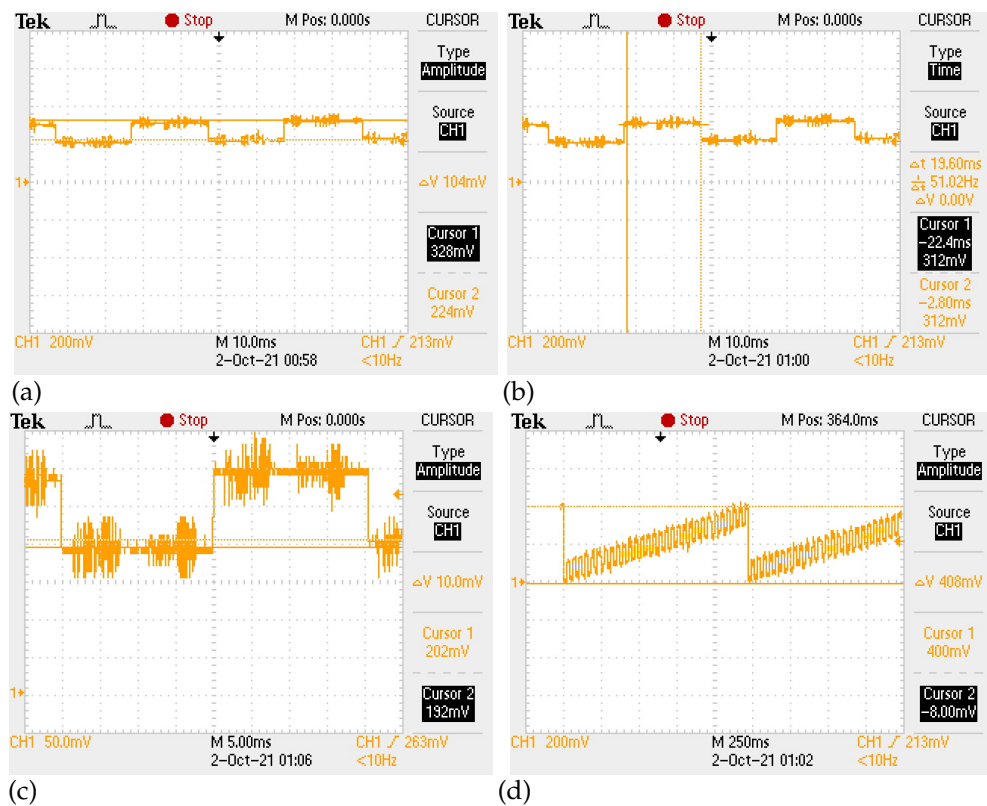


Figure 5.20: Oscilloscope screenshots of the stair-step waveform generated (a) Amplitude (b) Frequency (c) Step size (d) Start and stop potential

5.6.2 Transimpedance amplifier test

5.6.2.1 Biasing of the operational amplifier

A change in biasing voltage that is applied to the op-amp in the transimpedance amplifier affects the output voltage. Various voltages ranging from 1 V to 3.5 V are applied to the positive terminal of the op-amp. By applying these voltages to the positive terminal, the negative terminal is biased to the same potential. Figure 5.21 shows the output voltage recorded.

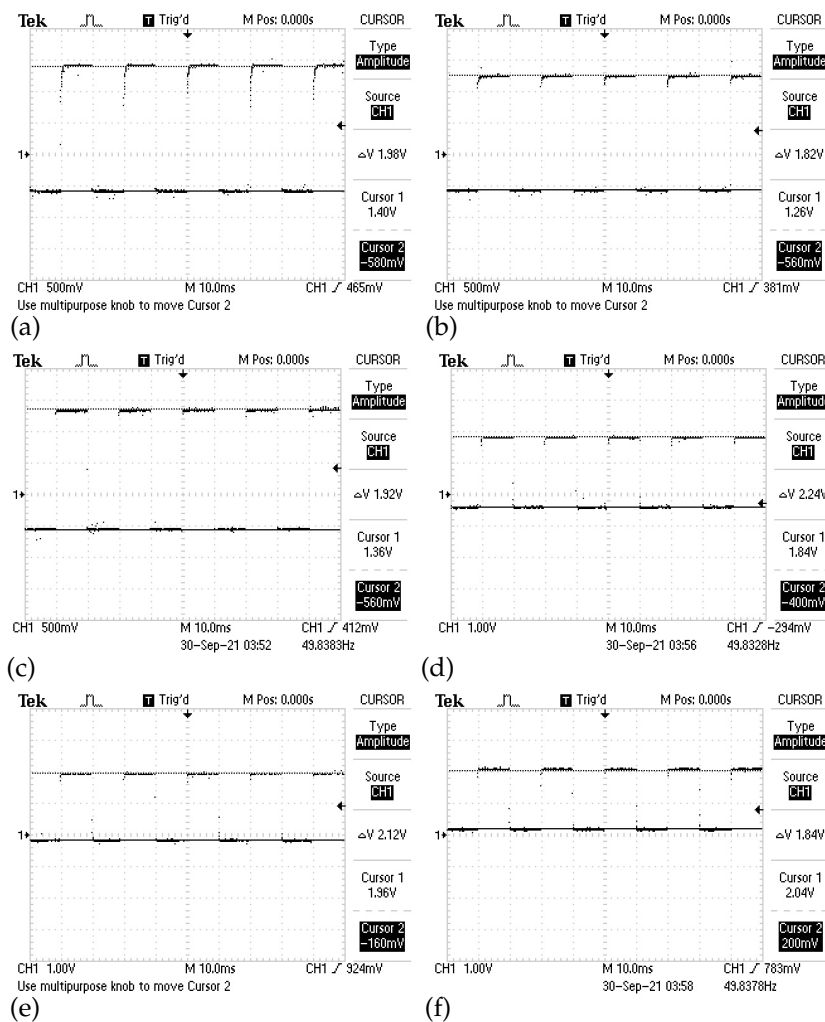


Figure 5.21: Oscilloscope screenshots of the transimpedance output with various biased input voltages (a) 1 V (b) 1.5 V (c) 2 V (d) 3 V (e) 3.3 V (f) 3.5 V

Table 5.6 summarises the results of Figure 5.21. The ADC on the Arduino can only process positive potentials, therefore when biasing the transistor, it is important to make sure that the output potential is positive. Lower biased voltages result in negative output voltages. As the biased voltage increases, the output voltage increases. At a biased voltage of 3.5 V, the output voltage reaches a positive voltage of 200 mV for its lower potential. Therefore, a voltage of 3.5 V is chosen as the biased voltage for the transimpedance amplifier.

Table 5.6: Transimpedance voltage biasing

Biased voltage	Vout max	Vout min
1 V	1.4 V	-580 mV
1.5 V	1.26 V	-560 mV
2 V	1.36 V	-560 mV
3 V	1.84 V	-400 mV
3.3 V	1.96 V	-160 mV
3.5 V	2.04 V	200 mV

5.6.2.2 Current measurement on 3V simplified wave

To test the working of the transimpedance amplifier, a simple 3 V step wave is applied to the sub-circuit and the results are compared with a Spice simulation. The sub-circuit only comprises of the transimpedance amplifier and dummy cell without the control amplifier, DAC, and Arduino. For this test, a simple $1\text{k}\Omega$ precision resistor is used as the dummy cell. The circuit simulated in Spice is shown in Figure 5.22.

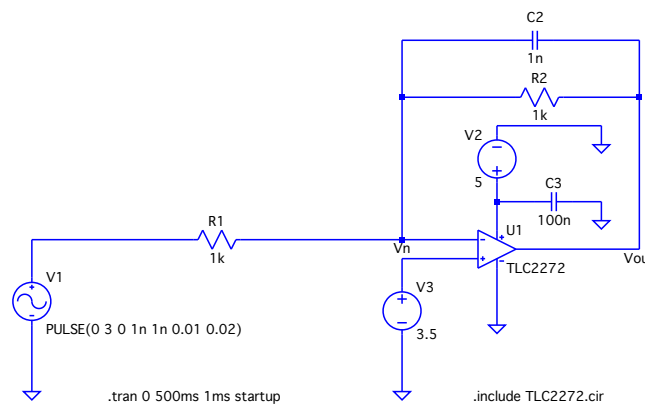


Figure 5.22: Spice simulation of 3 V

The voltage V_n of the actual circuit is compared with the Spice simulation in Figure 5.23. The spice simulation has a lower potential of 2.18 V and an upper potential of 3.5 V, compared to the actual potential of 2.2 V and 3.52 V. The error between the upper potential and lower potential is 0.92% and 0.57%.

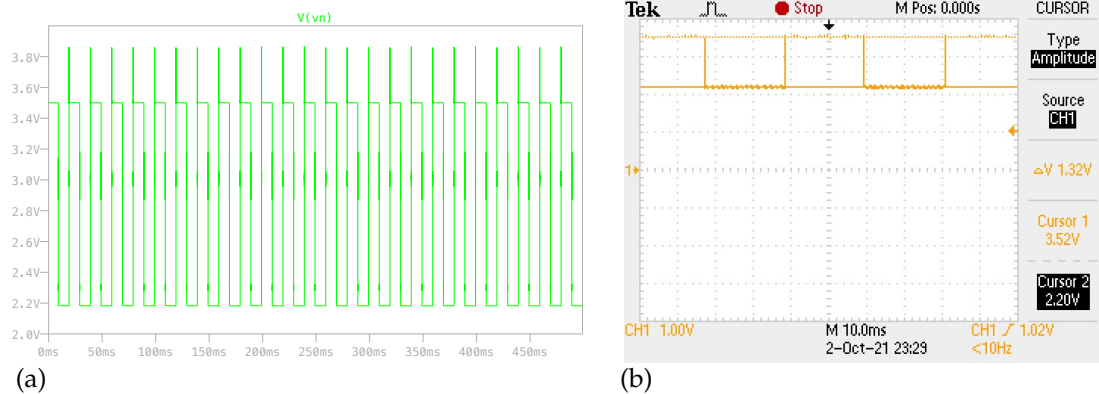


Figure 5.23: Transimpedance input V_n (a) Spice model (b) prototype

Voltage V_{out} of the actual circuit is compared with the Spice simulation in Figure 5.24. The Spice simulation has a lower potential of 4 V and an upper potential of 4.36 V, compared to the actual potential of 3.92 V and 4.32 V. The error is therefore calculated as 2% and 0.92%.

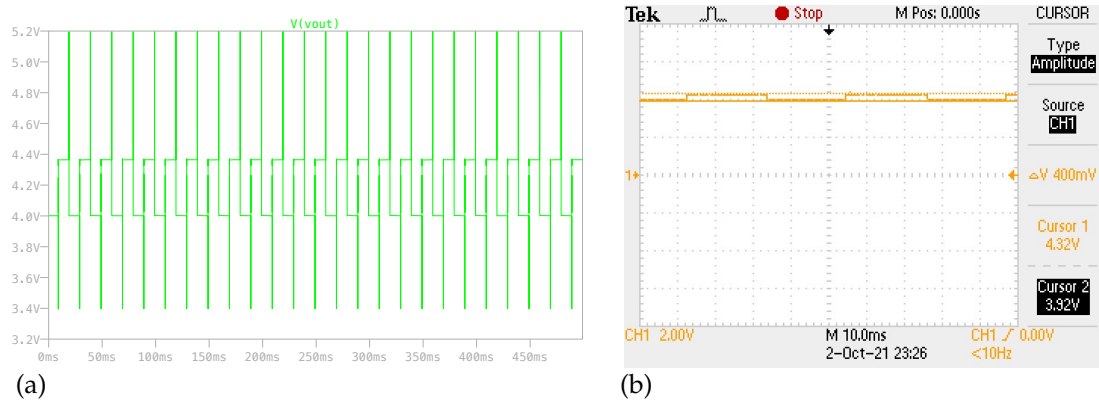


Figure 5.24: Transimpedance output V_{out} (a) Spice model (b) prototype

5.6.3 Full circuit current test

The entire circuit is tested with a dummy cell and compared with its corresponding Spice model and against a working commercial potentiostat. The potentiostat used in the tests is the PalmSens 4.

5.6.3.1 1 k Ω precision resistor dummy cell

The first test compared the designed potentiostat against its simulated Spice model when a 1 k Ω precision resistor as the dummy cell. A comparison of the current through the cell is shown in Figure 5.25. The current in the cell below includes both the forward and reverse current sampled at the last 25% of the pulse from the

input waveform. The peak difference between the forward and reverse currents of the simulated design and the prototype design are respectively 83.5 mV and 130 mV.

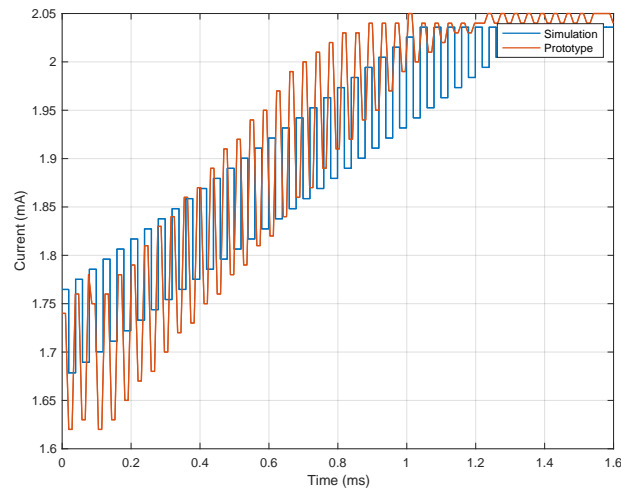


Figure 5.25: Output current of Spice model and prototype design

Figure 5.26 includes the forward and reverse currents of the commercial potentiostat, Palmsens 4. The current measured using the Palmsens 4 is much lower than that of the simulation and the prototype design as seen in Figure 5.26(a). This is due to the biased potential of the op-amp of the transimpedance amplifier. The results from Figure 5.26(a) are from the simulated and prototype design, where the biased voltage of the op-amp in the transimpedance amplifier is set at 3.5 V. By biasing the op-amp at 1.2 V, the simulated current matches that of the Palmsens 4 as shown in Figure 5.26(b). Both the Palmsens 4 and the simulated design have a peak difference between the forward and reverse current of 200 mV. It can be assumed that biasing the prototype at 1.2 V will change the measured current through the 1 k Ω resistor to match that of the commercial potentiostat text¹.

¹Due to time-constraints, analysis of the data was done away from the experimental setup. Therefore, it was only later found that changing the biased voltage will improve the working of the potentiostat

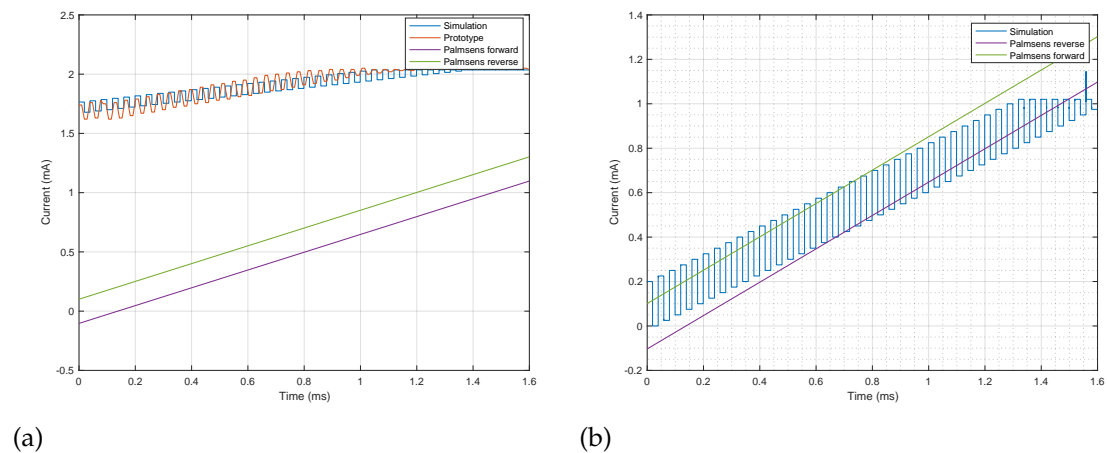


Figure 5.26: Output current (a) Spice and prototype model biased at 3.5 V (b) Spice model biased at 1.2 V

Figure 5.27 shows the current measured in the $1\text{k}\Omega$ dummy cell when a negative and positive voltage sweep is applied to the cell. The figure compares the Spice simulation and the prototype design. The figure indicates that the prototype follows the simulated results closely. By applying both a positive and negative voltage sweep to the cell, a peak current is able to be measured. Further calibration of the prototype is recommended to reduce the error between the prototype and the Spice simulation.

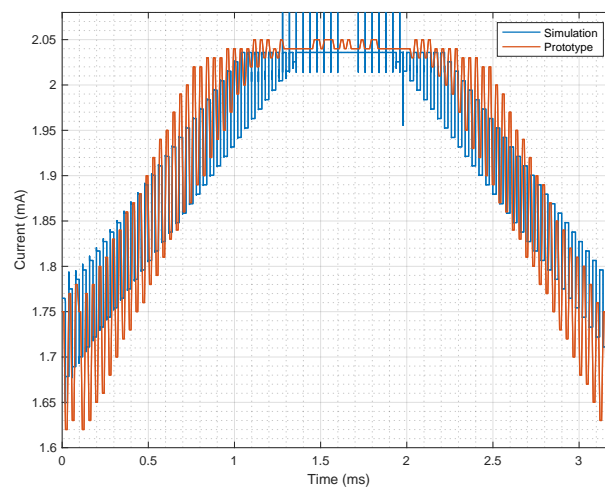


Figure 5.27: Output current when a positive and negative voltage sweep is applied

5.6.3.2 Randles circuit dummy cell

To further investigate the working of the prototype design beyond the $1\text{k}\Omega$ precision resistor as a dummy cell, the prototype is tested on a Randles equivalent circuit. A Randles circuit is one of the most common cell models used in electro-

chemistry and electrochemical impedance spectroscopy. It consists of an active electrolyte resistance in series with a parallel combination of an double-layer capacitor and an impedance of a faradaic reaction [59].

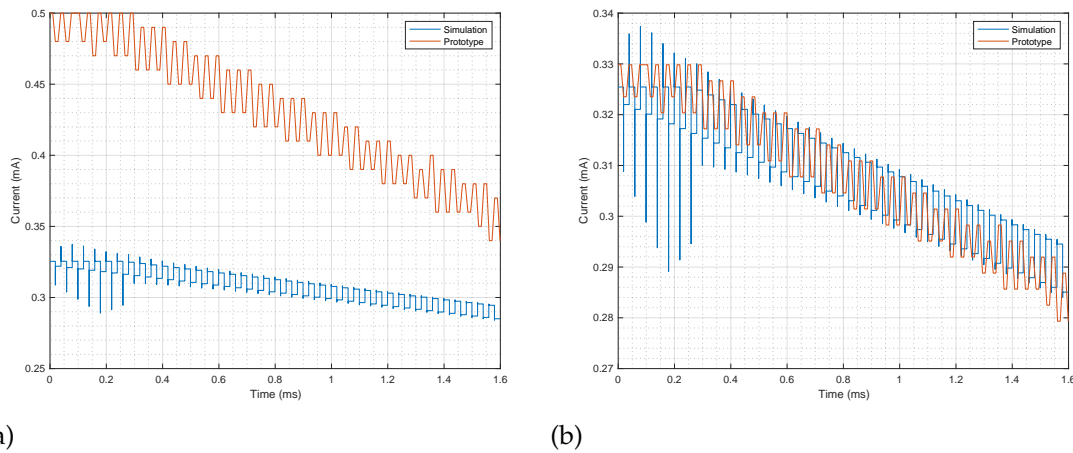


Figure 5.28: Output current with Randles circuit dummy cell (a) Uncalibrated prototype (b) Calibrated prototype

Figure 5.28 compares the prototype design to the simulated model when a stair-step wave is applied to a Randles equivalent dummy cell. Figure 5.28(a) shows the uncalibrated prototype compared to the Spice simulation. The uncalibrated prototype's measured current and the simulated current are non-identical. By calibrating the ADC measured values on the prototype design as shown in Figure 5.28(b), the measured current more accurately fits that of the simulated current.

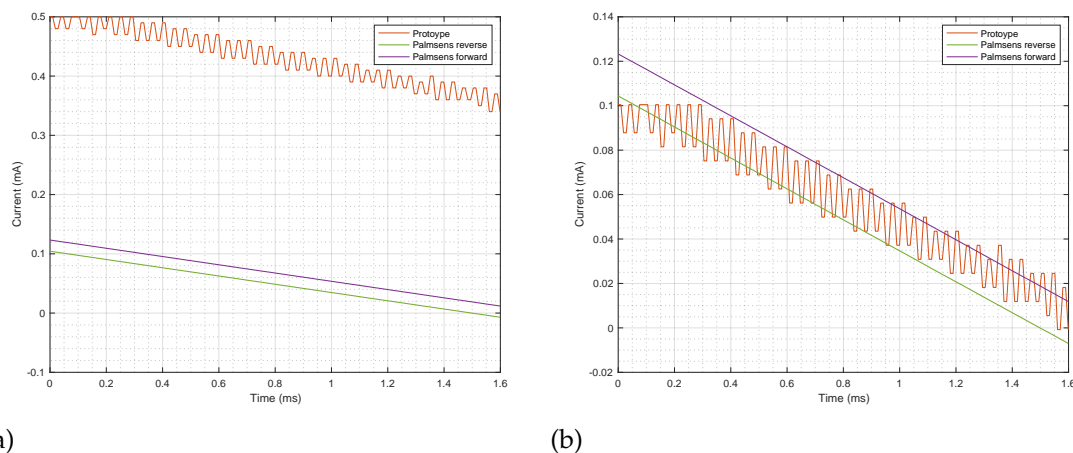


Figure 5.29: Output current (a) Uncalibrated prototype, (b) Calibrated prototype

Figure 5.29 compares the output current of the prototype and a commercial potentiostat. The measured current from the prototype is not identical to the forward and reverse currents of the commercial potentiostat. By calibrating the

ADC values that is measured in the prototype design, the measured current follows the current measured using the commercial potentiostat.

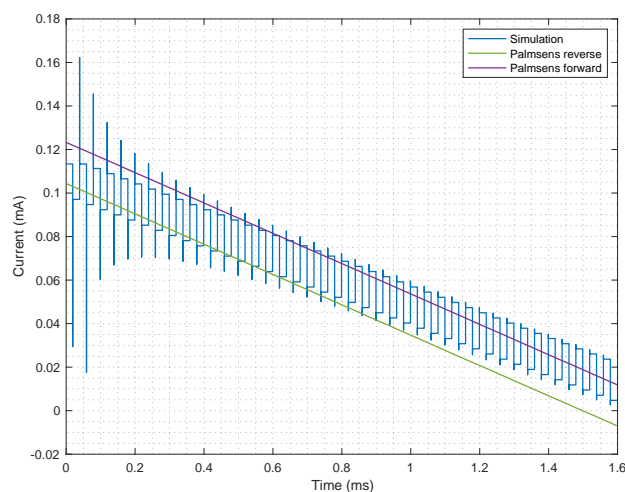


Figure 5.30: Output current of Spice simulation and commercial potentiostat

Figure 5.30 compares the output current of the commercial potentiostat to that of the Spice simulation when the biased voltage of the transimpedance amplifier is adjusted from 3.5 V to 1.2 V. By adjusting the biased voltage it is shown that the proposed design works as well as a commercial potentiostat. The difference between the forward and reverse currents of both the commercial potentiostat and the Spice simulation is 10 μA .

5.7 Summary

The first experiment investigated various concentrations of the electrolyte solution, the results indicate that 10 mM potassium ferrocyanide in 100 mM potassium chloride is the optimal concentration. The relationship between the peak current of the square wave voltammogram is found to be proportional to the concentration of the background electrolyte (potassium chloride). The cyclic voltammogram indicated that the redox reaction of the electrolyte solution is reversible.

A calibration curve is established for the biosensor by averaging multiple square wave voltammograms of the blank gold SPE in the electrolyte solution. The calibration curve has a peak current of 1.1 mA. The calibration curve is investigated under various circumstances. These include using an external reference electrode, treating the electrode with MCH, pre-treating the electrode with an ultrasonic treatment, changing the frequency of the applied stair-step wave, and using a platinum auxiliary electrode. The results indicate that using an external reference

electrode, treating the electrode with MCH or an ultrasonic cleaning decreases the peak current. A frequency of 50 Hz is chosen due its increased peak current. A comparison between gold and platinum as the auxiliary electrode show that gold yields a higher peak current.

The peak currents of square wave voltammograms are investigated when a gold electrode is immobilized with different concentrations of ssDNA probes. DNA solutions with TCEP are compared against a control sample, which is DNA solutions without TCEP. The results indicate a proportional relationship between the peak current and the concentration of the immobilized ssDNA probes. As the concentration of the immobilized ssDNA probes increase, the peak current decreases. TCEP is shown to increase the repeatability of the immobilized ssDNA probes and to increase binding of ssDNA probes to gold during the immobilization procedure. To further investigate binding, fluorescent microscopy, SEM, and EDX analysis is performed on the immobilized DNA on gold. The results from the visual analysis do not confirm binding.

The detection of the analyte (ssDNA targets) is done by comparing the peak currents of the square wave voltammograms of various concentrations of ssDNA targets to 1 μM of immobilized ssDNA probes. The results indicate that there is a proportional relationship between the concentration of the ssDNA targets and the peak current. As the concentration increases the peak current decreases. A LOD of 0.1 μM of ssDNA targets is seen. Concentrations smaller than the LOD are unable to be detected. The reason is investigated by performing multiple SWV measurements on the same electrode over 4500 s. The results indicate that repeated activation of an electrode increases the amount of electrode fouling, which reduces accuracy.

The potentiostat is tested and the results indicate that it is able to apply SWV to the sensor and sample the resulting current. Oscilloscope readings on the output of the DAC show that the measured applied stair-step wave matches the desired wave. The biased voltage of 3.5 V of the transimpedance amplifier is shown to result in a positive output voltage, which is required for the ADC. The Spice simulation of the transimpedance amplifier is compared to the experimental setup. An error between the output voltage, V_{out} , is found to be 2% and 0.92% for the lower and upper potential limit. A full circuit test is conducted using a 1 k Ω precision resistor, and a Randles circuit as the dummy cell. The results are compared against a commercial potentiostat and the Spice simulation. It is found that by changing the biased voltage to 1.2 V increases the accuracy of the forward and reverse currents compared to the commercial potentiostat. Calibration of the

ADC is also found to increase the accuracy.

The results from the experiments performed on the sensor and the potentiostat indicate the successful development of an electrochemical biosensor to measure the concentration of ssDNA.

Chapter 6

Discussion

6.1 Introduction

NCDs burden society and particularly low- and middle-income countries, as they often go undetected and undiagnosed. Around 41 million people die every year from NCDs. Early detection of diseases such as cancers and neurodegenerative diseases can save lives and lessen the dependence on health care systems, societies, friends, and families. Autophagy flux provides an important measure to detect these diseases and monitor their progression. Autophagy flux is also a useful tool to monitor the general health of not only patients suffering from diseases, but also everyone else. Autophagy flux may be a good indicator of health which generally fluctuates with changing exercise programs, diet, and sleep. However, there is no technology on the commercial market to date that can monitor autophagy flux and not only indicate whether the autophagic process is taking place. The development of low cost biosensors is the key to rectify the disproportionate access to diagnostic systems in low-and middle-income countries. Autophagy related biomarkers such as LC3-II offer new methods to detect certain autophagy related diseases such as Alzheimer's disease, breast cancer, as well as monitoring overall general health.

6.2 Overview of the project

In this study an electrochemical DNA biosensor is developed to detect and measure autophagy flux. cDNA of mRNA that encodes LC3-II is used in the sensor instead of mRNA. ssDNA probes are immobilized through covalent bonding onto a gold SPE to act as a recognition layer for the target. The ssDNA probes are designed to be complementary to the ssDNA targets. The analyte (ssDNA targets) are detected and measured when they hybridize with ssDNA probes. Using SWV, the

concentration of the ssDNA targets are measured directly from the peak current generated in SWV.

The simple implementation of immobilization of the ssDNA probes results in a measured peak current that decreases as the concentration of the ssDNA probes increases. When the target ssDNA hybridizes with the immobilized ssDNA probes, there is a further reduction in the peak current measured. This is in line with previous studies, which utilized the hybridization reaction to measure an analyte. One study used a SAM of thiolated DNA probes as sequence-specific electrochemical sexually transmitted disease sensor to detect target opa gene for detection of Gonorrhoea [60]. Another study which designed a selective electrochemical biosensor to diagnose breast cancer also implemented a SAM of thiolated ssDNA immobilized onto a gold electrode [61]. Although both studies characterized the biosensor using differential pulse voltammetry (DPV), the increased target concentration resulted in a decrease in peak current against the applied potential. Incorporating TCEP in the DNA solution resulted in a dramatic change in the peak current measured through SWV by increasing the amount of immobilized ssDNA probes through the specific binding of Au-S. This is consistent with literature [62].

A surprising finding in this study that is not recorded in this paper is the effect of MCH on hybridization efficiency. Peak currents generated from SWV of the sensor that is treated with MCH before the hybridization reaction had little difference from the sensor that is not treated with MCH. The reason MCH has little effect on hybridization may be due to the length of the ssDNA probes, which are short, therefore are stable enough to maintain a good orientation. Thiol modified DNA are also shown to generate an upright orientation compared to other linkers. The highly specific interaction of the ssDNA probes with the ssDNA target render the need for MCH unnecessary.

Gold SPEs are chosen as the transducer due to the strong affinity of thiolated DNA to bind to gold through the covalent S-H bond. SPEs are disposable and not intended for repeated use. This placed a limitation on the project. Characterization of the sensor requires repeated measurements of the immobilization and hybridization steps to establish a mean peak current for every concentration of ssDNA probes and ssDNA targets. To ensure that the gold substrate does not take part in the measurement process, unused SPEs are used for every iteration of the process. This led to the use of many SPEs, which increased the cost of the project as well delays in the completion of the project as new SPEs had to be ordered. Reusable SPEs were not available to use with voltammetric techniques such as SWV. A three-electrode configuration is required to ensure that the current and

potential characteristics of the WE is only measured and not the entire cell. A CE is required to ensure that no current is passed through the RE. Therefore, to save on the use of SPEs, IDEs are used in the fluorescent microscopy test. The surface conditions of the gold are similar and no electrochemical measurement is required for the test.

The project was also limited by the amount of ssDNA targets available. The volume of the ssDNA target solution only allowed of maximum concentration of 0.5 μM for use in the sensor. This is considerably small compared to the maximum concentration of 10 μM of ssDNA probes. Therefore, the change in the measured peak current by hybridization of small concentrations of ssDNA target are small, but can be increased to a more distinct change by comparing the effects of larger concentrations of ssDNA targets.

Reproducibility of measurement results were the biggest problem in this study. This is partly due to the changing environmental conditions within which the experiment took place, the lack of control in reproducing the same density of immobilized ssDNA probes, as well as the use of single-use SPEs. For future studies, the manufacturing of reusable SPEs for voltammetry measurements is recommended. The project was limited by the small concentration of ssDNA targets available. Future research should ensure that there is enough volume of a high concentration of ssDNA targets to understand the range of detection of the biosensor. The sensitivity of the sensor can be increased by additional steps. To increase the amount of immobilized ssDNA probes, the transducer surface can be functionalized with AuNPs. This increases the surface area of the transducer to allow area for more ssDNA probes to form a SAM with a controlled density. Sensitivity of the measurement can also be increased by including a redox indicator to the system. Methylene blue is recommended, as it specifically binds through intercalation to dsDNA with a stronger affinity than to ssDNA [63]. Incorporating a redox indicator to the sensor will change the biosensor from a label-free system to a labeled system.

6.3 Conclusion

This study successfully developed an electrochemical DNA biosensor to detect and measure autophagy flux. The project met all the objectives set in the introduction. The biosensor is characterized by its label-free electrochemical technique to detect and measure DNA concentration. Immobilization through covalent bonding of the thiol linker synthesized on the 5' of the DNA is confirmed through the inter-

pretation of the square wave voltammograms. The measurement technique of the analyte is chosen as the hybridization reaction of the ssDNA targets and the immobilized ssDNA probes. The successful hybridization is confirmed by the change in peak current of the square wave voltammograms. A low cost potentiostat is developed that is able to apply SWV to the sensor to form a complete biosensor. The working of the potentiostat is successfully tested with various dummy cells and compared to simulated circuits and a commercial potentiostat. The prototype biosensor successfully demonstrated through the intrinsic interaction of complementary ssDNA strands to form dsDNA, the DNA that encodes LC3-II can be detected. Immobilization of ssDNA increased significantly by using TCEP to expose the thiol bond on the thiolated probes. The sensor is able to detect small concentrations of ssDNA targets of $0.5 \mu\text{M}$. This project hopes to contribute in the ongoing research into autophagy flux and its relationship to various diseases and health. This prototype can be further developed with future research to monitor realtime changes in autophagy flux that relates to general health.

Appendices

Appendix A

Datasheets

A.1 Screen-printed electrode






Screen-Printed Gold Electrodes	Refs.	220AT	220BT
		C220AT	C220BT
		C223AT	C223BT



220AT - High temperature curing ink, WE 4 mm.

C223AT - High temperature curing ink, WE 1.6 mm.

C220AT - High temperature curing ink, WE 4 mm. Work in solution.

220BT - Low temperature curing ink, WE 4 mm.

C223BT - Low temperature curing ink, WE 1.6 mm.

C220BT - Low temperature curing ink, WE 4 mm. Work in solution.

Disposable **Gold Electrodes** are ideal for working with microvolumes, (refs. 220AT, 220BT, C223AT, C223BT) or by dipping them in solution (refs. C220AT, C220BT). Suitable for decentralized assays or to develop specific (bio)sensors.


C220AT and **C220BT** are specifically designed to work in solution by entirely immersing sensing area.



Also useful for undergraduate lab to avoid tedious polishing of solid electrodes.

Ceramic substrate: L33 x W10 x H0.5 mm
Electric contacts: Silver

The electrochemical cell consists of:
Working electrode: Gold
Auxiliary electrode: Gold
Reference electrode: Silver

Working electrode is available in two sizes: 4 mm diameter (refs. 220AT, C220AT, 220BT, C220BT) or 1.6 mm diameter (refs. C223AT, C223BT).



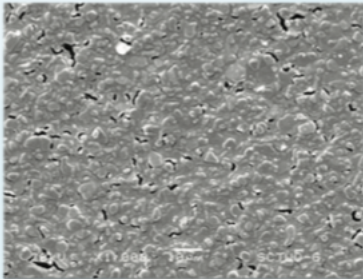
Screen-Printed Gold Electrodes

Refs.	220AT	220BT
	C220AT	C220BT
	C223AT	C223BT

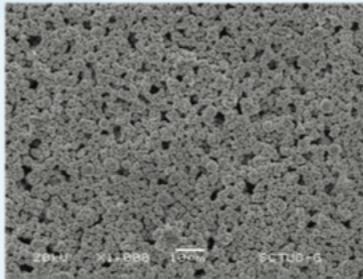
Electrodes screen-printed with high (AT) and low (BT) temperature curing inks which may have different properties depending on the application.

SEM images of working electrode

AT Models




BT Models




Screen-Printed Gold Electrodes are commercialised in 75 units packs. They should be stored at room temperature, protected from light in a dry place.

Also, specific **connectors** that act as an interface between the screen-printed electrode and any potentiostat (refs. DSC, CAC) and other accessories are available at [Dropsens](http://Dropsens.com).


Related products




8X220AT




CAC




FLWCL




CELL



STAT400





STAT8000



SPELEC


Full Catalogue





Parque Tecnológico de Asturias - Edif. CEEI. 33428 LLanera (Asturias), Spain
 (+34) 985 27 76 85 - info@dropsens.com - www.dropsens.com

Contact Form



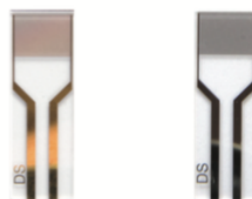
© Dropsens, S.L. 1.0

A.2 Interdigitated electrode

Interdigitated electrodes on glass substrate

01

Ref. G-IDEAU5, G-IDEAU10, G-IDEPT5, G-IDEPT10, G-IDEAG5, G-IDEUC5



Metrohm DropSens interdigitated electrodes (IDEs) are composed of two interdigitated electrodes with two connection tracks, made of same material, on a glass substrate.

Two dimensions of bands/gaps are available: 5 μm and 10 μm in gold or platinum (ref. G-IDEAU5, G-IDEAU10, G-IDEPT5, G-IDEPT10) and 5 μm in silver or copper (ref. G-IDEAG5 and ref. G-IDEUC5).

Glass substrate dimensions: L 22.8 x W 7.6 x H 0.7 mm

According to Zaretsky's definition of K_{cell} and by mathematical calculation:

Cell constant for 5 μm IDE: 0.0059 cm^{-1}
 Number of digits: 250 x 2
 Digit length: 6760 μm



Stereo microscope (left) and AFM 3D (right) images of G-IDEPT5, 5 μm bands/gaps IDE

Cell constant for 10 μm IDE: 0.0188 cm^{-1}
 Number of digits: 125 x 2
 Digit length: 6760 μm



Stereo microscope (left) and AFM 3D (right) images of G-IDEAU10, 10 μm bands/gaps IDE

The interdigitated electrodes are commercialized in packs of 20 units. They should be stored at room temperature, protected from light in a dry place.

Due to the small distances between the fingers of these electrodes, they are intended for use in clean room. In addition, for cleaning, simply pour a little ethanol solution over the electrodes and dry them under a gentle current of N_2 .

Specific cable connectors that act as an interface between interdigitated electrodes and any potentiostat (ref. CACIDE) are available at Metrohm DropSens.

www.metrohm-dropsens.com

A.3 MCP4922

The electrical characteristics of the device is presented in the datasheet that follows. Other characteristics of the device can be found in the full datasheet at: <https://ww1.microchip.com/downloads/en/devicedoc/22250a.pdf>



MICROCHIP MCP4902/4912/4922

8/10/12-Bit Dual Voltage Output Digital-to-Analog Converter with SPI Interface

Features

- MCP4902: Dual 8-Bit Voltage Output DAC
- MCP4912: Dual 10-Bit Voltage Output DAC
- MCP4922: Dual 12-Bit Voltage Output DAC
- Rail-to-Rail Output
- SPI Interface with 20 MHz Clock Support
- Simultaneous Latching of the Dual DACs with LDAC pin
- Fast Settling Time of 4.5 μ s
- Selectable Unity or 2x Gain Output
- External Voltage Reference Inputs
- External Multiplier Mode
- 2.7V to 5.5V Single-Supply Operation
- Extended Temperature Range: -40°C to +125°C

Applications

- Set Point or Offset Trimming
- Precision Selectable Voltage Reference
- Motor Control Feedback Loop
- Digitally-Controlled Multiplier/Divider
- Calibration of Optical Communication Devices

Related Products⁽¹⁾

P/N	DAC Resolution	No. of Channels	Voltage Reference (V _{REF})
MCP4801	8	1	Internal (2.048V)
MCP4811	10	1	
MCP4821	12	1	
MCP4802	8	2	
MCP4812	10	2	
MCP4822	12	2	External
MCP4901	8	1	
MCP4911	10	1	
MCP4921	12	1	
MCP4902	8	2	
MCP4912	10	2	
MCP4922	12	2	

Note 1: The products listed here have similar AC/DC performances.

Description

The MCP4902/4912/4922 devices are dual 8-bit, 10-bit, and 12-bit buffered voltage output Digital-to-Analog Converters (DACs), respectively. The devices operate from a single 2.7V to 5.5V supply with SPI compatible Serial Peripheral Interface. The user can configure the full-scale range of the device to be V_{REF} or 2 * V_{REF} by setting the Gain Selection Option bit (gain of 1 of 2).

The user can shut down both DAC channels by using SHDN pin or shut down the DAC channel individually by setting the Configuration register bits. In Shutdown mode, most of the internal circuits in the shutdown channel are turned off for power savings and the output amplifier is configured to present a known high resistance output load (500 k Ω , typical).

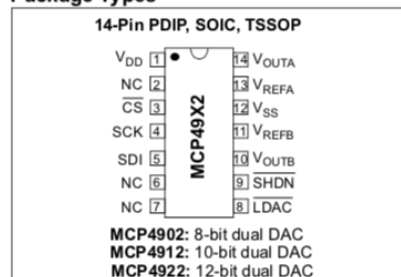
The devices include double-buffered registers, allowing synchronous updates of two DAC outputs, using the LDAC pin. These devices also incorporate a Power-on Reset (POR) circuit to ensure reliable power-up.

The devices utilize a resistive string architecture, with its inherent advantages of low DNL error and fast settling time. These devices are specified over the extended temperature range (+125°C).

The devices provide high accuracy and low noise performance for consumer and industrial applications where calibration or compensation of signals (such as temperature, pressure and humidity) are required.

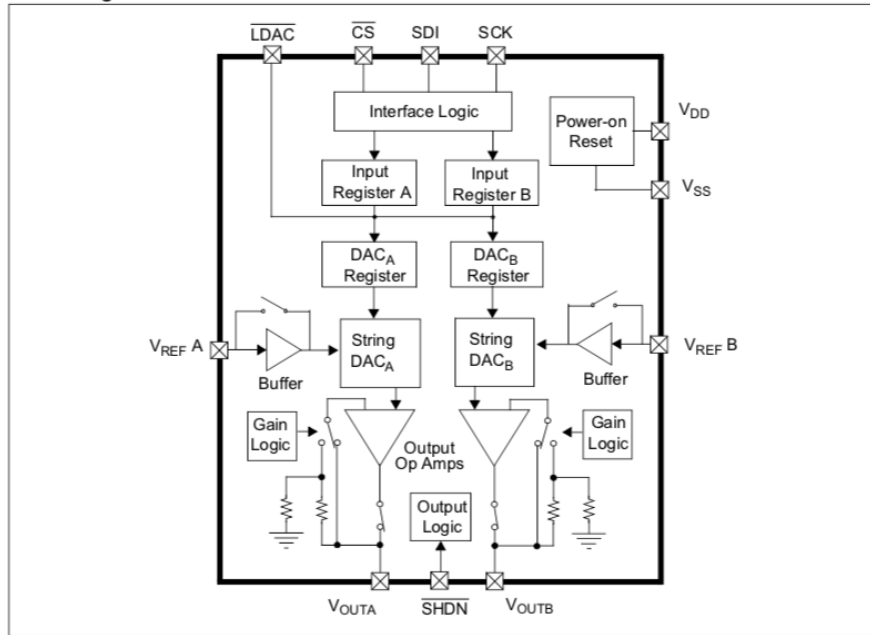
The MCP4902/4912/4922 devices are available in the PDIP, SOIC and TSSOP packages.

Package Types



MCP4902/4912/4922

Block Diagram



MCP4902/4912/4922

1.0 ELECTRICAL CHARACTERISTICS

Absolute Maximum Ratings †

V _{DD}	6.5V
All inputs and outputs w.r.t. V _{SS} -0.3V to V _{DD} +0.3V	
Current at Input Pins	±2 mA
Current at Supply Pins	±50 mA
Current at Output Pins	±25 mA
Storage temperature	-65°C to +150°C
Ambient temp. with power applied	-55°C to +125°C
ESD protection on all pins ≥ 4 kV (HBM), ≥ 400V (MM)	
Maximum Junction Temperature (T _J).....	+150°C

† **Notice:** Stresses above those listed under "Maximum Ratings" may cause permanent damage to the device. This is a stress rating only and functional operation of the device at those or any other conditions above those indicated in the operational listings of this specification is not implied. Exposure to maximum rating conditions for extended periods may affect device reliability.

ELECTRICAL CHARACTERISTICS

Electrical Specifications: Unless otherwise indicated, V_{DD} = 5V, V_{SS} = 0V, V_{REF} = 2.048V, Output Buffer Gain (G) = 2x, R_L = 5 kΩ to GND, C_L = 100 pF T_A = -40 to +85°C. Typical values are at +25°C.

Parameters	Sym	Min	Typ	Max	Units	Conditions
Power Requirements						
Operating Voltage	V _{DD}	2.7	—	5.5	V	
Operating Current	I _{DD}	—	350	700	μA	V _{DD} = 5V V _{DD} = 3V V _{REF} input is unbuffered, all digital inputs are grounded, all analog outputs (V _{OUT}) are unloaded. Code = 000h.
		—	250	500	μA	
Hardware Shutdown Current	I _{SHDN}	—	0.3	2	μA	Power-on Reset circuit is turned off
Software Shutdown Current	I _{SHDN_SW}	—	3.3	6	μA	Power-on Reset circuit stays on
Power-on-Reset Threshold	V _{POR}	—	2.0	—	V	
DC Accuracy						
MCP4902						
Resolution	n	8	—	—	Bits	
INL Error	INL	-1	±0.125	1	LSb	
DNL	DNL	-0.5	±0.1	+0.5	LSb	Note 1
MCP4912						
Resolution	n	10	—	—	Bits	
INL Error	INL	-3.5	±0.5	3.5	LSb	
DNL	DNL	-0.5	±0.1	+0.5	LSb	Note 1
MCP4922						
Resolution	n	12	—	—	Bits	
INL Error	INL	-12	±2	12	LSb	
DNL	DNL	-0.75	±0.2	+0.75	LSb	Note 1
Offset Error	V _{OS}	—	±0.02	1	% of FSR	Code = 0x000h

Note 1: Guaranteed monotonic by design over all codes.

Note 2: This parameter is ensured by design, and not 100% tested.

MCP4902/4912/4922

ELECTRICAL CHARACTERISTICS (CONTINUED)

Electrical Specifications: Unless otherwise indicated, $V_{DD} = 5V$, $V_{SS} = 0V$, $V_{REF} = 2.048V$, Output Buffer Gain (G) = 2x, $R_L = 5\text{ k}\Omega$ to GND, $C_L = 100\text{ pF}$, $T_A = -40$ to $+85^\circ\text{C}$. Typical values are at $+25^\circ\text{C}$.

Parameters	Sym	Min	Typ	Max	Units	Conditions
Offset Error Temperature Coefficient	$V_{OS}/^\circ\text{C}$	—	0.16	—	ppm/ $^\circ\text{C}$	-45°C to 25°C
		—	-0.44	—	ppm/ $^\circ\text{C}$	$+25^\circ\text{C}$ to 85°C
Gain Error	g_E	—	-0.10	1	% of FSR	Code = 0xFFFh, not including off-set error
Gain Error Temperature Coefficient	$\Delta G/^\circ\text{C}$	—	-3	—	ppm/ $^\circ\text{C}$	
Input Amplifier (V_{REF} Input)						
Input Range – Buffered Mode	V_{REF}	0.040	—	$V_{DD} - 0.040$	V	Note 2 Code = 2048
Input Range – Unbuffered Mode	V_{REF}	0	—	V_{DD}	V	$V_{REF} = 0.2V$ p-p, $f = 100\text{ Hz}$ and 1 kHz
Input Impedance	R_{VREF}	—	165	—	$\text{k}\Omega$	Unbuffered Mode
Input Capacitance – Unbuffered Mode	C_{VREF}	—	7	—	pF	
Multiplier Mode -3 dB Bandwidth	f_{VREF}	—	450	—	kHz	$V_{REF} = 2.5V \pm 0.2V$ p-p, Unbuffered, $G = 1x$
	f_{VREF}	—	400	—	kHz	$V_{REF} = 2.5V \pm 0.2V$ p-p, Unbuffered, $G = 2x$
Multiplier Mode – Total Harmonic Distortion	THD_{VREF}	—	-73	—	dB	$V_{REF} = 2.5V \pm 0.2V$ p-p, Frequency = 1 kHz
Output Amplifier						
Output Swing	V_{OUT}	—	0.01 to $V_{DD} - 0.04$	—	V	Accuracy is better than 1 LSB for $V_{OUT} = 10\text{ mV}$ to $(V_{DD} - 40\text{ mV})$
Phase Margin	θ_m	—	66	—	degrees	
Slew Rate	SR	—	0.55	—	V/ μs	
Short Circuit Current	I_{SC}	—	15	24	mA	
Settling Time	t_{settling}	—	4.5	—	μs	Within 1/2 LSB of final value from 1/4 to 3/4 full-scale range
Dynamic Performance (Note 2)						
DAC-to-DAC Crosstalk		—	10	—	nV-s	
Major Code Transition Glitch		—	45	—	nV-s	1 LSB change around major carry (0111...1111 to 1000...0000)
Digital Feedthrough		—	10	—	nV-s	
Analog Crosstalk		—	10	—	nV-s	

Note 1: Guaranteed monotonic by design over all codes.

Note 2: This parameter is ensured by design, and not 100% tested.

A.4 TLC2272

The electrical characteristics of the device is presented in the datasheet that follows. Other characteristics of the device can be found in the full datasheet at: <https://www.ti.com/product/TLC2272>

Product Folder
 Sample & Buy
 Technical Documents
 Tools & Software
 Support & Community

TLC2272, TLC2272A, TLC2272M, TLC2272AM
TLC2274, TLC2274A, TLC2274M, TLC2274AM
SLOS190H – FEBRUARY 1997 – REVISED MARCH 2016

TLC227x, TLC227xA: Advanced LinCMOS Rail-to-Rail Operational Amplifiers

1 Features

- Output Swing Includes Both Supply Rails
- Low Noise: 9 nV/ $\sqrt{\text{Hz}}$ Typical at $f = 1 \text{ kHz}$
- Low-Input Bias Current: 1-pA Typical
- Fully-Specified for Both Single-Supply and Split-Supply Operation
- Common-Mode Input Voltage Range Includes Negative Rail
- High-Gain Bandwidth: 2.2-MHz Typical
- High Slew Rate: 3.6-V/ μs Typical
- Low Input Offset Voltage: 950 μV Maximum at $T_A = 25^\circ\text{C}$
- Macromodel Included
- Performance Upgrades for the TLC272 and TLC274
- Available in Q-Temp Automotive

2 Applications

- White Goods (Refrigerators, Washing Machines)
- Hand-held Monitoring Systems
- Configuration Control and Print Support
- Transducer Interfaces
- Battery-Powered Applications

3 Description

The TLC2272 and TLC2274 are dual and quadruple operational amplifiers from Texas Instruments. Both devices exhibit rail-to-rail output performance for increased dynamic range in single- or split-supply applications. The TLC227x family offers 2 MHz of bandwidth and 3 V/ μs of slew rate for higher-speed applications. These devices offer comparable AC performance while having better noise, input offset voltage, and power dissipation than existing CMOS operational amplifiers. The TLC227x has a noise voltage of 9 nV/ $\sqrt{\text{Hz}}$, two times lower than competitive solutions.

The TLC227x family of devices, exhibiting high input impedance and low noise, is excellent for small-signal conditioning for high-impedance sources such as piezoelectric transducers. Because of the micropower dissipation levels, these devices work well in hand-held monitoring and remote-sensing applications. In addition, the rail-to-rail output feature, with single- or split-supplies, makes this family a great choice when interfacing with analog-to-digital converters (ADCs). For precision applications, the TLC227xA family is available with a maximum input offset voltage of 950 μV . This family is fully characterized at 5 V and $\pm 5 \text{ V}$.

The TLC227x also make great upgrades to the TLC27x in standard designs. They offer increased output dynamic range, lower noise voltage, and lower input offset voltage. This enhanced feature set allows them to be used in a wider range of applications. For applications that require higher output drive and wider input voltage range, see the TLV2432 and TLV2442 devices.

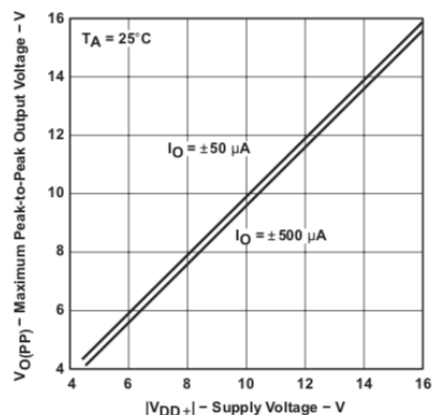
If the design requires single amplifiers, see the TLV2211, TLV2221 and TLV2231 family. These devices are single rail-to-rail operational amplifiers in the SOT-23 package. Their small size and low power consumption make them ideal for high density, battery-powered equipment.

Device Information⁽¹⁾

PART NUMBER	PACKAGE	BODY SIZE (NOM)
TLC2272	TSSOP (8)	4.40 mm × 3.00 mm
	SOIC (8)	3.91 mm × 4.90 mm
	SO (8)	5.30 mm × 6.20 mm
	PDIP (8)	6.35 mm × 9.81 mm
TLC2274	TSSOP (14)	4.40 mm × 5.00 mm
	SOIC (14)	3.91 mm × 8.65 mm
	SO (14)	5.30 mm × 10.30 mm
	PDIP (14)	6.35 mm × 19.30 mm

(1) For all available packages, see the orderable addendum at the end of the data sheet.

Maximum Peak-to-Peak Output Voltage vs Supply Voltage



An IMPORTANT NOTICE at the end of this data sheet addresses availability, warranty, changes, use in safety-critical applications, intellectual property matters and other important disclaimers. PRODUCTION DATA.



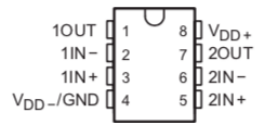
**TLC2272, TLC2272A, TLC2272M, TLC2272AM
TLC2274, TLC2274A, TLC2274M, TLC2274AM**

www.ti.com

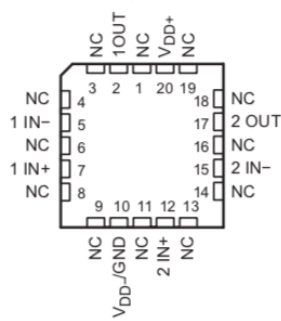
SLOS190H – FEBRUARY 1997 – REVISED MARCH 2016

5 Pin Configuration and Functions

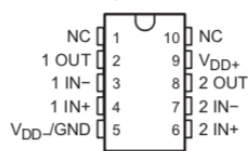
TLC2272
D, JG, P, or PW Package
8-Pin SOIC, CDIP, PDIP, or TSSOP
Top View



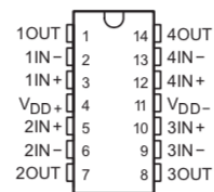
TLC2272
FK Package
20-Pin LCCC
Top View



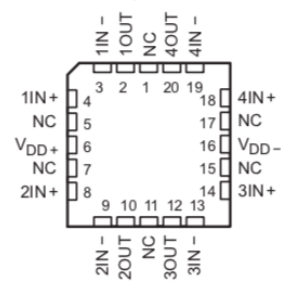
TLC2272
U Package
10-Pin CFP
Top View



TLC2274
D, J, N, PW, or W Package
14-Pin SOIC, CDIP, PDIP, TSSOP, or CFP
Top View



TLC2274
FK Package
20-Pin LCCC
Top View



TLC2272, TLC2272A, TLC2272M, TLC2272AM
TLC2274, TLC2274A, TLC2274M, TLC2274AM

SLOS190H – FEBRUARY 1997 – REVISED MARCH 2016

www.ti.com

Pin Functions

NAME	PIN					I/O	DESCRIPTION
	NO.						
	TLC2272			TLC2274			
D, JG, P, or PW	FK	U	D, J, N, PW, or W	FK			
1IN+	3	7	4	3	4	I	Non-inverting input, Channel 1
1IN-	2	5	3	2	3	I	Inverting input, Channel 1
1OUT	1	2	2	1	2	O	Output, Channel 1
2IN+	5	12	6	5	8	I	Non-inverting input, Channel 2
2IN-	6	15	7	6	9	I	Inverting input, Channel 2
2OUT	7	17	8	7	10	O	Output, Channel 2
3IN+	—	—	—	10	14	I	Non-inverting input, Channel 3
3IN-	—	—	—	9	13	I	Inverting input, Channel 3
3OUT	—	—	—	8	12	O	Output, Channel 3
4IN+	—	—	—	12	18	I	Non-inverting input, Channel 4
4IN-	—	—	—	13	19	I	Inverting input, Channel 4
4OUT	—	—	—	14	20	O	Output, Channel 4
V _{DD+}	8	20	9	4	6	—	Positive (highest) supply
V _{DD-}	—	—	—	11	16	—	Negative (lowest) supply
V _{DD-/GND}	4	10	5	—	—	—	Negative (lowest) supply
NC	—	1, 3, 4, 6, 8, 9, 11, 13, 14, 16, 18, 19	1, 10	—	1, 5, 7, 11, 15, 17	—	No Connection



www.ti.com

TLC2272, TLC2272A, TLC2272M, TLC2272AM
TLC2274, TLC2274A, TLC2274M, TLC2274AM

SLOS190H – FEBRUARY 1997 – REVISED MARCH 2016

6 Specifications

6.1 Absolute Maximum Ratings

over operating free-air temperature range (unless otherwise noted)⁽¹⁾

		MIN	MAX	UNIT
Supply voltage, V_{DD+} ⁽²⁾			8	V
V_{DD-} ⁽²⁾		-8		V
Differential input voltage, V_{ID} ⁽³⁾			±16	V
Input voltage, V_I (any input) ⁽²⁾		$V_{DD-} - 0.3$	V_{DD+}	V
Input current, I_I (any input)			±5	mA
Output current, I_O			±50	mA
Total current into V_{DD+}			±50	mA
Total current out of V_{DD-}			±50	mA
Duration of short-circuit current at (or below) 25°C ⁽⁴⁾		Unlimited		
Operating free-air temperature range, T_A	C level parts	0	70	°C
	I, Q level parts	-40	125	
	M level parts	-55	125	
Lead temperature 1,6 mm (1/16 inch) from case for 10 seconds	D, N, P or PW package		260	°C
Lead temperature 1,6 mm (1/16 inch) from case for 60 seconds	J or U package		300	°C
Storage temperature, T_{stg}		-65	150	°C

(1) Stresses beyond those listed under *Absolute Maximum Ratings* may cause permanent damage to the device. These are stress ratings only, which do not imply functional operation of the device at these or any other conditions beyond those indicated under *Recommended Operating Conditions*. Exposure to absolute-maximum-rated conditions for extended periods may affect device reliability.

(2) All voltage values, except differential voltages, are with respect to the midpoint between V_{DD+} and V_{DD-} .

(3) Differential voltages are at $IN+$ with respect to $IN-$. Excessive current will flow if input is brought below $V_{DD-} - 0.3$ V.

(4) The output may be shorted to either supply. Temperature or supply voltages must be limited to ensure that the maximum dissipation rating is not exceeded.

6.2 ESD Ratings

			VALUE	UNIT
$V_{(ESD)}$ Electrostatic discharge	Human-body model (HBM), per AEC Q100-002 ⁽¹⁾	Q-grade and M-grade devices in D and PW packages	±2000	V
	Charged-device model (CDM), per AEC Q100-011	Q-grade and M-grade devices in D and PW packages	±1000	

(1) AEC Q100-002 indicates that HBM stressing shall be in accordance with the ANSI/ESDA/JEDEC JS-001 specification.

6.3 Recommended Operating Conditions

			MIN	MAX	UNIT
$V_{DD±}$ Supply voltage		C LEVEL PARTS	±2.2	±8	V
		I LEVEL PARTS	±2.2	±8	
		Q LEVEL PARTS	±2.2	±8	
		M LEVEL PARTS	±2.2	±8	
V_I Input voltage		C LEVEL PARTS	V_{DD-}	$V_{DD+} - 1.5$	V
		I LEVEL PARTS	V_{DD-}	$V_{DD+} - 1.5$	
		Q LEVEL PARTS	V_{DD-}	$V_{DD+} - 1.5$	
		M LEVEL PARTS	V_{DD-}	$V_{DD+} - 1.5$	
V_{IC} Common-mode input voltage		C LEVEL PARTS	V_{DD-}	$V_{DD+} - 1.5$	V
		I LEVEL PARTS	V_{DD-}	$V_{DD+} - 1.5$	
		Q LEVEL PARTS	V_{DD-}	$V_{DD+} - 1.5$	
		M LEVEL PARTS	V_{DD-}	$V_{DD+} - 1.5$	

TLC2272, TLC2272A, TLC2272M, TLC2272AM
 TLC2274, TLC2274A, TLC2274M, TLC2274AM
 SLOS190H – FEBRUARY 1997 – REVISED MARCH 2016



www.ti.com

Recommended Operating Conditions (continued)

		MIN	MAX	UNIT	
T _A	Operating free-air temperature	C LEVEL PARTS	0	70	°C
		I LEVEL PARTS	-40	125	
		Q LEVEL PARTS	-40	125	
		M LEVEL PARTS	-55	125	

6.4 Thermal Information

THERMAL METRIC ⁽¹⁾	TLC2272					TLC2274					UNIT	
	D (SOIC)	P (PDIP)	PW (TSSOP)	FK (LCCC)	U (CFP)	D (SOIC)	N (PDIP)	PW (TSSOP)	FK (LCCC)	J (CDIP)		
	8-PIN	8-PIN	8-PIN	20-PIN	10-PIN	14-PIN	14-PIN	14-PIN	20-PIN	14-PIN		
R _{θJA}	Junction-to-ambient thermal resistance ⁽²⁾⁽³⁾	115.6	58.5	175.8	—	—	83.8	—	111.6	—	—	°C/W
R _{θJC(top)}	Junction-to-case (top) thermal resistance ⁽²⁾⁽³⁾	61.8	48.3	58.8	18	121.3	43.2	34	41.2	16	16.2	°C/W
R _{θJB}	Junction-to-board thermal resistance	55.9	35.6	104.3	—	—	38.4	—	54.7	—	—	°C/W
ψ _{JT}	Junction-to-top characterization parameter	14.3	25.9	5.9	—	—	9.4	—	3.9	—	—	°C/W
ψ _{JB}	Junction-to-board characterization parameter	55.4	35.5	102.6	—	—	38.1	—	53.9	—	—	°C/W
R _{θJC(bot)}	Junction-to-case (bottom) thermal resistance	—	—	—	—	8.68	—	—	—	—	—	°C/W

- (1) For more information about traditional and new thermal metrics, see the *Semiconductor and IC Package Thermal Metrics* application report, [SPRA953](#).
- (2) Maximum power dissipation is a function of T_{J(max)}, θ_{JA}, and T_A. The maximum allowable power dissipation at any allowable ambient temperature is P_D = (T_{J(max)} - T_A) / θ_{JA}. Operating at the absolute maximum T_J of 150°C can affect reliability.
- (3) The package thermal impedance is calculated in accordance with JEDEC 51-7 (plastic) or MIL-STD-883 Method 1012 (ceramic).

6.5 TLC2272 and TLC2272A Electrical Characteristics V_{DD} = 5 V

at specified free-air temperature, V_{DD} = 5 V; T_A = 25°C, unless otherwise noted.

PARAMETER	TEST CONDITIONS	MIN	TYP	MAX	UNIT	
V _{IO}	Input offset voltage V _{IC} = 0 V, V _{ODt} = ±2.5 V, V _O = 0 V, R _S = 50 Ω	TLC2272	300	2500	μV	
		TLC2272A				
		TLC2272	300	950		
		TLC2272A	3000	1500		
α _{VIO}	Temperature coefficient of input offset voltage V _{IC} = 0 V, V _{ODt} = ±2.5 V, V _O = 0 V, R _S = 50 Ω	2		μV/°C		
	Input offset voltage long-term drift ⁽²⁾	0.002		μV/mo		
I _{IO}	Input offset current V _{IC} = 0 V, V _{ODt} = ±2.5 V, V _O = 0 V, R _S = 50 Ω	All level parts	0.5	60	pA	
		C level part	T _A = 0°C to 80°C			
		I level part	T _A = -40°C to 85°C			
		Q level part	T _A = -40°C to 125°C			
		M level part	T _A = -55°C to 125°C			
I _B	Input bias current V _{IC} = 0 V, V _{ODt} = ±2.5 V, V _O = 0 V, R _S = 50 Ω	All level parts	1	60	pA	
		C level part	T _A = 0°C to 80°C			
		I level part	T _A = -40°C to 85°C			
		Q level part	T _A = -40°C to 125°C			
		M level part	T _A = -55°C to 125°C			
V _{ICR}	Common-mode input voltage R _S = 50 Ω; V _{IO} ≤ 5 mV	T _A = 25°C	-0.3	2.5	4	V
		Full Range ⁽¹⁾	0	2.5	3.5	

- (1) T_A = -55°C to 125°C.
- (2) Typical values are based on the input offset voltage shift observed through 168 hours of operating life test at T_A = 150°C extrapolated to T_A = 25°C using the Arrhenius equation and assuming an activation energy of 0.96 eV.



**TLC2272, TLC2272A, TLC2272M, TLC2272AM
TLC2274, TLC2274A, TLC2274M, TLC2274AM**

www.ti.com

SLOS190H – FEBRUARY 1997 – REVISED MARCH 2016

TLC2272 and TLC2272A Electrical Characteristics $V_{DD} = 5\text{ V}$ (continued)

at specified free-air temperature, $V_{DD} = 5\text{ V}$; $T_A = 25^\circ\text{C}$, unless otherwise noted.

PARAMETER	TEST CONDITIONS	MIN	TYP	MAX	UNIT	
V_{OH} High-level output voltage	$I_{OH} = -20\ \mu\text{A}$	$T_A = 25^\circ\text{C}$	4.85	4.99	V	
		Full Range ⁽¹⁾	4.85			
	$I_{OH} = -200\ \mu\text{A}$	$T_A = 25^\circ\text{C}$	4.25	4.65		
		Full Range ⁽¹⁾	4.25			
V_{OL} Low-level output voltage	$V_{IC} = 2.5\text{ V}$	$I_{OL} = 50\ \mu\text{A}$		0.01	V	
		$I_{OL} = 500\ \mu\text{A}$	$T_A = 25^\circ\text{C}$	0.09		0.15
			Full Range ⁽¹⁾			0.15
		$I_{OL} = 5\text{ mA}$	$T_A = 25^\circ\text{C}$	0.9		1.5
Full Range ⁽¹⁾			1.5			
A_{VD} Large-signal differential voltage amplification	$V_{IC} = 2.5\text{ V}$, $V_O = 1\text{ V to }4\text{ V}$; $R_L = 10\text{ k}\Omega^{(3)}$	C level part	$T_A = 25^\circ\text{C}$	15	35	V/mV
			$T_A = 0^\circ\text{C to }80^\circ\text{C}$	15		
		I level part	$T_A = 25^\circ\text{C}$	15	35	
			$T_A = -40^\circ\text{C to }85^\circ\text{C}$	15		
		Q level part	$T_A = 25^\circ\text{C}$	10	35	
		M level part	$T_A = -40^\circ\text{C to }125^\circ\text{C}$	10		
			$T_A = 25^\circ\text{C}$	10	35	
		$T_A = -55^\circ\text{C to }125^\circ\text{C}$	10			
	$V_{IC} = 2.5\text{ V}$, $V_O = 1\text{ V to }4\text{ V}$; $R_L = 1\text{ M}\Omega^{(3)}$		175			
r_{id} Differential input resistance			10^{12}		Ω	
r_i Common-mode input resistance			10^{12}		Ω	
C_i Common-mode input capacitance	$f = 10\text{ kHz}$, P package		8		pF	
z_o Closed-loop output impedance	$f = 1\text{ MHz}$, $A_V = 10$		140		Ω	
CMRR Common-mode rejection ratio	$V_{IC} = 0\text{ V to }2.7\text{ V}$, $V_O = 2.5\text{ V}$, $R_S = 50\ \Omega$	$T_A = 25^\circ\text{C}$	70	75	dB	
		Full Range ⁽¹⁾	70			
k_{SVR} Supply-voltage rejection ratio ($\Delta V_{DD} / \Delta V_{IO}$)	$V_{DD} = 4.4\text{ V to }16\text{ V}$, $V_{IC} = V_{DD} / 2$, no load	$T_A = 25^\circ\text{C}$	80	95	dB	
		Full Range ⁽¹⁾	80			
I_{DD} Supply current	$V_O = 2.5\text{ V}$, no load	$T_A = 25^\circ\text{C}$	2.2	3	mA	
		Full Range ⁽¹⁾		3		
SR Slew rate at unity gain	$V_O = 0.5\text{ V to }2.5\text{ V}$, $R_L = 10\text{ k}\Omega^{(3)}$, $C_L = 100\text{ pF}^{(3)}$	$T_A = 25^\circ\text{C}$	2.3	3.6	V/ μs	
		Full Range ⁽¹⁾	1.7			
V_n Equivalent input noise voltage	$f = 10\text{ Hz}$ $f = 1\text{ kHz}$		50		nV/ $\sqrt{\text{Hz}}$	
			9			
V_{NPP} Peak-to-peak equivalent input noise voltage	$f = 0.1\text{ Hz to }1\text{ Hz}$ $f = 0.1\text{ Hz to }10\text{ Hz}$		1		μV	
			1.4			
I_n Equivalent input noise current			0.6		fA/ $\sqrt{\text{Hz}}$	
THD+N Total harmonic distortion + noise	$V_O = 0.5\text{ V to }2.5\text{ V}$, $f = 20\text{ kHz}$, $R_L = 10\text{ k}\Omega^{(3)}$	$A_V = 1$		0.0013%		
		$A_V = 10$		0.004%		
		$A_V = 100$		0.03%		
Gain-bandwidth product	$f = 10\text{ kHz}$, $R_L = 10\text{ k}\Omega^{(3)}$, $C_L = 100\text{ pF}^{(3)}$		2.18		MHz	
B_{OM} Maximum output-swing bandwidth	$V_{OPP} = 2\text{ V}$, $A_V = 1$, $R_L = 10\text{ k}\Omega^{(3)}$, $C_L = 100\text{ pF}^{(3)}$		1		MHz	
t_s Settling time	$A_V = -1$, $R_L = 10\text{ k}\Omega^{(3)}$, Step = $0.5\text{ V to }2.5\text{ V}$, $C_L = 100\text{ pF}^{(3)}$	To 0.1%	1.5		μs	
		To 0.01%	2.6			
Φ_m Phase margin at unity gain	$R_L = 10\text{ k}\Omega^{(3)}$, $C_L = 100\text{ pF}^{(3)}$		50°		dB	
		Gain margin	$R_L = 10\text{ k}\Omega^{(3)}$, $C_L = 100\text{ pF}^{(3)}$	10		

(3) Referenced to 0 V.

Appendix B

Protocols

B.1 DNA preparation

1 Materials and methods

1.1 Cell culture

Mouse Embryonic Fibroblast (MEF) cells that stably express green fluorescent protein tagged to light chain 3 (MEF-GFP) and wild type MEF cells (MEF-CL) were maintained in Dulbecco's modified Eagle's medium (DMEM) (Life Technologies, # 41-965-039), supplemented with 10% fetal bovine serum (Biocrom, # S-0615) and penicillin-streptomycin (Life Technologies, # 15-140-122), at 37°C in a 5% CO₂ humidified atmosphere.

1.2 Chemicals

Rapamycin (Sigma-Aldrich, # R-0395) and spermidine (Sigma-Aldrich, # S-0266) were used as an mTOR-dependent and -independent autophagy inducers, and bafilomycin A₁ (LKT Laboratories Inc., # B-0025) as an autophagosome/lysosome fusion inhibitor.

1.3 Quantitative real-time PCR analysis

Total RNA was extracted from MEF cells using TRIzol (Thermo Fisher Scientific, # 15596026) and 1 µg RNA converted to double-stranded cDNA with LunaScript RT SuperMix Kit (New England BioLabs Inc., # E3010S) according to the manufacturers instructions. Quantitative analysis of gene expression (QRT-PCR) was performed with an ABI 7900HT (Applied Biosystems); each reaction was performed in triplicate by using 1 µL of cDNA, 6.25 µL Luna Universal qPCR Master Mix (New England BioLabs Inc., # M3003L), 0.25 µL primers (unmodified) and 4.75 µL ddH₂O. Primer pair sequences and cycling protocol are shown in Tables 1 and 3. A relative standard curve was used for linear regression analysis of unknown samples and data presented as fold change between samples.

1.4 Immobilization

Thiol modified MAP1lc3b forward primer is re-suspended in Tris-EDTA (TE) buffer solution (Sigma-Aldrich, # 93283) to achieve a stock concentration of 50 mM. For im-

mobilization, the stock solution is diluted to 5 mM and the di-thiol bonds reduced with 500 mM TCEP (Sigma-Aldrich, # C4706) for 2 hr. Gold electrodes are submerged in the reduced MAP11c3b forward primer solution and incubated overnight to immobilize oligonucleotides.

1.5 Preparation of single stranded DNA

Polymerase chain reaction was performed with an ABI 9800 (Applied Biosystems); each reaction was performed using 1 μ L of cDNA, 6.25 μ L Taq 2X Master Mix (New England BioLabs Inc., # M0270L), 0.25 μ L primers (unmodified forward and Fluorescein conjugated reverse) and 4.75 μ L ddH₂O. Primer pair sequences and cycling protocol are shown in Tables 1 and 3. To produce single stranded DNA, the the positive sense DNA is digested with RecJf exonuclease (New England BioLabs Inc., # M0264S) the negative sense DNA purified using Monarch PCR & DNA Cleanup Kit (New England BioLabs Inc., # T1030S) [could also use a more cost effective alternative].

1.6 Primers

Primers (Table 1) were designed and synthesized by Integrated DNA Technologies, Inc. (Belgium). Nucleotide sequences used in the primer design were retrieved from NCBI database (<https://ncbi.nlm.nih.gov/>) and aligned using BLAST to confirm gene specificity and obtain from literature.

Table 1: Sequences of primers of selected autophagy proteins and cargo

Primers	5' Modification	Sequence (5'-3' orientation)	Reference
MAP1lc3b_Forward	n/a	GACGGCTTCCTGTACATGGTTT	[1]
MAP1lc3b_Reverse	n/a	TGGAGTCTTACACAGCCATTGC	[1]
MAP1lc3b_Forward	Thiol C6 S-S	GACGGCTTCCTGTACATGGTTT	[1]
MAP1lc3b_Reverse	Fluorescein	TGGAGTCTTACACAGCCATTGC	[1]
p62/SQSTM1_Forward	n/a	TGTGGAACATGGAGGGAAGAG	[1]
p62/SQSTM1_Reverse	n/a	TGTGCCTGTGCTGGAAC TTTC	[1]
p62/SQSTM1_Reverse	Fluorescein	TGTGCCTGTGCTGGAAC TTTC	[1]
Beclin-1_Forward	n/a	GTGCGCTACGCCAGATC	[1]
Beclin-1_Reverse	n/a	GATGTGGAAGGTGGCATTGAA	[1]
Beclin-1_Reverse	Fluorescein	GATGTGGAAGGTGGCATTGAA	[1]
GAPDH_Forward	n/a	TGTGTCCGTCGTGGATCTGA	[1]
GAPDH_Reverse	n/a	CCTGCTTCACCACCTTCTTGA	[1]
GAPDH_Reverse	Fluorescein	CCTGCTTCACCACCTTCTTGA	[1]
LAMP2var1_Forward	n/a	TGGCTAATGGCTCAGCTTTC	[1]
LAMP2var1_Reverse	n/a	GCTATGGGCACAAGGAAGTT	[1]
LAMP2var1_Reverse	Fluorescein	GCTATGGGCACAAGGAAGTT	[1]

Table 2: Experimental conditions

Test	Test DNA	Scramble/Test DNA	cDNA
Sample 1	1 fg	1 mg/1 fg	1 fg
Sample 2	10 fg	1 mg/10 fg	10 fg
Sample 3	100 fg	1 mg/100 fg	100 fg
Sample 4	1 pg	1 mg/1 pg	1 pg
Sample 5	10 pg	1 mg/10 pg	10 pg
Sample 6	100 pg	1 mg/100 pg	100 pg
Sample 7	1 ng	1 mg/1 ng	1 μ g
Sample 8	10 ng	1 mg/10 ng	
Sample 9	100 ng	1 mg/100 ng	
Sample 10	1 μ g	1 mg/1 μ g	
Sample 11	10 μ g	1 mg/10 μ g	
Sample 12	100 μ g	1 mg/100 μ g	
Sample 13	1 mg	1 mg/1 mg	

Table 3: Cycling protocol for DNA amplification

Thermocycler conditions for PCR	Temp	Time
Initial Denaturation	Denat	95°C 5 min
	Denat	95°C 30 sec
Amplification (40 cycles)	Anneal	57°C 30 sec
	Extend	68°C 30 sec
Final extension	Extend	68°C 5 min
Hold	Anneal	4°C Infnit

B.2 Sybr nucleic acid stain



PROTOCOL

NanoDrop 3300

Sybr[®] Green I dsDNA Assay

Introduction

The Sybr[®] Green I dye is a fluorescent nucleic acid stain for quantitating double-stranded DNA (dsDNA). Used in conjunction with the micro-volume capability of the Thermo Scientific NanoDrop[™] 3300 Fluorospectrometer, the Sybr[®] Green I assay provides a highly sensitive means of dsDNA quantitation with minimal consumption of sample. The main disadvantage of general UV spectroscopy for dsDNA quantitation is the contribution of signal from single-stranded DNA (ssDNA) and other contaminants, such as protein and extraction buffers. Sybr[®] Green I reagent circumvents such contributions from interfering substances by exhibiting an emission maximum at 527nm when bound to dsDNA (unbound Sybr[®] Green I reagent exhibits minimal fluorescence in solution). The ability of the NanoDrop 3300 to measure as little as 1 ul of sample, allows significantly scaled-down reaction volumes, thereby using only a fraction of sample commonly needed for conventional cuvette-based fluorometers. The NanoDrop 3300 has demonstrated a detection range for dsDNA bound with Sybr[®] Green I reagent of 1 ng/ml– 1000 ng/ml and has proven to be 75 times more sensitive than using the Hoechst 33258 dye with this system. Readings taken at the lowest detection limit consume only 2 picograms of dsDNA per measurement.

Assay Supplies

Equipment:

- NanoDrop 3300 Fluorospectrometer
- 2uL pipettor
- Low retention nuclease free pipette tips

Materials:

- Low lint laboratory wipes
- Nuclease free sterile amber or foil covered 1.5 mL polypropylene tubes
- Nuclease free sterile clear 1.5 mL polypropylene tubes
- 10 uL sterile nuclease free low retention tips

Reagents:

- SYBR[®] Green I nucleic acid gel stain (Invitrogen Catalog Number - S-7567)
- Sterile Nuclease free 1X TE buffer pH 8.0 (10mM Tris, 1mM EDTA)
- Control dsDNA

Sybr[®] Green I Assay Protocol

This protocol is configured to provide enough volume for a maximum of five measurement replicates. This protocol has been observed to be effective for a final dye dilution in a range from 1:8000 to 1:10,000. As the dye intensity may be lot specific the investigator may change the dye dilution as necessary. The total reaction volume can also be scaled at the discretion of the investigator.

1. Dilute the Sybr[®] Green I reagent 1:100 in 1X TE pH 8.0. (This 1:100 dilution has shown to be stable for up to 6 hours at room temperature when protected from light.)

Example: For a 1:100 dye dilution transfer 10 ul of 10,000 X concentrated Sybr[®] Green I dye and 990 ul of 1X TE buffer into a clean amber or foiled 1.5ml microfuge tube and mix well with 1ml pipette.

2. Prepare a series of 2X serial dilutions of control dsDNA ranging from 2 ng/ml to 2,000 ng/ml in nuclease free tubes.

Example dilution series

dsDNA [ng/ml]	dsDNA uL	1X TE uL	Total Volume uL	*In assay dsDNA [ng/ml]
2000.0			178.3	1000.0
1000.0	78.3	78.3	156.6	500.0
500.0	56.6	56.6	113.2	250.0
50.0	13.2	118.8	132.0	25.0
10.0	32.0	128.0	160.0	5.0
4.0	60.0	90.0	150.0	2.0
2.0	50.0	50.0	100	1.0

*In assay describes the final concentration of dsDNA that present in the reaction.

3. Prepare a working Sybr[®] Green I dilution ranging from 1:4,000 to 1:5,000 in a 1.5 ml amber or foiled nuclease free tube (specific dilution of the Sybr[®] Green I working solution may be lot specific).

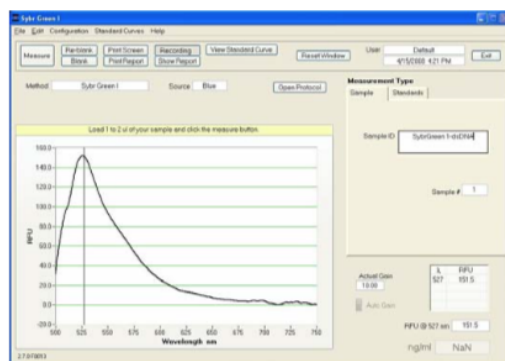
**Example: For a 1:4,500 working solution dilute the 1:100 Sybr[®] Green I reagent by transferring 22.2 ul of 1:100 Sybr[®] Green I reagent and 977.7 ul of 1X TE pH 8.0 to an amber or foiled tube and mix well.

PROTOCOL

NanoDrop 3300

4. Record the dsDNA concentrations on each tube and add 5 μ l of each standard dsDNA dilution to the respective amber tube. Centrifuge the samples briefly and transfer 5 μ l of the Sybr[®] Green I working solution to the bottom of the tube and centrifuge briefly once again.
5. Add 5 μ l of each unknown dsDNA sample into a labeled nuclease free amber tube, centrifuge the unknowns briefly, and add 5 μ l of the diluted Sybr[®] Green I reagent to the bottom of the tube and centrifuge briefly once again.
6. Prepare a reference standard by adding 5 μ l of 1X TE into a labeled nuclease free amber tube, centrifuge briefly, and add 5 μ l of the diluted Sybr[®] Green I reagent to the bottom of the tube and centrifuge briefly once again.
7. Finger vortex all samples and briefly centrifuge. Let the samples incubate for 5 minutes at room temperature.
8. Proceed to the standard curve protocol.

Example spectrum Syber Green I dsDNA sample



Standard Curve Protocol

1. Clean both sampling pedestals with 2 μ l of nuclease free de-ionized water.
2. Open upper arm and firmly blot the two pedestals with a dry lab wipe. Make sure there are no traces of lint on the pedestals before continuing.
3. Open the operating software. Click on the Nucleic Acid Quantitation button and select the SyberGreen method.
4. Add 2 μ l of assay buffer (no dye, no sample) to the lower pedestal. Lower the arm and click F3 or the Blank button. When the measurement is complete, lift the arm and use a dry laboratory wipe to blot the buffer from both the bottom and upper measurement surfaces. Use a fresh aliquot of buffer to verify a proper baseline.
5. Under Measurement type, click on the Standards tab. Highlight the Reference standard.
6. Mix the reference solution (assay buffer and dye, no sample) briefly and transfer 2 μ l of the solution onto the lower pedestal. Lower the arm and click F1 or the Measure button. A pop up window will ask for confirmation of the units. (Recommended ng/mL or pg/ μ L)
7. Measure up to 5 replicates of the reference solution using a fresh 2 μ l aliquot for each measurement.
8. Select Standard 1 to enter a value. Enter values for up to 7 standards.
9. Mix the standard solution briefly and transfer 2 μ l onto the lower pedestal. Lower the arm and click F1 or the Measure button. Measure up to 5 replicates of each standard using a fresh 2 μ l aliquot for each measurement.
10. Once the standard curve is completed, select the Standard Curve Type (Interpolation, Linear, 2^o polynomial, 3^o polynomial) that best fits the standards data set.
11. Click on the Sample tab under Measurement Type, and enter the unknown samples' respective ID information. If a dilution of the unknown sample was made, enter the dilution factor in the box below the sample ID window.
12. Add 2 μ l of the sample and use the F1 key or click the Measure button to initiate the measurement cycle. Use a fresh aliquot of sample for each measurement.

Rev 4/08

Appendix C

Code

C.1 Arduino code

```

// include the library code:
#include <SPI.h>
// Set Constants
const int dacChipSelectPin = 10;    // set pin 10 as the chip select for the DAC:
float step_DAC[100];
float amp_DAC[100];
int adcVout = A0;
int adcVn = A1;
float i_rev_arr[100];
float i_for_arr[100];
// Start setup function:
void setup() {
  Serial.begin(9600);
  pinMode(adcVout, INPUT);
  pinMode(adcVn, INPUT);
  pinMode(dacChipSelectPin, OUTPUT);
  digitalWrite(dacChipSelectPin, HIGH);
  // initialise SPI:
  SPI.begin();
  SPI.setBitOrder(MSBFIRST);        // Not strictly needed but just to be sure.
  SPI.setDataMode(SPI_MODE0);      // Not strictly needed but just to be sure.
  TCCR2B = TCCR2B & B11111000 | B00000001; // For PWM frequency of 31372.55 Hz
  pinMode(3, OUTPUT);
  pinMode(7, OUTPUT);
} // End setup function.
// Start loop function:
void loop() {
  digitalWrite(7, LOW); //virtual ground for op-amp
  float step = 10;
  float amp = 50;
  for (int i = 0; i < 40; i++){
    step = step+25;
    step_DAC[i] = step;
    step_DAC[i] = step / 3300;
    step_DAC[i] = step_DAC[i] * 4096;
    step_DAC[i] = (int)step_DAC[i];
    amp = amp +25;
    amp_DAC[i] = amp;
    amp_DAC[i] = amp / 3300;
    amp_DAC[i] = amp_DAC[i] * 4096;
    amp_DAC[i] = (int)amp_DAC[i];
    float xyz = amp_DAC[i];
    setDac(step_DAC[i], 0);
    delay(15);
    i_rev_arr[i] = sampleReverse();
    Serial.println(i_rev_arr[i]);
    Serial.println(i_rev_arr[i]);
    setDac(amp_DAC[i], 0);
    delay(15);
    i_for_arr[i] = sampleForward();
    Serial.println(i_for_arr[i]);
    Serial.println(i_for_arr[i]);
  }
  exit(0);
} // End of loop function.
float sampleReverse(){
  float adc_rev = 0;
  float v_rev = 0;
  float adc_avg_rev = 0;
  float adc_tot_rev = 0;
  float adc_rev_vn = 0;
  float v_rev_vn = 0;
  float adc_avg_rev_vn = 0;
  float adc_tot_rev_vn = 0;
  float i_rev = 0;
  for(int r=0; r<5; r++){
    delay(1);
    adc_rev = analogRead(adcVout);
    adc_tot_rev = adc_tot_rev + adc_rev;
    adc_rev_vn = analogRead(adcVn);
  }
}

```

```

    adc_tot_rev_vn = adc_tot_rev_vn + adc_rev_vn;
}
adc_avg_rev = adc_tot_rev/5;
v_rev =adc_avg_rev*5;
v_rev = v_rev/1023;
adc_avg_rev_vn = adc_tot_rev_vn/5;
v_rev_vn =adc_avg_rev_vn*5;
v_rev_vn = v_rev_vn/1023;
i_rev = v_rev - v_rev_vn; // divided by 1k = mA
i_rev = i_rev/4.14;
return i_rev;
}

float sampleForward(){
float adc_for =0;
float v_for =0;
float adc_avg_for =0;
float adc_tot_for =0;
float adc_for_vn =0;
float v_for_vn =0;
float adc_avg_for_vn =0;
float adc_tot_for_vn =0;
float i_for=0;
for(int f=0; f<5; f++){
    delay(1);
    adc_for = analogRead(adcVout);
    adc_tot_for = adc_tot_for + adc_for;
    adc_for_vn = analogRead(adcVn);
    adc_tot_for_vn = adc_tot_for_vn + adc_for_vn;
}
adc_avg_for = adc_tot_for/5;
v_for =adc_avg_for*5;
v_for = v_for/1023;
adc_avg_for_vn = adc_tot_for_vn/5;
v_for_vn =adc_avg_for_vn*5;
v_for_vn = v_for_vn/1023;
i_for = v_for - v_for_vn;
i_for = i_for/4.14;
return i_for;
}
// Function to set the DAC, Accepts the Value to be sent and the channel of the DAC to be used.
void setDac(int value, int channel) {
    byte dacRegister = 0b00110000; // Sets default DAC registers B00110000, 1st bit
    // chooses DAC, A=0 B=1, 2nd Bit bypasses input Buffer, 3rd bit sets output gain to 1x, 4th bit controls active
    // low shutdown. LSB are insignificant here.
    int dacSecondaryByteMask = 0b0000000011111111; // Isolates the last 8 bits of the 12 bit value,
    B0000000011111111.
    byte dacPrimaryByte = (value >> 8) | dacRegister; //Value is a maximum 12 Bit value, it is shifted to
    // the right by 8 bytes to get the first 4 MSB out of the value for entry into th Primary Byte, then ORed with
    // the dacRegister
    byte dacSecondaryByte = value & dacSecondaryByteMask; // compares the 12 bit value to isolate the 8 LSB and
    // reduce it to a single byte.
    // Sets the MSB in the primaryByte to determine the DAC to be set, DAC A=0, DAC B=1
    switch (channel) {
        case 0:
            dacPrimaryByte &= ~(1 << 7);
            break;
        case 1:
            dacPrimaryByte |= (1 << 7);
    }
    noInterrupts(); // disable interrupts to prepare to send data to the DAC
    digitalWrite(dacChipSelectPin,LOW); // take the Chip Select pin low to select the DAC:
    SPI.transfer(dacPrimaryByte); // send in the Primary Byte:
    SPI.transfer(dacSecondaryByte); // send in the Secondary Byte
    digitalWrite(dacChipSelectPin,HIGH); // take the Chip Select pin high to de-select the DAC:
    interrupts(); // Enable interrupts
}

```

Bibliography

- [1] World Health Organization., *Noncommunicable diseases*, 2021.
- [2] O. Landrove-Rodríguez *et al.*, “Non-communicable diseases: Risk factors and actions for their prevention and control in Cuba”, *Revista Panamericana de Salud Publica/Pan American Journal of Public Health*, vol. 42, pp. 1–8, 2018, ISSN: 16805348. DOI: 10.26633/RPSP.2018.23.
- [3] H. Sung *et al.*, “Global Cancer Statistics 2020: GLOBOCAN Estimates of Incidence and Mortality Worldwide for 36 Cancers in 185 Countries”, *CA: A Cancer Journal for Clinicians*, vol. 71, no. 3, pp. 209–249, 2021, ISSN: 0007-9235. DOI: 10.3322/caac.21660.
- [4] A. Raghavan and Z. A. Shah, “Neurodegenerative disease”, *Diet, Exercise, and Chronic Disease: The Biological Basis of Prevention*, pp. 339–390, 2014. DOI: 10.1201/b16783.
- [5] Alzheimer’s Association, “2019 Alzheimer’s disease facts and figures”, *Alzheimer’s & Dementia*, vol. 15, no. 3, pp. 321–387, Mar. 2019, ISSN: 1552-5260. DOI: 10.1016/j.jalz.2019.01.010.
- [6] P. A. H. Organization, *WHO outlines steps to save 7 million lives from cancer*, 2020.
- [7] A. Association, *Early Detection*, 2022.
- [8] T. Ichimiya *et al.*, “Autophagy and autophagy related diseases: A review”, *International Journal of Molecular Sciences*, vol. 21, no. 23, pp. 1–21, 2020, ISSN: 14220067. DOI: 10.3390/ijms21238974.
- [9] A. Di Meco *et al.*, “Autophagy Dysfunction in Alzheimer’s Disease: Mechanistic Insights and New Therapeutic Opportunities”, *Biological Psychiatry*, vol. 87, no. 9, pp. 797–807, 2020, ISSN: 18732402. DOI: 10.1016/j.biopsych.2019.05.008.

- [10] A. Udristioiu and D. Nica-Badea, "Autophagy dysfunctions associated with cancer cells and their therapeutic implications", *Biomedicine and Pharmacotherapy*, vol. 115, no. February, p. 108 892, 2019, ISSN: 19506007. DOI: 10.1016/j.biopha.2019.108892.
- [11] F. Madeo *et al.*, "Can autophagy promote longevity?", *Nature Cell Biology*, vol. 12, no. 9, pp. 842–846, 2010, ISSN: 14657392. DOI: 10.1038/ncb0910-842.
- [12] L. Galluzzi *et al.*, "Molecular definitions of autophagy and related processes", *The EMBO Journal*, vol. 36, no. 13, pp. 1811–1836, 2017, ISSN: 0261-4189. DOI: 10.15252/embj.201796697.
- [13] K. Kirkegaard *et al.*, "Cellular autophagy: Surrender, avoidance and subversion by microorganisms", *Nature Reviews Microbiology*, vol. 2, no. 4, pp. 301–314, 2004, ISSN: 17401526. DOI: 10.1038/nrmicro865.
- [14] Z. Yang and D. J. Klionsky, "Eaten alive: A history of macroautophagy", *Nature Cell Biology*, vol. 12, no. 9, pp. 814–822, 2010, ISSN: 14657392. DOI: 10.1038/ncb0910-814.
- [15] ———, "Mammalian autophagy: Core molecular machinery and signaling regulation", *Current Opinion in Cell Biology*, vol. 22, no. 2, pp. 124–131, 2010, ISSN: 09550674. DOI: 10.1016/j.ceb.2009.11.014.
- [16] D. Glick *et al.*, "Autophagy: Cellular and Molecular mechanisms", *Journal of Pathology*, vol. 221, no. 1, pp. 3–12, 2010, ISSN: 10969896. DOI: 10.1002/path.2697. Autophagy.
- [17] N. C. Chang, "Autophagy and Stem Cells: Self-Eating for Self-Renewal", *Frontiers in Cell and Developmental Biology*, vol. 8, no. March, pp. 1–11, Mar. 2020, ISSN: 2296-634X. DOI: 10.3389/fcell.2020.00138.
- [18] B. Loos *et al.*, "Defining and measuring autophagosome flux - Concept and reality", *Autophagy*, vol. 10, no. 11, pp. 2087–2096, 2014, ISSN: 15548635. DOI: 10.4161/15548627.2014.973338.
- [19] D. Grieshaber *et al.*, "Electrochemical biosensors - Sensor principles and architectures", *Sensors*, vol. 8, no. 3, pp. 1400–1458, 2008, ISSN: 14248220. DOI: 10.3390/s8031400.
- [20] M. U. Ahmed *et al.*, *Food Biosensors Food Chemistry, Function and Analysis*, 1st ed. Cambridge: The Royal Society of Chemistry 2017, 2017, pp. 1–21, ISBN: 9781782623908.
- [21] N. Bhalla *et al.*, "Introduction to biosensors", *Essays in Biochemistry*, vol. 60, no. 1, pp. 1–8, 2016, ISSN: 00711365. DOI: 10.1042/EBC20150001.

- [22] L. Zeng and Z. Xiao, "A Lateral Flow Biosensor for the Detection of Single Nucleotide Polymorphisms", in *Methods in Molecular Biology*, vol. 1572, Springer Science+Business Media LLC, 2017, pp. 421–430, ISBN: 9781493969104. DOI: 10.1007/978-1-4939-6911-1_27.
- [23] R. Renneberg *et al.*, "Frieder scheller and the short history of biosensors", *Advances in Biochemical Engineering/Biotechnology*, vol. 109, no. November 2014, pp. 1–18, 2007, ISSN: 07246145. DOI: 10.1007/10_2007_086.
- [24] P. Mehrotra, "Biosensors and their applications -A review", *Journal of Oral Biology and Craniofacial Research*, vol. 6, no. 2, pp. 153–159, May 2016, ISSN: 22124268. DOI: 10.1016/j.jobcr.2015.12.002.
- [25] P. Bergveld, "Development of an Ion-Sensitive Solid-State Device for Neurophysiological Measurements", *IEEE Transactions on Biomedical Engineering*, vol. BME-17, no. 1, pp. 70–71, Jan. 1970, ISSN: 1558-2531. DOI: 10.1109/TBME.1970.4502688.
- [26] V. Naresh and N. Lee, "A review on biosensors and recent development of nanostructured materials-enabled biosensors", *Sensors (Switzerland)*, vol. 21, no. 4, pp. 1–35, 2021, ISSN: 14248220. DOI: 10.3390/s21041109.
- [27] S. Suzuki *et al.*, "Ethanol and Lactic Acid Sensors Using Electrodes Coated with Dehydrogenase-Collagen Membranes", *Bulletin of the Chemical Society of Japan*, vol. 48, no. 11, pp. 3246–3249, 1975. DOI: 10.1246/bcsj.48.3246.
- [28] P. Competitive and B. Assay, *United States Patent (19)*, 1982.
- [29] B. Liedberg *et al.*, "Surface plasmon resonance for gas detection and biosensing", *Sensors and Actuators*, vol. 4, pp. 299–304, 1983, ISSN: 0250-6874. DOI: [https://doi.org/10.1016/0250-6874\(83\)85036-7](https://doi.org/10.1016/0250-6874(83)85036-7).
- [30] A. E. G. Cass *et al.*, "Ferrocene-mediated enzyme electrode for amperometric determination of glucose", *Analytical Chemistry*, vol. 56, no. 4, pp. 667–671, 1984. DOI: 10.1021/ac00268a018.
- [31] P. Poncharal *et al.*, "Electrostatic Deflections and Electromechanical Resonances of Carbon Nanotubes", *Science*, vol. 283, no. 5407, pp. 1513–1516, 1999. DOI: 10.1126/science.283.5407.1513.
- [32] G. Rocchitta *et al.*, "Enzyme biosensors for biomedical applications: Strategies for safeguarding analytical performances in biological fluids", *Sensors (Switzerland)*, vol. 16, no. 6, 2016, ISSN: 14248220. DOI: 10.3390/s16060780.

- [33] S. Saxena, *Applied microbiology*. Springer New Delhi Heidelberg New York Dordrecht London, 1953, vol. 171, p. 638, ISBN: 9788132222583. DOI: 10.1038/171638a0.
- [34] D. Thevenot *et al.*, "Electrochemical biosensors : Recommended definitions and classification", *Pure and Applied Chemistry*, vol. 71, pp. 2333–2348, 2014.
- [35] V. Mirceski *et al.*, "Square-wave voltammetry", *ChemTexts*, vol. 4, no. 4, pp. 1–14, 2018, ISSN: 21993793. DOI: 10.1007/s40828-018-0073-0.
- [36] K. V., "DNA Biosensors-A Review", *Journal of Bioengineering & Biomedical Science*, vol. 07, no. 02, 2017. DOI: 10.4172/2155-9538.1000222.
- [37] K.-K. Hamed *et al.*, "DNA Biosensors Techniques and Their Applications in Food Safety, Environmental Protection and Biomedical Research: A mini-review", *Journal of Cell and Developmental Biology*, vol. 3, no. 1, pp. 28–35, 2020. DOI: 10.36959/596/446.
- [38] X. Ni *et al.*, "Nucleic Acid Aptamers: Clinical Applications and Promising New Horizons", *Current Medicinal Chemistry*, vol. 18, no. 27, pp. 4206–4214, 2011, ISSN: 09298673. DOI: 10.2174/092986711797189600.
- [39] S. B. Nimse *et al.*, "Immobilization techniques for microarray: Challenges and applications", *Sensors (Switzerland)*, vol. 14, no. 12, pp. 22 208–22 229, 2014, ISSN: 14248220. DOI: 10.3390/s141222208.
- [40] N. R. Mohamad *et al.*, "An overview of technologies for immobilization of enzymes and surface analysis techniques for immobilized enzymes", *Biotechnology and Biotechnological Equipment*, vol. 29, no. 2, pp. 205–220, 2015, ISSN: 13102818. DOI: 10.1080/13102818.2015.1008192.
- [41] F. V. Oberhaus *et al.*, "Immobilization Techniques for Aptamers on Gold Electrodes for the Electrochemical Detection of Proteins: A Review", *Biosensors*, vol. 10, no. 5, 2020, ISSN: 20796374. DOI: 10.3390/bios10050045.
- [42] J. I. A. Rashid and N. A. Yusof, "The strategies of DNA immobilization and hybridization detection mechanism in the construction of electrochemical DNA sensor: A review", *Sensing and Bio-Sensing Research*, vol. 16, no. September, pp. 19–31, 2017, ISSN: 22141804. DOI: 10.1016/j.sbsr.2017.09.001.
- [43] E. E. Ferapontova, "Hybridization Biosensors Relying on Electrical Properties of Nucleic Acids", *Electroanalysis*, vol. 29, no. 1, pp. 6–13, 2017, ISSN: 15214109. DOI: 10.1002/elan.201600593.
- [44] R. J. Mackenzie, *DNA vs RNA: 5 key differences*, 2020.
- [45] Excedr, *What is RNase? The Basics of Ribonuclease*, 2021.

- [46] A. Margariti *et al.*, "XBP1 mRNA Splicing Triggers an Autophagic Response in Endothelial Cells through BECLIN-1 Transcriptional Activation", *Journal of Biological Chemistry*, vol. 288, no. 2, pp. 859–872, Jan. 2013, ISSN: 00219258. DOI: 10.1074/jbc.M112.412783.
- [47] H. Okayama and P. Berg, "High-efficiency cloning of full-length cDNA", *Molecular and Cellular Biology*, vol. 2, no. 2, pp. 161–170, 1982, ISSN: 0270-7306. DOI: 10.1128/mcb.2.2.161-170.1982.
- [48] Metrohm DropSens, *Dropsens Screen Printed Electrodes*, 2021.
- [49] B. Liu and J. Liu, "Methods for preparing DNA-functionalized gold nanoparticles, a key reagent of bioanalytical chemistry", *Analytical Methods*, vol. 9, no. 18, pp. 2633–2643, 2017, ISSN: 17599679. DOI: 10.1039/c7ay00368d.
- [50] bio SYNTHESIS, "Instruction of reduction reaction using TCEP", *Bio Synthesis*, pp. 1–2, 2018.
- [51] H. Ravan *et al.*, "Strategies for optimizing DNA hybridization on surfaces", *Analytical Biochemistry*, vol. 444, no. 1, pp. 41–46, 2014, ISSN: 10960309. DOI: 10.1016/j.ab.2013.09.032.
- [52] S. Tripathy and S. G. Singh, "Label-Free Electrochemical Detection of DNA Hybridization: A Method for COVID-19 Diagnosis", *Transactions of the Indian National Academy of Engineering*, vol. 5, no. 2, pp. 205–209, Jun. 2020, ISSN: 2662-5415. DOI: 10.1007/s41403-020-00103-z.
- [53] E. G. Hvastkovs and D. A. Buttry, "Recent advances in electrochemical DNA hybridization sensors", *Analyst*, vol. 135, no. 8, pp. 1817–1829, 2010, ISSN: 13645528. DOI: 10.1039/c0an00113a.
- [54] S. Mendoza *et al.*, "Voltammetric Techniques", in *Agricultural and Food Electroanalysis*, Chichester, UK: John Wiley & Sons, Ltd, Jul. 2015, pp. 21–48, ISBN: 9781118684030. DOI: 10.1002/9781118684030.ch2.
- [55] F. Scholz, "Voltammetric techniques of analysis: the essentials", *ChemTexts*, vol. 1, no. 4, pp. 1–24, 2015, ISSN: 21993793. DOI: 10.1007/s40828-015-0016-y.
- [56] E. E. Ferapontova, "DNA Electrochemistry and Electrochemical Sensors for Nucleic Acids", *Annual Review of Analytical Chemistry*, vol. 11, no. 1, pp. 197–218, 2018, ISSN: 1936-1327. DOI: 10.1146/annurev-anchem-061417-125811.
- [57] L. Wiggins, *No Title*, 2014.

- [58] H. Wang *et al.*, "Self-assembled monolayer of ssDNA on Au(1 1 1) substrate", *Surface Science*, vol. 480, no. 1-2, pp. 1–6, 2001, ISSN: 00396028. DOI: 10.1016/S0039-6028(01)01007-X.
- [59] J. E. B. Randles, "Kinetics of rapid electrode reactions", *Discussions of the Faraday Society*, vol. 1, p. 11, 1947, ISSN: 0366-9033. DOI: 10.1039/df9470100011.
- [60] R. Singh *et al.*, "DNA biosensor for detection of *Neisseria gonorrhoeae* causing sexually transmitted disease", *Journal of Biotechnology*, vol. 150, no. 3, pp. 357–365, Nov. 2010, ISSN: 01681656. DOI: 10.1016/j.jbiotec.2010.09.935.
- [61] A. Benvidi *et al.*, "A highly sensitive and selective electrochemical DNA biosensor to diagnose breast cancer", *Journal of Electroanalytical Chemistry*, vol. 750, pp. 57–64, 2015, ISSN: 15726657. DOI: 10.1016/j.jelechem.2015.05.002.
- [62] D. Kang *et al.*, "Comparing the properties of electrochemical-based DNA sensors employing different redox tags", *Analytical Chemistry*, vol. 81, no. 21, pp. 9109–9113, 2009, ISSN: 00032700. DOI: 10.1021/ac901811n.
- [63] E. Farjami *et al.*, "DNA interactions with a Methylene Blue redox indicator depend on the DNA length and are sequence specific", *Analyst*, vol. 135, no. 6, pp. 1443–1448, 2010, ISSN: 13645528. DOI: 10.1039/c0an00049c.